

Regulation of mRNA decapping across atomic and mesoscopic scales

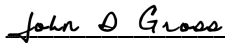
by  
Ryan W Tibble


DISSERTATION  
Submitted in partial satisfaction of the requirements for degree of  
DOCTOR OF PHILOSOPHY

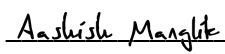
in  
Chemistry and Chemical Biology

in the  
GRADUATE DIVISION  
of the  
UNIVERSITY OF CALIFORNIA, SAN FRANCISCO

Approved:

DocuSigned by:  
  
C876331A93DC4B1... John D Gross  
Chair

DocuSigned by:  
  
DocuSigned by:  
43B... Geeta Narlikar

  
4C1E8A184D2E493... Aashish Manglik

---

Committee Members

Copyright 2021

by

Ryan William Tibble

## ACKNOWLEDGEMENTS

There are numerous people who shaped both my personal and scientific paths that has led to the writing of this dissertation. Their wisdom, insights, perspective, and support have pushed me to be a better scientist and person in my endeavor to understand the world around us. First and foremost, my PhD thesis advisor Dr. John Gross' unending support has encouraged me to pursue the important biological questions with rigor and curiosity. My project has taken me in unanticipated directions but John's enthusiasm has been contagious and my scientific development is all the better as a result. His affable nature is a welcoming presence in the lab, and I am equally excited to discuss science with him as I am my struggles, visions, and the ordinary day-to-day. I am also grateful for the team of scientists John has entrusted to carry out the work past and present as their guidance and discussions have influenced the experimentalist mind in me.

Outside of John's lab, UCSF is an enriching community to be a part of and many individuals who I interacted with—sometimes once or over many times—also contributed to my growth during graduate school. Thesis committee meetings with Drs. Geeta Narlikar and Aashish Manglik were always impactful, and I left them mulling over a critical insight or perspective that stretched my thinking in new directions. Annually presenting my research to the CCB program led me to be a better scientific communicator and was a constant reminder of the power in discussing diverse scientific projects with my peers. My CCB cohort was a source of many midday musings on the state of science and life. I am thankful to have gotten to know them over the years.

My professional scientific journey began as an undergraduate interested in anything chemistry and I am indebted to Dr. F. Jon Kull for the offer to join his lab. His lab introduced me to protein biochemistry and structural biophysics and provided me with the freedom to explore a myriad of techniques. During those formative years in the lab, I became friends and colleagues

with many people who shared with me the ups and downs of science. Their impact on me was transformative and is the reason I value teaching, mentorship, and personal growth.

My personal journey in science started much earlier with the whisking together of inedible spice concoctions and attempting to be helpful to Mom and Dad in their jobs as a papermaker and electrician, respectively. I am so incredibly thankful of their love since Day One and whose constant reminder of being proud parents keeps me from venturing too far astray. And to the rest of my family who helped me grow in innumerable ways and remind me to stay true to myself.

Finally, my partner Kaitlin has been the source of so much joy in my life. Her optimism and ceaseless kindness have been vital to my well-being amidst the chaos. She often knows me better than I do, and I am at my best when we are experiencing life's moments together. I look forward to the journey that lies ahead knowing we will be walking side-by-side.

## CONTRIBUTIONS

Work in this dissertation has been previously published in the following volumes of *Nucleic Acids Research* and *Nature Chemical Biology*:

Paquette, D. R.\*, Tibble, R. W.\*, Daifuku, T., Gross, J. D. Control of mRNA decapping by autoinhibition. *Nucleic Acids Research* **46**, 6318-6329 (2018).

Tibble, R. W., Depaix, A., Kowalska, J., Jemielity, J., Gross, J. D. Biomolecular condensates amplify mRNA decapping by biasing enzyme conformation. *Nature Chemical Biology* **17**, 615-623 (2021).

## Regulation of mRNA decapping across atomic and mesoscopic scales

Ryan W. Tibble

### ABSTRACT

During transcription in the nucleus, messenger RNA (mRNA) is endowed with modifications that serve as important markers for its regulation in the cell. This includes the addition of a 7-methylguanosine cap ( $m^7G$ ) at the 5' end, which is important for nuclear export, translation, and degradation of transcripts. Numerous mRNA quality control pathways end in the degradation of transcripts and pathogens can degrade RNA during infection to favor their survival. Removal of the cap structure, or decapping, commits mRNA to degradation and is a highly controlled step in post-transcriptional regulation. The conserved eukaryotic decapping complex Dcp1/Dcp2 is regulated through an intricate network of protein-protein interactions that can inhibit and accelerate decapping. While many of the interfaces required for these interactions have been studied, a mechanistic understanding of their consequences have not been well-characterized. This work describes a mechanism for autoinhibition of decapping and how the protein cofactors Edc3 and Edc1 relieve this autoinhibition to activate decapping through conformational changes in the Dcp2 active site. Furthermore, these regulatory mechanisms contribute to *in vitro* phase separation that causes localized sites of repressed and accelerated mRNA decapping. Together, these findings demonstrate how regulation at the ångstrom scale is coupled to microscopic behavior to enhance the catalytic power of decapping, which ensures mRNA degradation occurs only when specific conditions are met.

# TABLE OF CONTENTS

<b>Chapter 1: Introduction.....</b>	<b>1</b>
References .....	7
<b>Chapter 2: Control of mRNA decapping by autoinhibition .....</b>	<b>12</b>
Abstract.....	13
Introduction .....	13
Results .....	15
Discussion.....	25
Methods .....	29
Supplemental Figures.....	34
Supplemental Tables .....	38
References .....	41
<b>Chapter 3: Biomolecular condensates amplify mRNA decapping by biasing enzyme concentration .....</b>	<b>48</b>
Abstract.....	49
Introduction .....	49
Results .....	51
Discussion.....	65
Methods .....	67
Supplemental Figures.....	77

Supplemental Tables .....	87
References .....	90
<b>Chapter 4: Additional biochemical and biophysical studies of the decapping complex at ångstrom and mesoscopic scales .....</b>	<b>95</b>
Results .....	96
Tables .....	104
References .....	105
<b>Chapter 5: Concluding Remarks.....</b>	<b>108</b>



# LIST OF FIGURES

## Chapter 2: Control of mRNA decapping by autoinhibition

Figure 2.1: The C-terminal extension of Dcp2 inhibits decapping .....	16
Figure 2.2: Two motifs are required for autoinhibition of Dcp1:Dcp2 <sub>ext</sub> .....	18
Figure 2.3: Y220 stabilizes a cap-occluded state and alleviates inhibition .....	19
Figure 2.4: Y220G mutation quenches ms- $\mu$ sec dynamics in Dcp2 <sub>core</sub> .....	21
Figure 2.5: Edc3 alleviates autoinhibition of Dcp1:Dcp2 <sub>ext</sub> .....	22
Figure 2.6: Edc3 alleviates autoinhibition and promotes RNA binding .....	24
Figure 2.7: Edc1 and Edc3 coordinate to activate the Dcp1:Dcp2 <sub>ext</sub> complex.....	25
Figure 2.8: Model for autoinhibition, Edc3 alleviation and Edc3/Edc1 combined activation ...	27
Figure S2.1: Dcp1:Dcp2 containing C-terminal extension is monodisperse .....	34
Figure S2.2: Identification and characterization of inhibitory motifs in Dcp2 C-terminal extension .....	35
Figure S2.3: Amino-acid conservation in cap-occluded conformation.....	36
Figure S2.4: W43 and Y220G mutations quench ms- $\mu$ s dynamics in Dcp2 <sub>core</sub> and Y220G allows for observation of cap binding by NMR.....	36
Figure S2.5: Edc3 interaction with Dcp1:Dcp2 <sub>ext</sub> and activity with Dcp1:Dcp2 <sub>HLM-1</sub> .....	37
Figure S2.6: Comparison of rates with Edc3 and Edc1 of Dcp1:Dcp2 <sub>ext</sub> and Dcp1:Dcp2 <sub>core</sub> .	37
Figure S2.7: Coomassie stained SDS-PAGE of purified proteins used in this study.....	38

## Chapter 3: Biomolecular condensates amplify mRNA decapping by biasing enzyme concentration

Figure 3.1: Edc3 enhances Dcp1/Dcp2 <sub>ext</sub> phase separation .....	52
Figure 3.2: Interactions underlying Dcp1/Dcp2 <sub>ext</sub> and Dcp1/Dcp2 <sub>ext</sub> /Edc3 phase separation differ .....	54
Figure 3.3: The ability of phase-separated Dcp1/Dcp2 <sub>ext</sub> to decap RNA is modulated by Edc3.....	56
Figure 3.4: Edc3 couples activation of decapping to phase separation.....	58
Figure 3.5: The Dcp2 C-terminus stabilizes an autoinhibited conformation required for regulation of decapping in condensates .....	60
Figure 3.6: Maximum activation of Dcp1/Dcp2 <sub>ext</sub> in condensates requires Edc3.....	64
Figure S3.1: Edc3 alters physical properties of Dcp1/Dcp2 <sub>ext</sub> liquid droplets .....	77
Figure S3.2: Edc3 alters Dcp1/Dcp2 <sub>ext</sub> mobility in droplets.....	78
Figure S3.3: Synthesis and decapping of dually labelled 5' capped 35 nt RNA probe.....	79
Figure S3.4: Monitoring decapping of dual-labeled 35mer RNA using fluorescence polarization .....	80
Figure S3.5: Edc3 sequesters Dcp1/Dcp2 <sub>ext</sub> in condensates to cooperatively activate decapping .....	80
Figure S3.6: Edc3 alters Dcp1/Dcp2 <sub>ext</sub> enrichment and RNA mobility in liquid droplets.....	81
Figure S3.7: Generation of segmentally-labeled Dcp1/Dcp2 <sub>ext</sub> for NMR .....	82
Figure S3.8: <sup>1</sup> H/ <sup>13</sup> C-HSQC of ligated Dcp1/Dcp2 <sub>ext</sub> .....	83
Figure S3.9: Edc3(Lsm) reduces chemical shift perturbations (CSPs) of Dcp1/Dcp2 <sub>ext</sub> to more closely resemble the chemical shifts of Dcp1/Dcp2 <sub>core</sub> .....	84

Figure S3.10: Several resonances in the catalytic domain of Dcp2 report on the inactive—  
 precatalytic equilibrium ..... 85

Figure S3.11: Dcp1/Dcp2<sub>ext</sub> conformational equilibria is important for substrate recognition,  
 liquid-like behavior, and proper regulation of decapping in condensates ..... 86

**Chapter 4: Additional biochemical and biophysical studies of the decapping  
 complex at ångstrom and mesoscale levels**

Figure 4.1: Aromatic residues in Dcp2 that interact with m<sup>7</sup>G have different effects on activity  
 and specificity ..... 97

Figure 4.2: Residues along the interfacial helix of the Dcp2 NRD undergo coordinated  
 movements that enable m<sup>7</sup>G recognition by W43..... 98

Figure 4.3: Dcp1/Dcp2 dimers observed in solved crystal structure 2QKM ..... 101

Figure 4.4: Analytical ultracentrifugation (AUC) of Dcp1/Dcp2(1-504) and Dcp1/Dcp2  
 (1-266) ..... 101

Figure 4.5: Decapping in aged Dcp1/Dcp2/Edc3 condensates restores size and RNA  
 exchange to resemble liquid-like condensates more closely ..... 103

**Chapter 5: Concluding Remarks**

Figure 5.1: Model of how phase separation regulates mRNA decapping ..... 108

## LIST OF TABLES

### Chapter 2: Control of mRNA decapping by autoinhibition

Table S2.1: Table of constructs used in this study .....	39
Table S2.2: Dynamic Light Scattering (DLS) of Dcp1:Dcp2 <sub>ext</sub> and Dcp1:Dcp2 <sub>core</sub> .....	39
Table S2.3: Mean $k_{obs}$ of 1.5 $\mu$ M Dcp1:Dcp2 constructs .....	40

### Chapter 3: Biomolecular condensates amplify mRNA decapping by biasing enzyme concentration

Table S3.1: Protein constructs used in this study .....	87
Table S3.2: Values for half-time of recovery and the fraction of mobile molecules obtained from fitting to FRAP curves .....	88
Table S3.3: Dcp1/Dcp2 <sub>ext</sub> decapping rates in Bulk and Dilute phases .....	88
Table S3.4: Dcp1/Dcp2 <sub>ext</sub> decapping rates in Bulk and Dilute Phase with variable Edc3 .....	88
Table S3.5: Dcp1/Dcp2 <sub>ext</sub> decapping rates with addition of Edc3 Lsm and YjeF N domains .	88
Table S3.6: Equilibrium dissociation constants ( $K_D$ ) for various Dcp2 constructs determined by fluorescence polarization .....	88
Table S3.7: Dcp1/Dcp2 <sub>ext</sub> (Y220G) and Dcp1/Dcp2 <sub>ext</sub> WT decapping rates in Bulk and Dilute Phase at variable Edc3 concentrations .....	89
Table S3.8: Edc1/Dcp1/Dcp2 decapping rates in Bulk and Dilute Phase at variable Edc3 concentrations .....	89

### Chapter 4: Additional biochemical and biophysical studies of the decapping complex at ångstrom and mesoscopic scales

Table 4.1: Effect of Dcp2 aromatic mutations on decapping rates and specificity for methylated cap .....	104
Table 4.2: Qualitative evaluation of mutations in Dcp2 on ms- $\mu$ s dynamics.....	104

# CHAPTER 1

## INTRODUCTION

The biological state of a cell is dictated by environmental inputs and requires robust responses to stress, the cell cycle, and differentiation. To adequately adapt to these inputs, the cell undergoes a genetic reprogramming that leads to changes in its RNA composition. Cellular RNAs are extensively processed and modified throughout their lifetime, which leads to the recruitment of RNA-binding proteins (RBPs). The temporal composition of RBPs is important for regulating subsequent functional consequences on a specific RNA and RBPs often coordinate with one another to influence this outcome. As a result, elucidating how RBPs interact with each other to modify RNA is critical to understanding how cells ensure their viability under ever-changing conditions.

mRNA are a major class of RNA that dictate the protein machinery present in the cell and their proper regulation is crucial to maintaining homeostasis. During transcription in the nucleus, mRNA are capped at their 5'-end with 7-methylguanosine ( $m^7G$ ) and a polyadenosine (poly-A) tail on the 3'-end, which are vital modifications for the stability and recruitment of translation machinery to mRNA. In addition, several classes of viruses encode their own capping enzymes in order to promote translation of viral proteins and prevent activation of host immune responses, underscoring the importance of the 5'-cap in mRNA function.

Because of their role in promoting translation, removal of the 5'-cap and poly-A tail from mRNA is a major form of post-transcriptional control of gene expression important for cell development, growth, and antiviral response. Loss of the  $m^7G$  cap, or decapping, proceeds trimming of the poly-A tail (deadenylation) and leads to the rapid 5'-3' degradation of a transcript by a conserved 5'-exonuclease<sup>1-3</sup>. Decapping is at the convergence of multiple mRNA degradation pathways in the cell: bulk mRNA decay, microRNA (miRNA) mediated decay, nonsense-mediated decay (NMD), AU-rich elements (ARE) decay, and other transcript-specific

quality control mechanisms<sup>4-6</sup>. Moreover, decapping is largely irreversible and represents a final checkpoint in mRNA turnover. As a result, a myriad of protein cofactors coordinate assembly across the length of a mRNA transcript to form a highly regulated decapping complex.

Decapping is carried out by Dcp2, an enzyme of the Nudix (Nucleotide diphosphate moiety linked to X) hydrolase family that is conserved in eukaryotes<sup>7,8</sup>. Dcp2 contains a bipartite active site that is formed between a structured N-terminal domains<sup>9-11</sup>. While the structured domains are absolutely conserved, Dcp2 contains a variable intrinsically disordered region (IDR) C-terminal to these domains<sup>12</sup>. In the more well-studied yeast orthologues of Dcp2, several short linear motifs (SLiMs) have been identified that mediate protein-protein interactions and impart both positive and negative regulation of decapping<sup>13,14</sup>. In addition, removal of the IDR is lethal to yeast subjected to heat shock<sup>15</sup>. While not yet deeply characterized, putative SLiMs similar to those in yeast Dcp2 have been identified in other eukaryotes, suggesting the mechanisms of regulation may be conserved<sup>12</sup>.

The cofactor Dcp1 is often tightly associated with Dcp2 to form a minimal decapping complex *in vitro*<sup>7</sup>. Dcp1 has been shown to directly activate and promote specificity for m<sup>7</sup>G cap recognition in Dcp2<sup>9,11,16</sup>. Additionally, Dcp1 serves as a platform for bridging multiple components involved in 5'-3' decay, including the decapping activators Edc1/2 (PNRC1/2 in higher eukaryotes), the 5' exonuclease Xrn1, and the IDR of Dcp2<sup>17-19</sup>. Thus, Dcp1 serves as integrator of cellular signals to allosterically regulate Dcp2 activity.

As mentioned previously, the IDR of yeast Dcp2 contains multiple SLiMs and helical leucine motifs (HLMs) are the most abundant. HLMs in Dcp2 have been shown to directly interact with the proteins Edc3, Pat1, and Upf1. Despite all interacting with Dcp2 through the same interface, these cofactors regulate overlapping but distinct mRNAs *in vivo*<sup>20</sup>. In addition, both Edc3 and Pat1 interact with the helicase Dhh1 (DDX6 in humans), which has an important role in assessing mRNA translation fidelity and couples degradation to poor translation efficiency<sup>12,21</sup>. Finally, Pat1 interacts with Xrn1 and the heteromeric LSm1-7 complex that

recognizes the 3'-end of a transcript that has undergone deadenylation, linking deadenylation, decapping, and degradation<sup>22-25</sup>. As a result of the ability to recognize numerous factors, mRNA decapping and degradation can be controlled in a coordinated, context-dependent manner to remove specific transcripts from the translating pool that are no longer needed or are harmful to the cell.

Previous *in vivo* studies of decapping in yeast identified SLiMs in the Dcp2 IDR distinct from HLMs that prevented non-specific degradation of mRNA<sup>13</sup>. This negative regulation of decapping had not been described before and its mechanism was unclear. Chapter 1 of this thesis identifies inhibitory motifs (IMs) in Dcp2 from *Schizosaccharomyces pombe* and demonstrates these motifs directly autoinhibit decapping activity *in vitro*<sup>26</sup>. Furthermore, we define a direct regulatory role for Edc3 whereby its interaction with HLMs alleviates autoinhibition to restore catalysis. The mechanism of activation we described is shared by Pat1 and we posit it can be extended generally to other decapping cofactors that interact with HLMs<sup>27</sup>. These results highlight another mechanism of regulatory control placed on mRNA decapping to prevent aberrant degradation events.

The decapping complex and numerous other cofactors involved in 5'-3' mRNA decay colocalize in cytoplasmic foci known as Processing Bodies, or P-bodies<sup>28-30</sup>. These structures are conserved across eukaryotes and are stabilized by many redundant interactions that cause robust formation even when key components have been genetically deleted<sup>31,32</sup>. While many types of RNAs colocalize to P-bodies they share a common feature: they are translationally repressed due to the absence of translation factors and ribosomes<sup>33</sup>. Many studies have examined the global role of P-bodies in mRNA decay but a consensus has been difficult to reach<sup>30,34-37</sup>. Recent advances in developing fluorescent reporter mRNA have provided the field with the ability to study P-bodies at single-molecule resolution<sup>38,39</sup>. These studies have demonstrated P-body function is context-dependent, serving as both sites of active mRNA



decay and storage<sup>38,40-42</sup>. An exciting area of research involves identifying new mechanisms of regulation within these structures dense in factors involved in all aspects of 5'-3' mRNA decay.

In addition to being sites of regulated mRNA decay, P-bodies are dynamic structures that change in size and abundance depending on cell state. For example, P-bodies become more abundant and multiple microns in diameter under cellular stress, but can be completely cleared or less than one micron in diameter during development and normal growth conditions, respectively<sup>31</sup>. Thus, P-bodies do not represent a defined heterooligomeric protein structure nor an irreversible protein aggregate. Over the last few years, P-bodies have been classified as a biomolecular condensate, which is a membraneless, liquid-like, phase-separated compartment in cells<sup>43,44</sup>. Numerous biomolecular condensates have been described and many are involved in RNA processing. Subsequently, biomolecular condensates have emerged as a unique mechanism to spatially regulate RNA biochemistry and provide a framework for examining the functional consequences of P-body formation.

Condensate formation is promoted by numerous weak, multivalent interactions between proteins and nucleic acids, leading to their enrichment at concentrations that can greatly exceed those observed in the surrounding solution<sup>43</sup>. Such a dense and concentrated environment can lead to emergent phenomena that would otherwise not be observed. This includes the enhancement of biochemical reactions due to increased enzyme and substrate concentrations and enhanced specificity in substrate recognition<sup>45-47</sup>. Biochemistry can also be repressed in droplets by preventing productive interactions between reaction components because of differential sequestration or increased non-specific interactions. Furthermore, the environment within condensates can lead to conformational changes in resident molecules that may result in different biochemical outcomes<sup>48-50</sup>. Elucidating the consequences of phase separation on biochemical processes is essential to progressing our understanding of how cells utilize condensates to maintain cell viability.

Studying regulation in P-bodies is difficult because of their dynamic behavior and complex composition. However, several factors enriched in P-bodies undergo phase separation *in vitro*, which presents a powerful means to dissect the consequences outlined above. The Dcp1/Dcp2 decapping complex is the most enriched protein in yeast P-bodies and undergoes phase separation<sup>51</sup>. Given the critical role of decapping in 5'-3' mRNA degradation, studying how condensate formation influences Dcp1/Dcp2 activity affords a rigorous and systematic approach to discerning how mRNA decay can be regulated in P-bodies. In Chapter 2, we show decapping can be inhibited and repressed in condensates and phase separation expands the catalytic range of Dcp2<sup>52</sup>. The differential activity we observed is dependent on the interactions underlying condensate formation and we find these interactions are allosterically coupled to the conformation of the Dcp2 active site. Thus, this work extends the mechanism we describe in Chapter 1 to encompass regulation of decapping at the micron scale and has implications for how P-body formation can ensure fidelity in mRNA decay.

Dcp2 is a dynamic enzyme at the atomic and mesoscopic scales: undergoing large conformational changes during its catalytic cycle and exhibiting differential exchange kinetics in cellular P-bodies<sup>2,41,53,54</sup>. Previous work identified residues that mediate structural fluctuations necessary for cap recognition and organization of the pH-sensitive catalytic triad<sup>16,55,56</sup>. In yeast, HLMs are crucial for ensuring Dcp2 localizes to and is retained in P-bodies<sup>53</sup>. Underpinning much of the work in this thesis has been our ongoing efforts to expand our understanding of how Dcp2 dynamics are linked to catalysis. In Chapter 1, we identify a residue in Dcp2 that alleviates autoinhibition and bypasses Edc3 activation<sup>26</sup>. We find this mutation quenches interdomain motions between the structured domains of Dcp2 and, in Chapter 2, show this mutation prevents formation of an inactive state required for regulation of decapping in condensates<sup>52</sup>. In Chapter 3, we identify an interface that we predict serves as a molecular 'switchboard' to mediate the conformational state of Dcp2. At the mesoscale, we observed in Chapter 2 that Dcp2 exchange in condensates can be altered by composition and in Chapter 3,

we show Dcp2 catalysis is important for maintaining a liquid-like state in condensates. Altogether, these results highlight how catalysis and dynamics are inextricably linked across organizational scales to afford the cell with the ability to maximize biochemical potential.

## REFERENCES

1. Beelman, C. A. *et al.* An essential component of the decapping enzyme required for normal rates of mRNA turnover. *Nature* **382**, 642–646 (1996).
2. Mugridge, J. S., Collier, J. & Gross, J. D. Structural and molecular mechanisms for the control of eukaryotic 5'–3' mRNA decay. *Nat. Struct. Mol. Biol.* **25**, 1077–1085 (2018).
3. Nagarajan, V. K., Jones, C. I., Newbury, S. F. & Green, P. J. XRN 5'→3' exoribonucleases: Structure, mechanisms and functions. *Biochim. Biophys. Acta BBA - Gene Regul. Mech.* **1829**, 590–603 (2013).
4. Kurosaki, T., Popp, M. W. & Maquat, L. E. Quality and quantity control of gene expression by nonsense-mediated mRNA decay. *Nat. Rev. Mol. Cell Biol.* **20**, 406–420 (2019).
5. Franks, T. M. & Lykke-Andersen, J. The Control of mRNA Decapping and P-Body Formation. *Mol. Cell* **32**, 605–615 (2008).
6. Guo, H., Ingolia, N. T., Weissman, J. S. & Bartel, D. P. Mammalian microRNAs predominantly act to decrease target mRNA levels. *Nature* **466**, 835–840 (2010).
7. Dunckley, T. & Parker, R. The DCP2 protein is required for mRNA decapping in *Saccharomyces cerevisiae* and contains a functional MutT motif. *EMBO J.* **18**, 5411–5422 (1999).
8. Wang, Z., Jiao, X., Carr-Schmid, A. & Kiledjian, M. The hDcp2 protein is a mammalian mRNA decapping enzyme. *Proc. Natl. Acad. Sci.* **99**, 12663–12668 (2002).
9. Deshmukh, M. V. *et al.* mRNA Decapping Is Promoted by an RNA-Binding Channel in Dcp2. *Mol. Cell* **29**, 324–336 (2008).
10. She, M. *et al.* Crystal structure and functional analysis of Dcp2p from *Schizosaccharomyces pombe*. *Nat. Struct. Mol. Biol.* **13**, 63–70 (2006).
11. She, M. *et al.* Structural Basis of Dcp2 Recognition and Activation by Dcp1. *Mol. Cell* **29**, 337–349 (2008).

12. Jonas, S. & Izaurralde, E. The role of disordered protein regions in the assembly of decapping complexes and RNP granules. *Genes Dev.* **27**, 2628–2641 (2013).
13. He, F. & Jacobson, A. Control of mRNA decapping by positive and negative regulatory elements in the Dcp2 C-terminal domain. *RNA* **21**, 1633–1647 (2015).
14. Harigaya, Y., Jones, B. N., Muhlrads, D., Gross, J. D. & Parker, R. Identification and Analysis of the Interaction between Edc3 and Dcp2 in *Saccharomyces cerevisiae*. *Mol. Cell. Biol.* **30**, 1446–1456 (2010).
15. Fromm, S. A. *et al.* The structural basis of Edc3- and Scd6-mediated activation of the Dcp1:Dcp2 mRNA decapping complex. *EMBO J.* **31**, 279–290 (2012).
16. Floor, S. N., Borja, M. S. & Gross, J. D. Interdomain dynamics and coactivation of the mRNA decapping enzyme Dcp2 are mediated by a gatekeeper tryptophan. *Proc. Natl. Acad. Sci.* **109**, 2872–2877 (2012).
17. Wurm, J. P., Overbeck, J. & Sprangers, R. The *S. pombe* mRNA decapping complex recruits cofactors and an Edc1-like activator through a single dynamic surface. *RNA* **22**, 1360–1372 (2016).
18. Mugridge, J. S., Ziemniak, M., Jemielity, J. & Gross, J. D. Structural basis of mRNA-cap recognition by Dcp1–Dcp2. *Nat. Struct. Mol. Biol.* **23**, 987–994 (2016).
19. Braun, J. E. *et al.* A direct interaction between DCP1 and XRN1 couples mRNA decapping to 5' exonucleolytic degradation. *Nat. Struct. Mol. Biol.* **19**, 1324–1331 (2012).
20. He, F., Celik, A., Wu, C. & Jacobson, A. General decapping activators target different subsets of inefficiently translated mRNAs. *eLife* **7**, e34409 (2018).
21. Radhakrishnan, A. *et al.* The DEAD-Box Protein Dhh1p Couples mRNA Decay and Translation by Monitoring Codon Optimality. *Cell* **167**, 122-132.e9 (2016).
22. Charenton, C. *et al.* A unique surface on Pat1 C-terminal domain directly interacts with Dcp2 decapping enzyme and Xrn1 5'–3' mRNA exonuclease in yeast. *Proc. Natl. Acad. Sci.* **114**, E9493–E9501 (2017).

23. Sharif, H. & Conti, E. Architecture of the Lsm1-7-Pat1 Complex: A Conserved Assembly in Eukaryotic mRNA Turnover. *Cell Rep.* **5**, 283–291 (2013).
24. Sharif, H. *et al.* Structural analysis of the yeast Dhh1-Pat1 complex reveals how Dhh1 engages Pat1, Edc3 and RNA in mutually exclusive interactions. *Nucleic Acids Res.* **41**, 8377–8390 (2013).
25. Tuck, A. C. *et al.* Mammalian RNA Decay Pathways Are Highly Specialized and Widely Linked to Translation. *Mol. Cell* **0**, (2020).
26. Paquette, D. R., Tibble, R. W., Daifuku, T. S. & Gross, J. D. Control of mRNA decapping by autoinhibition. *Nucleic Acids Res.* **46**, 6318–6329 (2018).
27. Lobel, J. H., Tibble, R. W. & Gross, J. D. Pat1 activates late steps in mRNA decay by multiple mechanisms. *Proc. Natl. Acad. Sci.* **116**, 23512–23517 (2019).
28. Sheth, U. & Parker, R. Decapping and Decay of Messenger RNA Occur in Cytoplasmic Processing Bodies. *Science* **300**, 805–808 (2003).
29. Parker, R. & Sheth, U. P Bodies and the Control of mRNA Translation and Degradation. *Mol. Cell* **25**, 635–646 (2007).
30. Luo, Y., Na, Z. & Slavoff, S. A. P-Bodies: Composition, Properties, and Functions. *Biochemistry* **57**, 2424–2431 (2018).
31. Rao, B. S. & Parker, R. Numerous interactions act redundantly to assemble a tunable size of P bodies in *Saccharomyces cerevisiae*. *Proc. Natl. Acad. Sci.* **114**, E9569–E9578 (2017).
32. Teixeira, D. & Parker, R. Analysis of P-Body Assembly in *Saccharomyces cerevisiae*. *Mol. Biol. Cell* **18**, 2274–2287 (2007).
33. Teixeira, D., Sheth, U., Valencia-Sanchez, M. A., Brengues, M. & Parker, R. Processing bodies require RNA for assembly and contain nontranslating mRNAs. *RNA* **11**, 371–382 (2005).
34. Hubstenberger, A. *et al.* P-Body Purification Reveals the Condensation of Repressed mRNA Regulons. *Mol. Cell* **68**, 144-157.e5 (2017).

35. Wang, C. *et al.* Context-dependent deposition and regulation of mRNAs in P-bodies. *eLife* **7**, e29815 (2018).
36. Chan, L. Y., Mugler, C. F., Heinrich, S., Vallotton, P. & Weis, K. Non-invasive measurement of mRNA decay reveals translation initiation as the major determinant of mRNA stability. *eLife* **7**, e32536 (2018).
37. Brengues, M., Teixeira, D. & Parker, R. Movement of Eukaryotic mRNAs Between Polysomes and Cytoplasmic Processing Bodies. *Science* **310**, 486–489 (2005).
38. Horvathova, I. *et al.* The Dynamics of mRNA Turnover Revealed by Single-Molecule Imaging in Single Cells. *Mol. Cell* **68**, 615-625.e9 (2017).
39. Tutucci, E. *et al.* An improved MS2 system for accurate reporting of the mRNA life cycle. *Nat. Methods* **15**, 81–89 (2018).
40. Aizer, A. *et al.* The Dynamics of Mammalian P Body Transport, Assembly, and Disassembly In Vivo. *Mol. Biol. Cell* **19**, 4154–4166 (2008).
41. Aizer, A. *et al.* Quantifying mRNA targeting to P-bodies in living human cells reveals their dual role in mRNA decay and storage. *J. Cell Sci.* **127**, 4443–4456 (2014).
42. Hutchins, E. J., Piacentino, M. L. & Bronner, M. E. P-bodies are sites of rapid RNA decay during the neural crest epithelial—mesenchymal transition. *bioRxiv* 2020.07.31.231860 (2020) doi:10.1101/2020.07.31.231860.
43. Banani, S. F., Lee, H. O., Hyman, A. A. & Rosen, M. K. Biomolecular condensates: organizers of cellular biochemistry. *Nat. Rev. Mol. Cell Biol.* **18**, 285–298 (2017).
44. Boeynaems, S. *et al.* Protein Phase Separation: A New Phase in Cell Biology. *Trends Cell Biol.* **28**, 420–435 (2018).
45. Zhang, Y., Narlikar, G. J. & Kutateladze, T. G. Enzymatic Reactions inside Biological Condensates. *J. Mol. Biol.* **433**, 166624 (2021).
46. Lyon, A. S., Peeples, W. B. & Rosen, M. K. A framework for understanding the functions of biomolecular condensates across scales. *Nat. Rev. Mol. Cell Biol.* **22**, 215–235 (2021).

47. Peebles, W. & Rosen, M. K. Mechanistic dissection of increased enzymatic rate in a phase-separated compartment. *Nat. Chem. Biol.* **17**, 693–702 (2021).
48. Brady, J. P. *et al.* Structural and hydrodynamic properties of an intrinsically disordered region of a germ cell-specific protein on phase separation. *Proc. Natl. Acad. Sci.* **114**, E8194–E8203 (2017).
49. Kim, T. H. *et al.* Phospho-dependent phase separation of FMRP and CAPRIN1 recapitulates regulation of translation and deadenylation. *Science* **365**, 825–829 (2019).
50. Langdon, E. M. *et al.* mRNA structure determines specificity of a polyQ-driven phase separation. *Science* **360**, 922–927 (2018).
51. Fromm, S. A. *et al.* In Vitro Reconstitution of a Cellular Phase-Transition Process that Involves the mRNA Decapping Machinery. *Angew. Chem. Int. Ed.* **53**, 7354–7359 (2014).
52. Tibble, R. W., Depaix, A., Kowalska, J., Jemielity, J. & Gross, J. D. Biomolecular condensates amplify mRNA decapping by biasing enzyme conformation. *Nat. Chem. Biol.* **17**, 615–623 (2021).
53. Xing, W., Muhrad, D., Parker, R. & Rosen, M. K. A quantitative inventory of yeast P body proteins reveals principles of composition and specificity. *eLife* **9**, e56525 (2020).
54. Wurm, J. P. & Sprangers, R. Dcp2: an mRNA decapping enzyme that adopts many different shapes and forms. *Curr. Opin. Struct. Biol.* **59**, 115–123 (2019).
55. Aglietti, R. A., Floor, S. N., McClendon, C. L., Jacobson, M. P. & Gross, J. D. Active Site Conformational Dynamics Are Coupled to Catalysis in the mRNA Decapping Enzyme Dcp2. *Structure* **21**, 1571–1580 (2013).
56. Wurm, J. P., Holdermann, I., Overbeck, J. H., Mayer, P. H. O. & Sprangers, R. Changes in conformational equilibria regulate the activity of the Dcp2 decapping enzyme. *Proc. Natl. Acad. Sci.* **114**, 6034–6039 (2017).



## CHAPTER 2

### Control of mRNA decapping by autoinhibition

David R. Paquette<sup>1,3\*</sup>, Ryan W. Tibble<sup>2,3\*</sup>, Tristan S. Daifuku<sup>3</sup>, and John D. Gross<sup>1,2,3</sup>

Author affiliations:

<sup>1</sup> Integrative Program in Quantitative Biology, Graduate Group in Biophysics division, University of California, San Francisco, California, 94158, USA

<sup>2</sup> Program in Chemistry and Chemical Biology, University of California, San Francisco, California, 94158, USA

<sup>3</sup> Department of Pharmaceutical Chemistry, University of California, San Francisco, California, 94158, USA

\* These authors contributed equally

*This chapter adapted from:*

Paquette, D. R.\*, Tibble, R. W.\*, Daifuku, T., Gross, J. D. Control of mRNA decapping by autoinhibition. *Nucleic Acids Research* **46**, 6318-6329 (2018).

## ABSTRACT

5' mediated cytoplasmic RNA decay is a conserved cellular process in eukaryotes. While the functions of the structured core domains in this pathway are understood, the role of abundant intrinsically disordered regions (IDRs) is lacking. Here we reconstitute the Dcp1:Dcp2 complex containing a portion of the disordered C-terminus and show its activity is autoinhibited by linear interaction motifs. Enhancers of decapping (Edc) 1 and 3 cooperate to activate decapping by different mechanisms: Edc3 alleviates autoinhibition by binding IDRs and destabilizing an inactive form of the enzyme, whereas Edc1 stabilizes the transition state for catalysis. Both activators are required to fully stimulate an autoinhibited Dcp1:Dcp2 as Edc1 alone cannot overcome the decrease in activity attributed to the C-terminal extension. Our data provide a mechanistic framework for combinatorial control of decapping by protein cofactors, a principle that is likely conserved in multiple 5' mRNA decay pathways.

## INTRODUCTION

Eukaryotic 5'-3' mRNA decay is preceded and permitted by removal of the m<sup>7</sup>GpppN (N any nucleotide) cap structure and is a critical, conserved cellular process from yeast to humans<sup>1-3</sup>. There are multiple decapping enzymes in eukaryotic cells<sup>4</sup>, and the maintenance of the m<sup>7</sup>G cap in eukaryotes is required for numerous cellular processes including: splicing<sup>5,6</sup>, nuclear export<sup>7</sup>, canonical translation and transcript stability<sup>8,9</sup>, and quality control pathways<sup>10,11</sup>. Recent evidence suggests that caps containing m<sup>6</sup>A<sub>m</sub> as the first-transcribed nucleotide are protected from decapping and 5'-3' decay<sup>12</sup>. Critically, mRNA decay is important during development<sup>13</sup>. Furthermore, the cap structure and polyA tail differentiate the mRNA from other cellular RNAs, a feature viruses try to coopt to protect and translate their messages<sup>14</sup>. Hydrolysis of the cap structure usually marks the transcript for degradation. Consequently, decapping and 5'-3' decay pathways are tightly controlled and rely on cofactors<sup>15</sup>. A key question in the field is how the activity of decapping enzymes are controlled by different protein interaction networks.

The major cytoplasmic decapping enzyme in yeast is the Dcp1:Dcp2 holoenzyme. Dcp2 is a bi-lobed enzyme consisting of a regulatory (NRD) and NUDIX containing catalytic domain (CD). The NRD binds Dcp1, an EVH1-like scaffold, which recruits cofactors through an aromatic cleft that recognizes a short proline-rich motif found in Edc1-type coactivators<sup>16</sup>, including its yeast paralog Edc2 and mammalian PNRC2<sup>17</sup>. Additionally, Edc1-type coactivators contain a conserved short linear (Dcp2) activation motif that stimulates the catalytic step of decapping. Crystallographic and solution NMR analyses of Dcp1:Dcp2 with m<sup>7</sup>GDP product and substrate analog reveal the activation motif stabilizes the regulatory and catalytic domains of the enzyme in orientations compatible with formation of a composite active site<sup>18</sup>. In the absence of Edc1 or related cofactors, Dcp1:Dcp2 is dynamic and forms nonproductive interactions with substrate RNA<sup>18</sup>, which reduce catalytic efficiency. In several crystal structures of Dcp1:Dcp2, the composite active site is occluded (PDBID: 2QKM, 5J3Y, 5QK1), and it has been suggested that these forms of the enzyme exist in solution as nonproductive states of unknown function<sup>18–20</sup>.

Edc1 has genetic interactions with Edc3 in yeast and both proteins form physical interactions with Dcp1:Dcp2<sup>21</sup>, suggesting they work together to promote decapping. Edc3 is important for decapping and subsequent 5'-3' decay of pre-mRNA and mRNA targets in budding yeast<sup>22,23</sup>, general decapping in fission yeast<sup>24</sup>, and decay of miRNA targets in *Drosophila*<sup>25</sup>; while mutations in human Edc3 are associated with defects in neuronal development<sup>26</sup>. Edc3 binds to fungal Dcp2 or metazoan Dcp1 through interactions with C-terminal extensions containing short leucine rich helical motifs (HLMs)<sup>27</sup>. Recent crystallographic and genetic experiments in *S. cerevisiae* determined Pat1, a central component of the decapping machinery, also interacts with HLMs in Dcp2, demonstrating the importance of HLMs in mediating protein-protein interactions to control decay<sup>28</sup>. Moreover, the HLMs are important for recruitment to P-bodies *in vivo*<sup>20</sup> and for phase-separation *in vitro*<sup>27</sup>. However, the molecular mechanisms for how Edc3 stimulates decapping are not well understood.

Genetic studies in budding yeast indicate the disordered C-terminus of Dcp2 is a major site of regulation of decapping. He and Jacobson identified regions in the C-terminus that recruit positive regulators of decapping, including Edc3 and Pat1, to promote turnover of specific transcripts<sup>29</sup>. The same study also demonstrated that a distinct proline- and phenylalanine-rich region in the C-terminus negatively regulates decapping and excision of this region bypasses the requirement for activation of decapping by Edc3<sup>29</sup>. These results suggest Dcp2 is autoinhibited, but a biochemical and structural understanding of how the C-terminus acts to inhibit decapping and how activators of decapping alleviate this inhibition is unknown due to the difficulty in preparing constructs of Dcp2 containing the disordered region.

Here we reconstitute an extended construct of *S. pombe* Dcp1:Dcp2 from recombinant components and show that it is autoinhibited by its C-terminal extension. Within this extension, we identify a proline-rich region that contains two inhibitory motifs that when removed restore enzymatic activity. We demonstrate that the addition of Edc3 alleviates the inhibitory role of the C-terminal extension by stimulating the catalytic step of decapping. Edc3 also promotes substrate binding. We show that a fraction of the autoinhibited complex is recalcitrant to Edc1 activation and that Edc3 works synergistically to make the complex more amenable to Edc1 dependent activation. Finally, we identify a conserved amino acid in the structured core domain of Dcp2 which when mutated quenches ms- $\mu$ s dynamics of Dcp2, restores activity of the inhibited complex, and bypasses the Edc3 mediated alleviation of inhibition. We propose a model for autoinhibition of the decapping complex that occurs through stabilization of a cap-occluded Dcp2 conformation, which exists in solution and has appeared in numerous crystal structures.

## **RESULTS**

### **A segment of the C-terminus in Dcp2 inhibits decapping**

The C-terminus of *S. pombe* Dcp2 is predicted to be highly disordered (**Fig. 2.1a**). To determine its functional role in decapping, Dcp1 was co-expressed with the C-terminally extended

Dcp2 (Dcp1:Dcp2<sub>ext</sub>) and purified to homogeneity. A C-terminal boundary ending at residue 504 was chosen by sequence conservation and optimization of expression (**Table S2.1**). This construct contains regions of the protein that were excised in prior biochemical studies due to sub-optimal expression levels<sup>30,31</sup>. Decapping activity of Dcp1:Dcp2<sub>ext</sub> was compared with that containing only the structured core domains (Dcp1:Dcp2<sub>core</sub>) comprised of Dcp1 and Dcp2 with the N-terminal regulatory (NRD) and catalytic domain (CD) using a cap-radiolabeled RNA as substrate. The rate of decapping by Dcp1:Dcp2<sub>core</sub> was faster than Dcp1:Dcp2<sub>ext</sub> (**Fig. 2.1b**). Fitted rate-constants indicated Dcp1:Dcp2<sub>ext</sub> was consistently slower than Dcp1:Dcp2<sub>core</sub> (**Fig. 2.1c,d**); this effect was not dependent on enzyme preparation. Dcp1:Dcp2<sub>ext</sub> purified as a well-resolved, homogeneous peak on gel-filtration and is monodisperse under decapping reaction conditions, as indicated by dynamic light-scattering (**Fig. S2.1** and **Table S2.2**). These data suggest the C-terminal extension of Dcp2 has sequence motifs that can inhibit the decapping activity of the structured, core domains.

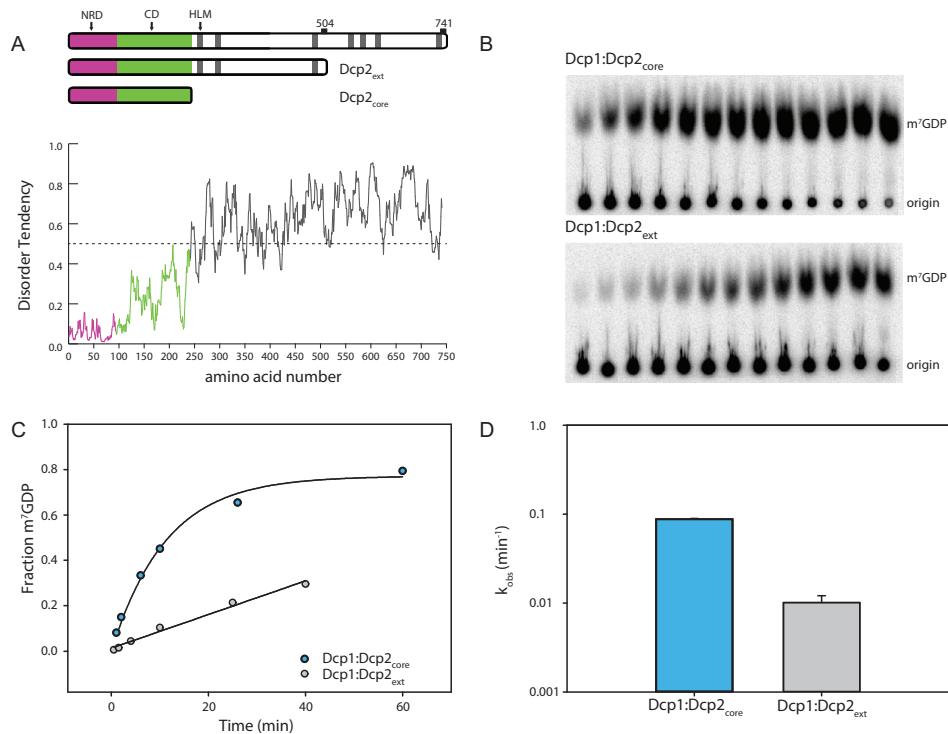


**Figure 2.1: The C-terminal extension of Dcp2 inhibits decapping.** a, Block diagram of the domains of *S. pombe* Dcp2. The magenta box (1-94) comprises the N-terminal regulatory domain (NRD) and the green (95-243) comprises the catalytic domain, which contains the Nudix helix. Grey bars are helical leucine-rich

motifs (HLMs). The disorder tendency plot below was calculated using the IUPRED server<sup>53</sup>. Where regions above the dotted line have a higher propensity for being disordered. **b**, Representative raw TLC (thin-layer chromatography) showing the formation of m<sup>7</sup>GDP product over 40 minutes. The lower spots are the RNA origin and the upper are the cleaved cap. **c**, Representative plot of fraction m<sup>7</sup>GDP product versus time comparing the catalytic core (Dcp1:Dcp2<sub>core</sub>) and inhibited C-terminally extended Dcp1:Dcp2<sub>ext</sub>. **d**, A log-scale plot of the empirically determined rates from **c**, where the error bars are the population standard deviation,  $\sigma$ . Difference in measured rates are significant as determined by unpaired t-test.

## Two motifs are required for autoinhibition of Dcp1:Dcp2

Having determined that Dcp1:Dcp2<sub>ext</sub> was less active than Dcp1:Dcp2<sub>core</sub>, we next asked which regions in the C-terminal extension confer inhibition. Since the C-terminal extension of Dcp2 is predicted to be disordered, we hypothesized that inhibition of decapping may be mediated by linear interaction motifs. Candidate inhibitory motifs were queried by analysis of sequence conservation amongst the most closely related fission yeast, as linear motifs are known to evolve rapidly due to a lack of restraints imposed by three-dimensional structure<sup>32,33</sup>. Using this approach, we identified two possible inhibitory motifs: a proline-rich sequence (PRS) that aligns to the inhibitory element identified in budding yeast<sup>29</sup> previously shown to bind fission yeast Dcp1<sup>34</sup>, and a highly conserved stretch of amino acids that strongly resembles Dcp1-binding motifs in Edc1-like coactivators (**Fig. 2.2a, Fig. S2.2**). We term these regions IM1 and IM2, respectively. Next, we queried whether deletion of these conserved regions, alone or in combination, would alleviate autoinhibition. The Dcp1:Dcp2 complexes where either putative IM1 or IM2 were deleted alone or in tandem were purified to homogeneity (**Fig. S2.1**). Deletion of a region containing IM1 (residues 267-350 in Dcp2) revealed that it partially contributes to autoinhibition in Dcp1:Dcp2<sub>ext</sub> (**Fig. 2.2b,c**); this region was previously observed to have no effect on decapping activity when added in *trans* to Dcp1:Dcp2<sub>core</sub><sup>34</sup>. Likewise, deletion of IM2 restored activity in Dcp1:Dcp2<sub>ext</sub> to a similar degree as deletion of IM1 (**Fig. 2.2b,c**). Furthermore, we found that a peptide of IM2 (residues 399-432) directly interacts with Dcp1:Dcp2<sub>core</sub> in *trans* (**Fig. S2.2c**). The combined removal of these regions fully restored the activity of Dcp1:Dcp2<sub>ext</sub> to that of Dcp1:Dcp2<sub>core</sub> (**Fig. 2.2b,c**). Additionally, internal deletions of nonconserved regions in the C-terminal extension did not show an increase in activity relative to Dcp1:Dcp2<sub>ext</sub> (**Fig. S2.2d**). We

conclude that the two linear motifs we identified in the C-terminal extension of fission yeast Dcp2, IM1 and IM2, are responsible for the autoinhibition of Dcp1:Dcp2.

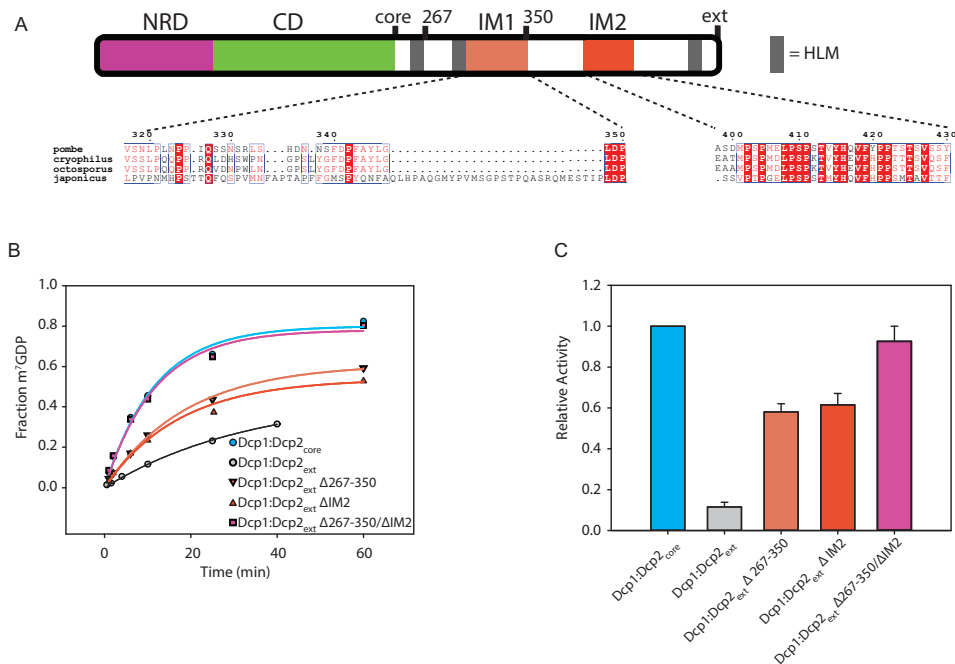


**Figure 2.2: Two motifs are required for autoinhibition of Dcp1:Dcp2<sub>ext</sub>.** **a**, Block diagram colored as in Fig. 2.1. with IM1 and IM2 regions colored and the sequence conservation<sup>54</sup> for each motif shown below. IM1 contains proline and phenylalanine residues similar to the negative regulatory element identified in budding yeast (Fig. S2.2B), while IM2 is absolutely conserved in all fission yeast. **b**, Plot with fits for fraction of m<sup>7</sup>GDP versus time comparing the activity of Dcp1:Dcp2<sub>ext</sub> where either IM1, IM2 or both are internally deleted. **c**, Bar graph of the relative enzymatic activity of the various Dcp1:Dcp2<sub>ext</sub> complexes compared to Dcp1:Dcp2<sub>core</sub>. Each IM contributes to the inhibitory effect of the c-terminal regulatory region (CRR). The error bars are the population standard deviation,  $\sigma$ . Differences in observed rates are significant except for Dcp1:Dcp2<sub>core</sub> relative to Dcp1:Dcp2(Δ267-350/ΔIM2) and Dcp1:Dcp2(Δ267-350) relative to Dcp1:Dcp2(ΔIM2) as determined by unpaired t-test.

### A conserved surface on the catalytic domain of Dcp2 is required for autoinhibition

Enzymes that are regulated by autoinhibition typically exist in an inactive conformation that is distinct from the catalytically active form, which can block substrate recognition and catalysis<sup>35</sup>. Typically, this entails linear interaction motifs interacting with core domains, which maintains the enzyme in the inactive state. We and others have suggested that the ATP-bound, closed Dcp1:Dcp2 structure (Song et al 2008, PDB 2QKM) could resemble an inactive conformation of the enzyme since the substrate binding site is occluded<sup>20,36</sup>. Recently, it was shown by NMR that this closed form of Dcp1:Dcp2 is significantly populated in solution<sup>18</sup>. We hypothesized the autoinhibited form of Dcp1:Dcp2 might correspond to this cap-occluded

conformation. This conformation is stabilized by several conserved residues that anchor the NRD to the CD of Dcp2, including W43, D47 and Y220 (**Fig. S2.3**). In this conformation, Y220 blocks access of W43 and D47 of the NRD to cap. When Dcp2 is bound to  $m^7G$  of cap in the catalytically-active conformation, Y220 is displaced and W43 and D47 of the NRD make essential interactions with  $m^7G$  (**Fig. 2.3a**)<sup>34,37</sup>. Therefore, we reasoned mutation of Y220 would destabilize the cap-occluded form of Dcp1:Dcp2, permitting it to more readily populate the cap-accessible, active conformation. Mutation of Y220 to glycine enhanced decapping activity of the Dcp1:Dcp2<sub>core</sub> by 1.5-fold (**Fig. 2.3b**) and we were able to observe cap binding in Dcp2<sub>core</sub> by NMR (**Fig. S2.4**). We next assessed the effect of the Y220G mutation in Dcp1:Dcp2<sub>ext</sub> and observed a 6-fold increase in activity relative to wild-type Dcp1:Dcp2<sub>ext</sub> (**Fig. 2.3b**). These data suggest the cap-occluded conformation of Dcp1:Dcp2, which is observed in solution and in many crystal structures, could resemble the autoinhibited form of the enzyme containing the C-terminal extension.

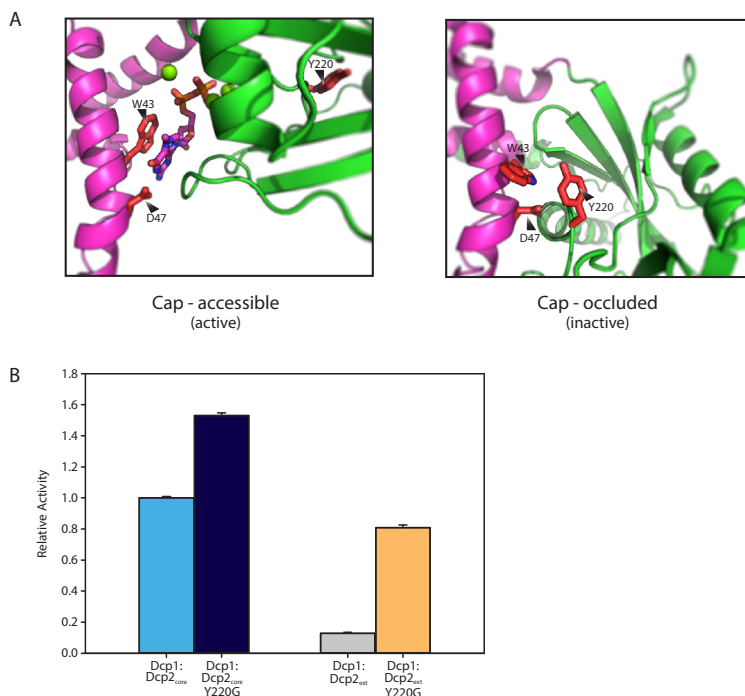


**Figure 2.3: Y220 stabilizes a cap-occluded state and alleviates inhibition.** **a**, W43 and D47 that coordinate the  $m^7G$  cap exist in conformations where they are either accessible or occluded by interaction with the conserved Y220G. **b**, Plot of the relative activity of WT or Y220G Dcp1:Dcp2<sub>ext</sub> compared to the same mutation in Dcp1:Dcp2<sub>core</sub>. Dcp1:Dcp2<sub>ext</sub> exhibits a greater increase in  $k_{obs}$  when Y220 is mutated as determined by an *in vitro* decapping assay. The error bars are the population standard deviation,  $\sigma$ . All differences in reported rates are significant as determined by unpaired t-test.



The Y220G mutation may activate decapping by destabilizing the cap-occluded conformation. To test this possibility, we used dynamic NMR spectroscopy. Previously, it had been noted that Dcp2 experiences global motions on the millisecond to microsecond timescale (ms- $\mu$ s dynamics) where the NRD and the CD sample open and closed, cap-occluded forms, with Dcp1 enhancing the population of the latter state<sup>18,19</sup>. W43 was identified as a “gatekeeper” required for these dynamics<sup>19</sup>. Since Y220 makes interactions with W43 in the cap-occluded state, we reasoned the Y220 mutation would also quench global ms- $\mu$ s dynamics, resulting in the reappearance of broadened cross-peaks. Upon mutation of Y220 to glycine in Dcp2<sub>core</sub>, the expected cross-peaks from both the NRD and CD reappeared (**Fig. S2.4**), indicating dynamics were quenched similarly to the previously reported W43 mutation (**Fig. 2.4a**)<sup>19</sup>. To corroborate that mutation of Y220 quenched the collective dynamics, we used CPMG spectroscopy on <sup>13</sup>C-methyl ILVMA side-chain labeled Dcp2. Consistent with previous experiments, significant dephasing of transverse magnetization from collective ms- $\mu$ s motions in wild-type Dcp2 could be attenuated with increasing CPMG pulse rate (**Fig. 2.4b**, black filled circles)<sup>18,19</sup>. In contrast to the wild-type, these dynamics are not present for the Y220G mutant (**Fig. 2.4b**, blue circles). We conclude that the Y220G mutation shifts the equilibrium from cap-occluded to the open conformation.

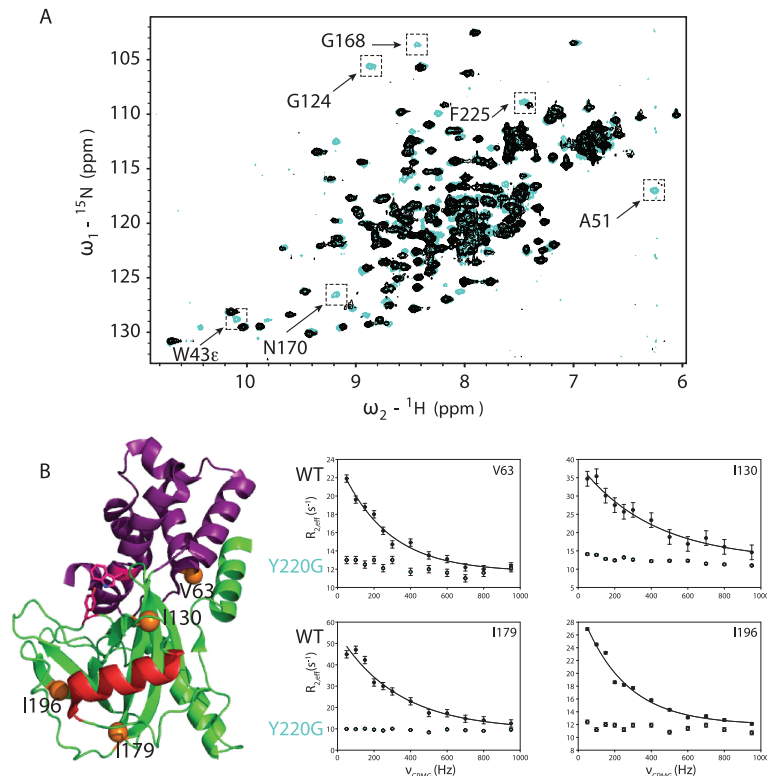


**Figure 2.4: Y220G mutation quenches ms- $\mu$ sec dynamics in Dcp2<sub>core</sub>.** **a**, Shown are the  $^{15}\text{N}$  HSQC spectra of WT Dcp2 residues 1-243 (black) and Dcp2 Y220G (cyan). Selected residues with significant changes upon mutation are indicated. **b**, Location of the four representative residues whose sidechain dynamics are presented are shown as orange spheres on the ATP-bound structure of DCP2 (2QKM), where the NRD is magenta, CD is green, catalytic Nudix helix is red and W43 and Y220 are displayed as sticks. Selected CPMG dispersion data at 800 MHz for WT (black circles) or Y220G (cyan circles). WT data fit well to a two-site exchange model (Black lines), whereas Y220G data did not, indicating ms- $\mu$ s dynamics are strongly reduced.

### Edc3 alleviates autoinhibition of Dcp1:Dcp2<sub>ext</sub> by stimulating the catalytic step

Since the inhibitory motifs of Dcp2 are proximal to known Edc3 binding sites (the HLMs) we tested if Edc3 could alleviate autoinhibition. When Dcp1:Dcp2<sub>ext</sub> was incubated with saturating concentrations of Edc3, a stable complex was observed and decapping activity was completely restored to rates observed for Dcp1:Dcp2<sub>core</sub> (**Fig. 2.5a,b; Fig. S2.5; Table S2.3**). Having identified a mutation in the catalytic domain of Dcp2<sub>core</sub> that destabilizes autoinhibition, we next examined whether this mutation bypasses activation by Edc3. Introduction of the Y220G mutation into Dcp1:Dcp2<sub>ext</sub> markedly attenuates stimulation by Edc3 and closely resembles the extent of activation observed for Dcp1:Dcp2<sub>HLM-1</sub>, which is a construct of Dcp1:Dcp2<sub>core</sub> containing a single Edc3 binding site (**Fig. 2.5c**). The differential activation observed for Dcp1:Dcp2:Edc3 complexes

with and without the C-terminal extension containing autoinhibitory motifs indicates Edc3 utilizes multiple mechanisms to enhance decapping.

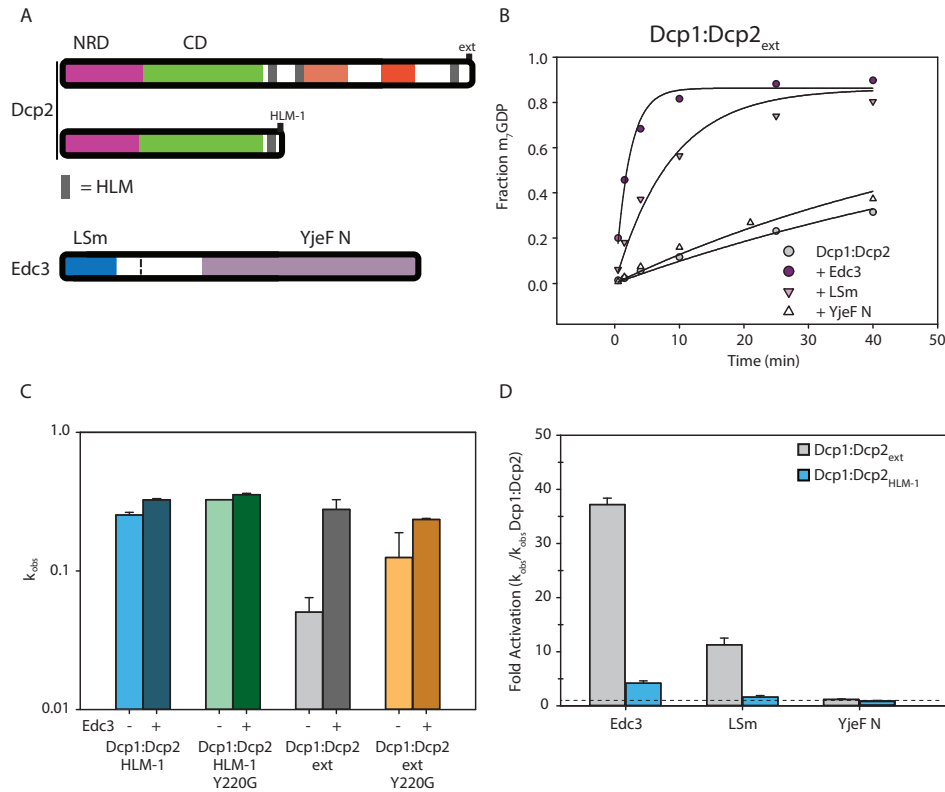


**Figure 2.5: Edc3 alleviates autoinhibition of Dcp1:Dcp2<sub>ext</sub>.** **a**, Block diagram of the Dcp2 and Edc3 used in the subsequent decapping assays. Edc3 consists of an LSM domain that interacts with HLMs and a YjeF N domain that provides an RNA binding surface when dimerized. **b**, Decapping activity of Dcp1:Dcp2<sub>ext</sub> incubated with excess Edc3, LSM domain or YjeF N domain. **c**, Logscale plot of decapping rate of Dcp1:Dcp2<sub>HLM-1</sub> [blue], Dcp1:Dcp2<sub>HLM-1</sub> Y220G [green], Dcp1:Dcp2<sub>ext</sub> [gray], or Dcp1:Dcp2<sub>ext</sub> Y220G [yellow] where the darker bar is the rate with excess Edc3. The error bars are the population standard deviation,  $\sigma$ . Differences in observed rates are significant except for Dcp1:Dcp2<sub>HLM-1</sub> Y220G relative to Dcp1:Dcp2<sub>HLM-1</sub> Y220G:Edc3 and Dcp1:Dcp2<sub>ext</sub> Y220G relative to Dcp1:Dcp2<sub>ext</sub> Y220G:Edc3 as determined by unpaired t-test. **d**, Comparison of the relative fold activation of Dcp1:Dcp2<sub>ext</sub> versus Dcp1:Dcp2<sub>HLM-1</sub> with the various Edc3 constructs.

Edc3 is known to interact with HLMs in the C-terminus of Dcp2 through its N-terminal LSM domain and has been shown to bind RNA through its C-terminal YjeF N domain<sup>20,38</sup>. To dissect the contributions from these domains in enhancing decapping, we compared their activation of Dcp1:Dcp2<sub>HLM-1</sub> and Dcp1:Dcp2<sub>ext</sub> (**Fig. 2.5d**, **Fig. S2.5b**). The Edc3 LSM domain was sufficient to increase the activity of Dcp1:Dcp2<sub>ext</sub> to levels comparable with Dcp1:Dcp2<sub>core</sub>; whereas addition of the Edc3 YjeF N domain in isolation had no effect on decapping activity (**Fig. 2.5d**). These

results indicate binding of the Edc3 LSM domain to the HLMs in Dcp2 is sufficient to alleviate autoinhibition of the C-terminal regulatory region of Dcp2, but full-activation requires the Yjef N domain. In contrast to Dcp1:Dcp2<sub>ext</sub>, the LSM domain of Edc3 does not provide any substantial increase in activity of Dcp1:Dcp2<sub>HLM-1</sub>; whereas a 5-fold increase in decapping is observed upon addition of full-length Edc3. These observations suggest Edc3 activates decapping both by alleviating autoinhibition to enhance the catalytic step and by promoting RNA binding.

To test these possibilities, we measured rates of decapping by Dcp1:Dcp2 in the presence and absence of saturating Edc3 under single-turnover conditions. This approach allows us to determine the contributions of Edc3 activation to RNA binding ( $K_m$ ) and the catalytic step of decapping ( $k_{max}$ ). Compared to Dcp1:Dcp2<sub>HLM-1</sub>, Dcp1:Dcp2<sub>ext</sub> had a significant 6-fold reduction in  $k_{max}$ , indicating autoinhibition occurs in the catalytic step (**Fig. 2.6a-d**, compare lower curves in **a,b**; light blue and light gray bars in **c,d**). When kinetics for Dcp1:Dcp2<sub>ext</sub> were performed in the presence of Edc3, there was a substantial 6-fold increase in  $k_{max}$  and concomitant 5-fold decrease in  $K_m$  relative to Dcp1:Dcp2<sub>ext</sub> alone (**Fig. 2.6b,d**). Thus, the observed 30-fold stimulation of Dcp1:Dcp2<sub>ext</sub> by Edc3 (**Fig. 2.5c,d**) can be broken down as 6-fold from alleviation of autoinhibition by the its LSM domain binding HLMs in the extended C-terminus of Dcp2, and 5-fold deriving from RNA binding by Edc3. The effects of Edc3 on Dcp1:Dcp2<sub>ext</sub> activity are in contrast to Dcp1:Dcp2<sub>HLM-1</sub>, which in the presence of Edc3 had a similar 5-fold decrease in  $K_m$  but not a significant change in  $k_{max}$  (**Fig. 2.6a,c**). The observed 5-fold decrease in  $K_m$  for both Dcp1:Dcp2<sub>HLM-1</sub> and Dcp1:Dcp2<sub>ext</sub> is in good agreement with the reported ability of Edc3 to bind RNA and suggests Edc3 predominantly provides additional RNA binding capacity in the absence of autoinhibition<sup>37,39</sup>. Therefore, the mechanism of activation by Edc3 is a combination of binding to HLMs in order to alleviate autoinhibition and enhance the catalytic step while providing an additional RNA binding surface to increase Dcp2 substrate affinity.

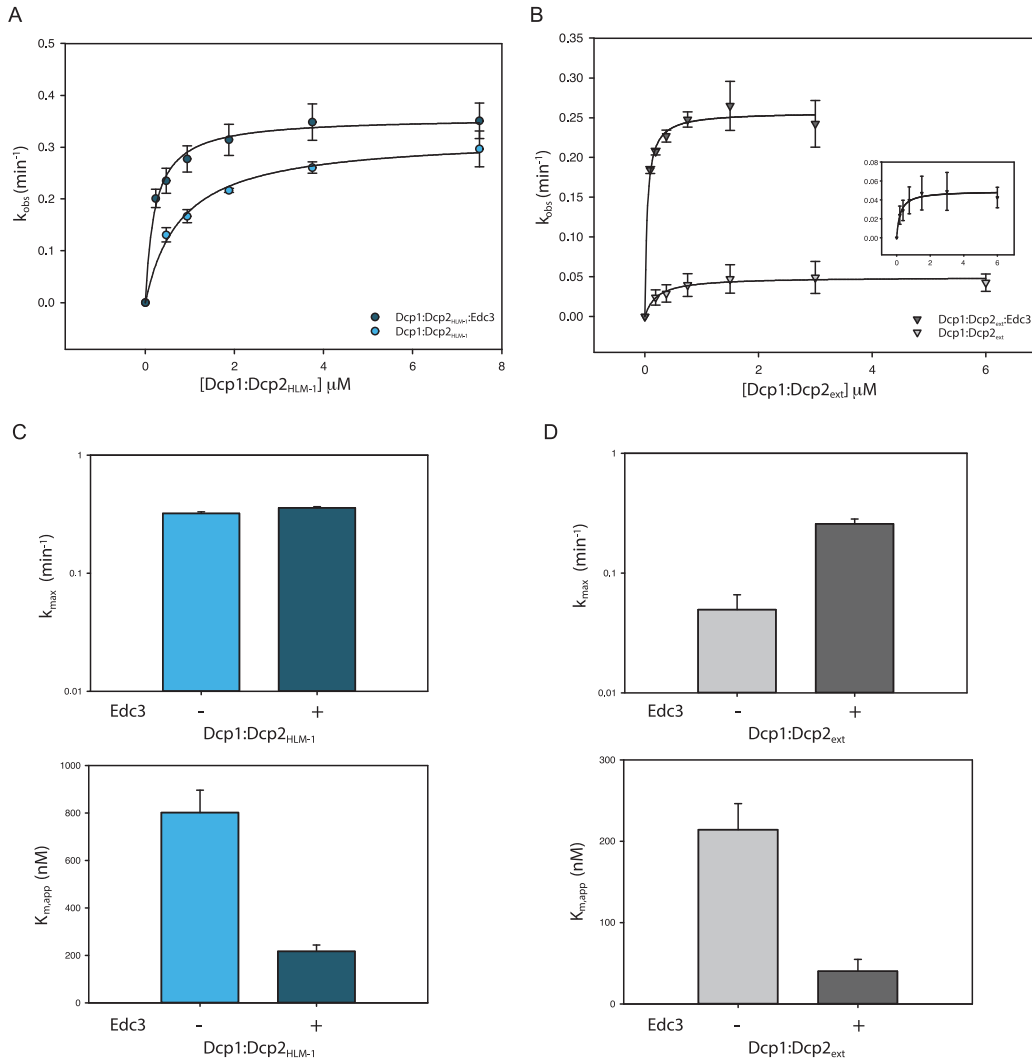


**Figure 2.6: Edc3 alleviates autoinhibition and promotes RNA binding.** **a**, Plot of  $k_{obs}$  versus Dcp1:Dcp2<sub>HLM-1</sub> concentration in the absence (light blue) or presence (dark blue) of saturating concentrations of Edc3. Error bars represent population standard deviation,  $\sigma$ . **b**, Plot of  $k_{obs}$  versus Dcp1:Dcp2<sub>ext</sub> concentration in the absence (light gray) or presence (dark gray) of saturating concentrations of Edc3. Error bars represent population standard deviation,  $\sigma$ . **c**, Comparison of fitted  $k_{max}$  (top) and  $K_{m,app}$  (bottom) values from panel **a** for Dcp1:Dcp2<sub>HLM-1</sub> with or without saturating Edc3 (colored as in panel **a**). There is not a significant change in  $k_{max}$  upon addition of Edc3 (as determined by unpaired t-test) but  $K_{m,app}$  is 5-fold decreased. **d**, Comparison of fitted  $k_{max}$  (top) and  $K_{m,app}$  (bottom) values from panel **b** for Dcp1:Dcp2<sub>ext</sub> with or without saturating Edc3 (colored as in panel **b**). There is a 6-fold increase in  $k_{max}$  upon incubation with Edc3 and  $K_{m,app}$  decreases by 5-fold. Error bars are population standard deviation,  $\sigma$ .

### Edc3 and Edc1 work together to activate decapping by Dcp1:Dcp2<sub>ext</sub>

Edc1 stimulates the catalytic step of decapping by stabilizing the composite cap binding site of Dcp2 formed by the N-terminal regulatory and catalytic domains<sup>18</sup>. Here we have shown Edc3 alleviates autoinhibition by binding sites distal from the Dcp1:Edc1 interaction site, which suggests these activators could work together to promote decapping. To test this possibility, we

titrated a peptide of *sp*Edc1 (residues 155-180) that contains the minimal Dcp1 binding and Dcp2 activation motifs (Edc1-DAM, see ref<sup>40</sup>) against Dcp1:Dcp2<sub>ext</sub> or Dcp1:Dcp2<sub>core</sub> and determined if Edc3 changed the threshold of activation, defined as a concentration of Edc1-DAM required for one-half maximal activity ( $K_{1/2}$ ) (**Fig. 2.7a**). For experiments with Dcp1:Dcp2<sub>ext</sub>, the  $K_{1/2}$  was shifted 3.5-fold higher compared to the Dcp1:Dcp2<sub>core</sub> (**Fig. 2.7b**). In addition, even at saturating concentrations, Edc1 was unable to fully overcome the inhibitory effect of the Dcp2 C-terminal extension in the absence of Edc3. In contrast, addition of Edc3 returned the  $K_{1/2}$  for Edc1-DAM activation of Dcp1:Dcp2<sub>ext</sub> to within error of Dcp1:Dcp2<sub>core</sub> and rescued the maximal observed rate. A maximum rate of 6.2  $\text{min}^{-1}$  was observed when Edc1 and Edc3 were present at saturating concentrations, which is greater than the maximum rate observed for the Dcp1:Dcp2<sub>core</sub> saturated with Edc1. These observations suggest Edc1-DAM alone is not sufficient to fully activate decapping of Dcp1:Dcp2<sub>ext</sub> and instead requires Edc3 to fully stimulate the rate of the autoinhibited complex greater than 500-fold (**Fig. S2.6**).

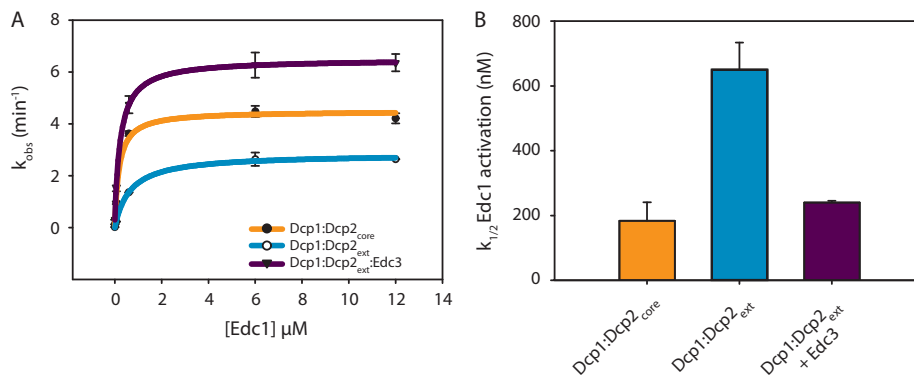


**Figure 2.7: Edc1 and Edc3 coordinate to activate the Dcp1:Dcp2<sub>ext</sub> complex.** **a**, Plot of  $k_{\text{obs}}$  versus Edc1 concentration for the catalytic core (orange), autoinhibited complex (cyan), or the autoinhibited complex (Dcp1:Dcp2<sub>ext</sub>) saturated with Edc3 (purple). Error bars are population standard deviation,  $\sigma$ . **b**, Bar graphs showing the  $k_{1/2}$  Edc1 activation (apparent  $k_d$ ) determined from the fits in panel **a** for Edc1 dependent activation with same colors as in **A**. Error bars are standard error.

## DISCUSSION

The structures of a majority of the globular domains of the mRNA decay proteins are available and have provided key insights into how these factors interact with one another to mediate decay<sup>27</sup>. While progress has been made on this front, much less is known regarding the

regulatory functions of intrinsically disordered regions (IDRs) that are replete in these proteins. Here, we have determined that the disordered C-terminal extension of fungal Dcp2 contains two motifs (IM1 and IM2) that inhibit decapping activity. The inhibitory effect of the disordered extension likely relies on an underlying cap-occluded conformation, which is stabilized by a conserved aromatic side-chain in the CD of Dcp2. Edc3 alleviates autoinhibition by binding the HLMs that are proximal to the inhibitory motifs and provides increased RNA binding affinity through its RNA binding domain. Stimulation of Dcp1:Dcp2<sub>ext</sub> by Edc1 requires Edc3 to achieve maximal activation (~500-fold), and we provide evidence that such control of decapping is achieved by factors acting on distinct conformational substates.

Decapping by Dcp1:Dcp2 requires formation of a composite active site shaped by residues lining the NRD and the CD of Dcp2. The core complex is dynamic in solution, sampling an open form where residues that line the composite active site are far apart, or a closed form where residues on the NRD that engage cap to promote catalysis are occluded<sup>18</sup>. Several observations suggest the closed, cap-occluded form of Dcp1:Dcp2 is representative of the autoinhibited form containing the C-terminal extension (**Fig. 2.8a**). First, this conformation has been observed in a variety of crystal structures and in solution<sup>18,37,38,40,41</sup>. Second, it is incompatible with cap recognition, since essential residues of the NRD that contact the m<sup>7</sup>G moiety (W43 and D47) are blocked by a conserved amino acid on the CD (Y220) (**Fig. S2.3**). Third, mutation of a conserved Tyr predicted to stabilize this nonproductive state increases the catalytic activity, destabilizes the “occluded” state in solution and disrupts the inhibitory effect of the Dcp2 extension (**Figs. 2.3,2.4**). Fourth, the C-terminal extension reduces that catalytic step of decapping, consistent with the composite active site of Dcp2 being occluded.

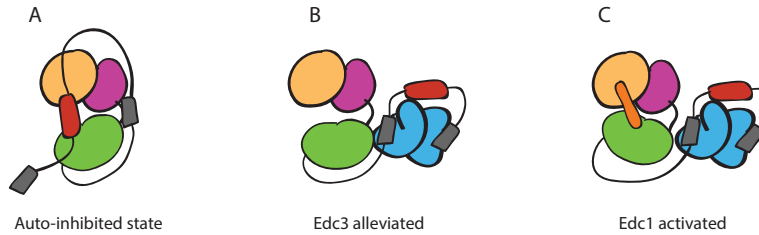


**Figure 2.8: Model for autoinhibition, Edc3 alleviation and Edc3/Edc1 combined activation.** **a**, Autoinhibited conformation of the decapping holoenzyme. Dcp1 is yellow-gold, and the NRD and CD of Dcp2 are magenta and green, respectively. IM1&IM2, shown in red, stabilize this inactive conformation by making contacts with the core domains. The grey boxes are HLMs. **b**, Edc3, shown in cyan, alleviated inhibition by binding to the HLMs, which disrupts the IM1&IM2 interaction with the Dcp1:Dcp2<sub>core</sub>. **c**, Representation of the activated Dcp1:Dcp2 structure where Edc1, orange, stabilizes a composite active site formed by the NRD and CD. Edc3 frees up the Dcp1:Edc1 binding site from IM1 & IM2.

In budding yeast, there is clear evidence of autoinhibition, as excision of a short linear motif in the C-terminus bypasses the requirement for Edc3 for degradation of target transcripts (29). Notably, introduction of the equivalent Y220 mutation in budding yeast resulted in a temperature sensitive phenotype, suggesting the cap-occluded conformation may be important for maintaining proper mRNA degradation *in vivo*<sup>42</sup>. The autoinhibitory linear motif identified in budding yeast Dcp2 has similarity to IM1 of fission yeast, whereas IM2 appears to be unique to fission yeast (**Fig. S2.2a,b**). Future studies will be required to identify Edc3 dependent mRNAs in fission yeast and how they are dependent on autoinhibition as described here.

Dcp1:Dcp2<sub>core</sub> makes fast excursions between the open and cap-occluded states<sup>19,34</sup>, so it is likely the inhibitory motifs in the C-terminal extension stabilize the closed, cap-occluded form by direct interactions with the structured core domains. In support of this hypothesis, the inhibitory motifs found in the C-terminal extension of Dcp2 bind the structured domains of Dcp1:Dcp2<sub>core</sub> in *trans* (**Fig. S2.2c** and <sup>34</sup>). We cannot exclude the possibility that the inhibitory motifs may stabilize another conformation of the enzyme that is catalytically impaired, such as the open form; or inhibitory motifs could sterically block interactions with substrate. These modes of autoinhibition are reminiscent of the eukaryotic tyrosine kinase superfamily, where motifs flanking the functional domains stabilize an inactive conformation of the enzyme, with structural variation amongst family



members<sup>43</sup>. Detailed structural studies will be required to define the precise mode of autoinhibition.

How does Edc3 alleviate autoinhibition and allow full activation by Edc1? The Lsm domain of Edc3 is sufficient to alleviate autoinhibition in Dcp1:Dcp2<sub>ext</sub> and it binds the HLMs found in the Dcp2 C-terminal extension (**Fig. 2.8b**). Prior NMR studies indicate Edc1 and IM1 of the Dcp2 C-terminal extension bind the same surface on Dcp1<sup>34</sup>; moreover, we show here that IM2 binds Dcp1:Dcp2<sub>core</sub> in *trans* and that Edc3 can lower the threshold for activation by Edc1. A working model for activation of decapping by Edc3 is that binding to HLMs found in the Dcp2 C-terminal extension is coupled to remodeling of the IM1 and IM2 interaction with the structured, core domains, allowing the enzyme to undergo a conformational change from an inactive to an active, cap-accessible conformation that is stabilized by Edc1 (**Fig. 2.8c**). In this way, the coactivators Edc3 and Edc1 coordinate to destabilize the inactive, autoinhibited form and consolidate the catalytically active conformation, respectively.

Our biochemical and biophysical data are consistent with genetic studies in budding yeast that indicate decapping coactivators work together to promote 5' mediated decay. First, synthetic growth defects are observed when Edc1 and Edc3 are deleted in yeast strains where Dcp2 is essential<sup>21</sup>. Second, deletion of an inhibitory motif in budding yeast Dcp2 bypasses the requirement of Edc3 for decapping on specific RNAs<sup>29</sup>. Third, additional proteins such as Scd6 and Pat1 have synthetic genetic interactions with Edc3 and form physical interactions with the HLMs found in the C-terminal extension of Dcp2<sup>28</sup>. Clearly the combinatorial control of Dcp1:Dcp2 activity we observe *in vitro* by Edc1 and Edc3 is well supported by functional studies in cells and the general principles observed here may be applicable to other activators such as Scd6 and Pat1.

In general, any protein that contains an HLM interaction domain such as the LSm domain of Edc3 would promote alleviation of autoinhibition from the Dcp2 C-terminal extension. The fusion of an HLM interaction domain to an RNA binding domain could further increase the

activation of the decapping enzyme through increased RNA binding capacity. For example, the C-terminal extension of Dcp2 could provide rationale for Pat1's strong effect on decapping *in vivo*<sup>44,45</sup>, since Pat1 can bind HLMS and is linked to the Lsm1-7 complex<sup>46-49</sup> that binds oligoadenylated RNA intermediates during bulk 5'-3' decay. Further studies will be required to investigate how pathway specific activators such as Pat1 activate decapping through interactions with the C-terminal extension of Dcp2.

We suggest the observations reported in this work on fungal proteins could be conserved in metazoans. The HLM of the fungal Dcp2 has been transferred to a long C-terminal extension of Dcp1<sup>27</sup>. A structure of the Edc3 LSM domain and the HLM in Dcp1 from *D. melanogaster* is consistent with this interaction being evolutionarily important<sup>20</sup>. Transfer of regulatory short linear interaction motifs to different subunits of a conserved complex is a common theme in eukaryotic biology<sup>27,32</sup>. An important area for future research is to determine if the inhibitory motifs of Dcp2 have also been transferred to different subunits of the decapping complex by evolutionary rewiring.

In this work, we have characterized an additional mechanism responsible for regulating mRNA decay by showing that elements in the C-terminus of Dcp2 inhibit decapping at the catalytic step. Addition of Edc3 alleviates autoinhibition to promote catalysis and is required for full stimulation of Dcp1/Dcp2 by Edc1. This combinatorial activation suggests decapping by Dcp2 can be controlled across multiple log units of activity to coordinate decay. Such exquisite regulation of decapping reflects the importance of 5'-3' mRNA decay in maintaining cellular homeostasis.

## **METHODS**

### **Protein expression and purification**

A pRSF containing polycistronic His-Gb1-tev-Dcp1:Dcp2(1-504)-strepII was used to coexpress the C-terminally extended Dcp1:Dcp2 complexes. Both the Dcp1 and Dcp2 sequences were codon-optimized for *Escherichia coli* from Integrated DNA Technologies and were cloned

into a pRSF vector using Gibson assembly. The Dcp2 sequence contained a ribosome binding site (rbs) upstream and the Dcp1 was cloned behind the endogenous T7 promoter and rbs within the vector. The His-Gb1-tev-Dcp1:Dcp2(1-504)-strepII were expressed in *E. coli* BL21(DE3) (New England Biolabs) grown in LB medium. Cells were grown at 37 °C until they reached an OD<sub>600</sub> = 0.6-0.8, when they were transferred to 4 °C for 30 minutes before induction by addition of 0.5mM IPTG (final concentration). Cells were induced for 16-18 hours at 18 °C. Cells were harvested at 5,000g, lysed by sonication (50% duty cycle, 3x1min), and clarified at 16,000g in lysis buffer (buffer composition goes here). The protein complex was purified in a two-step affinity purification: Ni-NTA agarose affinity column followed by strep-tactin high-capacity superflow and elution with 5mM d-desthiobiotin. The His-Gb1 tag was removed by addition of TEV protease overnight at 4 °C. The complex was further purified by size-exclusion chromatography on a GE Superdex 200 16/60 column in storage buffer (50mM HEPES, 100mM NaCl, 5% glycerol, 5mM DTT pH 7.5). The purified complex was concentrated, 20% v/v (final) glycerol was added, and then flash frozen in LN2 for kinetics studies. Dcp1:Dcp2(1-504) internal deletion constructs (IM1, IM2 and IM1&IM2) were generated by whole-plasmid PCR with 5'Phosphorylated primers. Dcp1:Dcp2 (1-504) Y220G was generated using whole-plasmid PCR with mutagenic divergent primers. A His-TRX-tev-Edc3 containing plasmid was generated by Gibson cloning *S. pombe* Edc3 cDNA into a pET30b plasmid which already contained a His-TRX-tev coding sequence. The LSM and YjeF N domain containing plasmids were created by whole-plasmid PCR with 5'-phosphorylated primers. The Edc3 constructs were purified as described<sup>30</sup> with a modification to elute constructs from size-exclusion chromatography in the storage buffer described above.

### **Kinetic assays**

Single-turnover *in vitro* decapping assays were carried out as previously described<sup>49</sup>. Slight alteration to the buffer (brought up volume in storage buffer with additional 20% v/v glycerol). A <sup>32</sup>P-labeled 355-nucleotide RNA substrate (containing a 15-nucleotide poly(A) tail)

derived from *S. cerevisiae* MFA2 mRNA was used for all the decapping assays; where the m<sup>7</sup>G cap is radiolabeled on the  $\alpha$  phosphate such that, upon decapping, the excised m<sup>7</sup>GDP product could be detected by TLC and autoradiography. Reactions were initiated by mixture of 30  $\mu$ L 3 $\times$  protein solution with 60  $\mu$ L 1.5 $\times$  RNA solution at 4  $^{\circ}$ C; final Dcp1:Dcp2 concentration was 1.5 $\mu$ M and the final RNA concentration was <100 pM. For decapping assays containing Edc3; Edc3 was added in 4-fold molar excess and the mixture was incubated at RT for 20 minutes before transferring to the 4  $^{\circ}$ C block. For decapping assays containing Edc1, the peptide (synthesized by Peptide2.0) was added at the indicated concentration and the mixture was incubated at RT for 20 minutes before transferring to the 4  $^{\circ}$ C block. Samples were equilibrated for at least 30 minutes on the 4  $^{\circ}$ C block before initiating. Time points were quenched by addition of excess EDTA, TLC was used to separate the RNA from the product m<sup>7</sup>GDP, and the fraction decapped was quantified with a GE Typhoon scanner and ImageQuant software. Fraction m<sup>7</sup>GDP versus time were plotted and fit to a 1<sup>st</sup>-order exponential to obtain  $k_{obs}$ ; in the case of Dcp1:Dcp2(1-504) when the kinetics were too slow to obtain reliable exponential fits,  $k_{obs}$  was obtained from a linear fit of the initial rates by division of the slope by the empirically derived endpoint.

### **NMR Spectroscopy**

ILVMA methyl labeling of Dcp2 was carried out in D<sub>2</sub>O M9 minimal media with <sup>15</sup>NH<sub>4</sub>Cl and <sup>12</sup>C/<sup>2</sup>H-glucose as the sole nitrogen and carbon sources, respectively, and labeled precursors (Ile: 50 mg L<sup>-1</sup>, Leu/Val: 100 mg L<sup>-1</sup>, Met: 250 mg L<sup>-1</sup>, Ala: 100 mg L<sup>-1</sup>) were added 40 minutes prior to induction. Following overnight induction with 1 mM IPTG, cells were lysed by sonication and clarified at 16,000g. Dcp2 was purified by incubating clarified lysate with nickel resin followed by elution with 250 mM imidazole. The His-GB1-TEV tag was then removed by digestion with TEV protease and untagged Dcp2 was run over a Superdex 75 size exclusion chromatography column equilibrated with pH 7.0 NMR buffer (21.1 mM NaH<sub>2</sub>PO<sub>4</sub>, 28.8 mM Na<sub>2</sub>PO<sub>4</sub>, 200 mM NaCl,

100 mM Na<sub>2</sub>SO<sub>4</sub>, 5 mM DTT). All <sup>1</sup>H-<sup>15</sup>N HSQC and CPMG experiments were performed with 250 μM protein at 303K on a Bruker Avance 800 spectrometer equipped with a cryogenic probe.

For CPMG analysis, dispersion curves were acquired with a 40-ms constant-time delay wherein the pulse frequency was varied between 50 and 950 Hz. FuDA (gift from D.F. Hansen, University College London, London, UK, <http://www.biochem.ucl.ac.uk/hansen/fuda/>) was used to extract intensities, which were converted to relaxation rates using procedures outlined in<sup>50</sup>. Errors in R<sub>2,eff</sub> are reported as the pooled standard deviation determined using procedures outlined in<sup>51</sup>. Dispersion curves were fit to a two-site exchange model using the program `cpmg_fitd8` (gift from D. Korzhnev and L. Kay, University of Toronto, Toronto, ON).

### **Dynamic light scattering**

Samples of Dcp1:Dcp2<sub>core</sub> and Dcp1:Dcp2<sub>ext</sub> were prepared in a mock decapping reaction buffer lacking RNA substrate. 3X protein solutions were mixed 1:2 with a mock substrate solution that did not contain any RNA. The final protein concentration in the solution was 1.5 μM and the final buffer composition of the reactions was as follows: 50mM TrisCl (pH 7.5 @ 25 °C), 12.5mM Hepes, 50mM NH<sub>4</sub>Cl, 25mM NaCl, 5mM MgCl<sub>2</sub>, 1mM DTT, 0.01% NP-40, 5% glycerol, 6U RNAsin, 0.1 mg/mL Acetylated-BSA. A control solution without protein was made the same way by leaving the protein out of the 3X solution. 30 μL of each sample was added to a corning black, clear bottom 384 well plate, which was spun down at ~150 xg to remove any air bubbles. Measurements were made using a DynaPro Plate Reader II system (Wyatt Technology) with a 60 mW laser at ~830nm; this instrument has been modified by Wyatt Technology to have a larger beam width. Data were acquired and processed using the software Dynamics, version 1.7 (Wyatt Technology). The laser power was auto adjusted by the software and the detector angle was 158°. Each radius value reported represents two independent measurements at 25 °C.

### Fluorescence polarization (FP) assay

N-terminally labelled 5FAM-IM2 peptide was synthesized by Peptide 2.0. The buffer used for analysis was the standard decapping reaction buffer as described<sup>49</sup>. 45µL of 2X labeled peptide (6.8 nM) in 2X reaction buffer was mixed with an equal amount of protein in storage buffer (50mM Hepes (pH 7.5), 100mM NaCl, 5mM DTT, 20% glycerol). This was 2-fold serial diluted into a 1X labeled peptide (3.4 nM) in 1X reaction buffer. 40µL of each dilution was loaded into a Greiner black 384 well nonbinding plate and left to equilibrate for one hour at 25 °C. FP measurements were made using an Analyst plate reader (LJL Biosystems). All assays were performed in at least duplicate and the average values were plotted using Sigma Plot. Curve fitting for estimation of  $K_D$  was performed using equations derived as previously described<sup>52</sup>.

### NMR $m^7$ GDP titration

<sup>15</sup>N-labeled *S. pombe* Dcp2 for titration experiments was expressed with a N-terminal His-GB1-TEV tag in *E. coli* grown in M9 minimal media containing <sup>15</sup>N-ammonium chloride (<sup>15</sup>NH<sub>4</sub>Cl) as the sole nitrogen source and purified as described in the main text. For NMR titrations with  $m^7$ GDP, Dcp2 was exchanged into nucleotide binding buffer (50 mM Hepes pH 7.0, 150 mM NaCl, 2 mM MgCl<sub>2</sub>, 5 mM DTT) using a BioRad desalting column. Titrations were carried out at 100 µM protein with equimolar addition of  $m^7$ GDP and MgCl<sub>2</sub>. Chemical shift perturbations were determined using the standard Euclidian equation:

$$\sqrt{(\delta H_{bound} - \delta H_{free})^2 + (0.2(\delta N_{bound} - \delta N_{free}))^2}$$

where the factor of 0.2 is used as a scaling factor for the nitrogen spectral width. Titration data were fitted to the standard hyperbolic binding equation if the observed perturbation between apo and 20 mM  $m^7$ GDP for any residue was greater than the mean plus one standard deviation. Experimental  $K_D$  values are reported as  $\pm$  standard error.

## SUPPLEMENTAL FIGURES

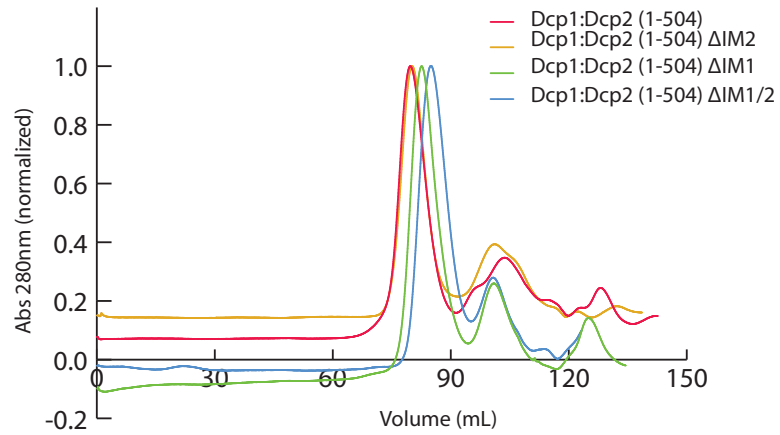


**Figure S2.1: Dcp1:Dcp2 containing C-terminal extension is monodisperse. a,** Size exclusion chromatography of various Dcp1:Dcp2<sub>ext</sub> complexes with and without excisions of the noted inhibitory motifs on a GE Superdex 200 16/60 column.

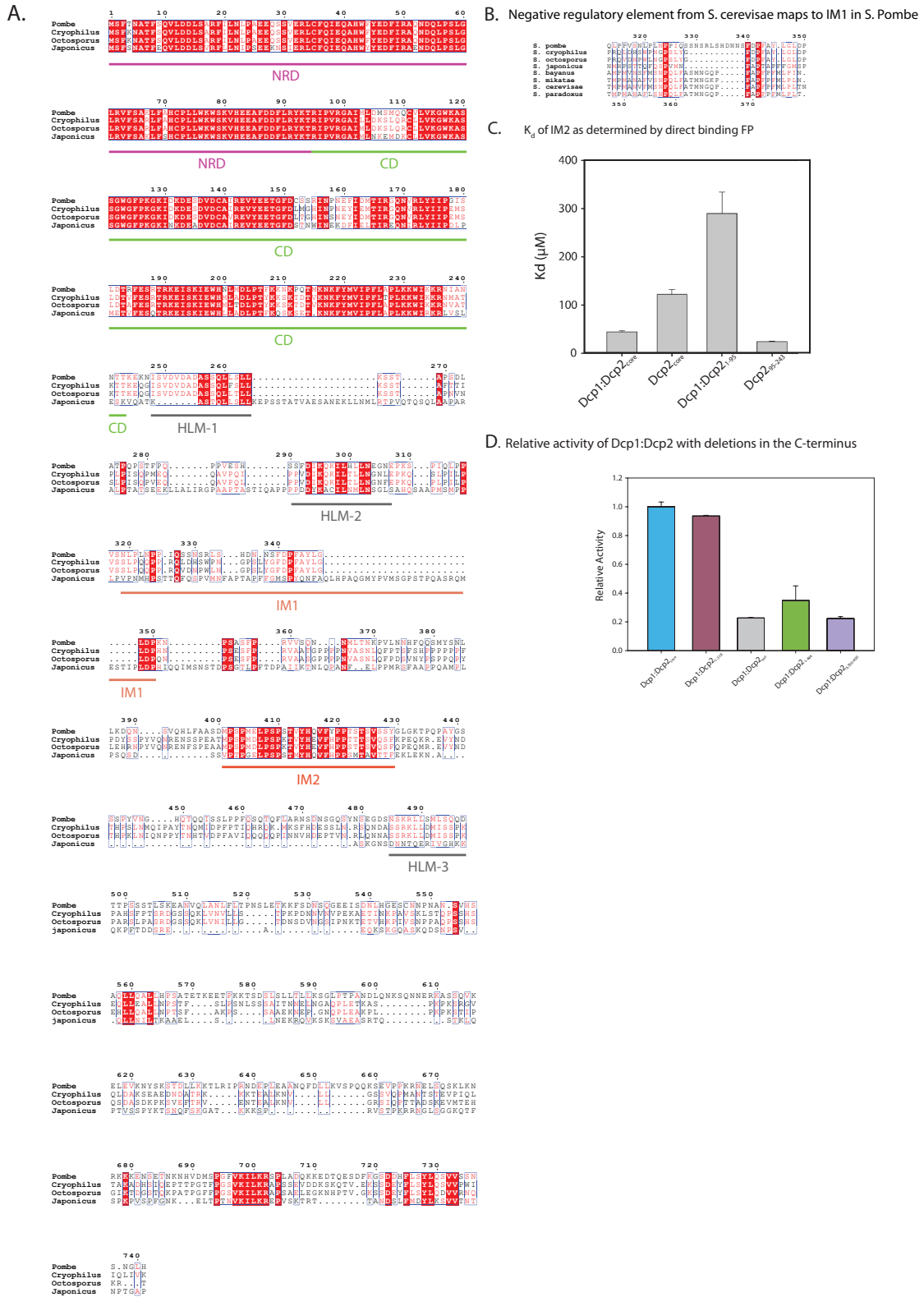


**Figure S2.2: Identification and characterization of inhibitory motifs in Dcp2 C-terminal extension.**  
**a,** Sequence alignment of fission yeast Dcp2 proteins showing the boundaries of the NRD and CD, and the locations of the HLMs and IM1/IM2 in the Dcp1:Dcp2<sub>ext</sub>. **b,** Sequence alignment of IM1 from



Schizosaccharomyces (top four sequences) identified in this study aligned to the negative regulatory sequence in the C-terminus of Saccharomyces (bottom four sequences) identified by He and Jacobson. Numbering above alignment corresponds to position in *S. pombe* sequence and numbering below corresponds to *S. cerevisiae* sequence. **c**, Apparent  $K_d$  ( $\mu$ M) for the IM2 peptide (Dcp2399-434) in *trans* for the protein components listed as determined by direct binding fluorescence polarization. Errors are population standard deviation,  $\sigma$ . **d**, Relative activity of Dcp1:Dcp2 constructs with regions of the Dcp2 C-terminus removed as determined by an *in vitro* decapping assay. Errors are population standard deviation,  $\sigma$ .

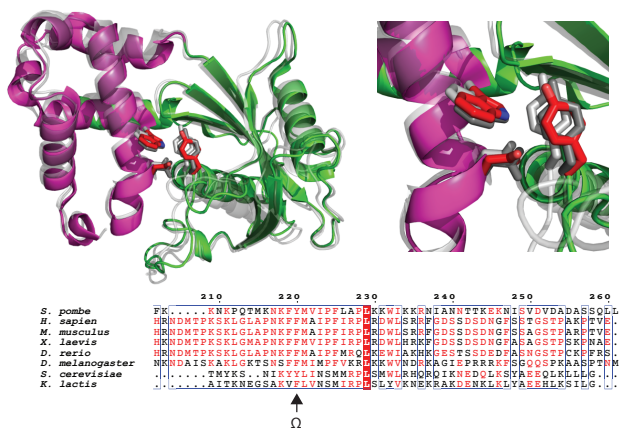


**Figure S2.3: Amino-acid conservation in cap-occluded conformation.** Alignment of ATP bound form of Dcp2 (2QKM) colored as in Figure 4a with 5QK1 and 5J3Y showing the common cap-occluded conformation, where W43, D47 and Y220 make contacts. Alignments below show that Y220 is a conserved aromatic.

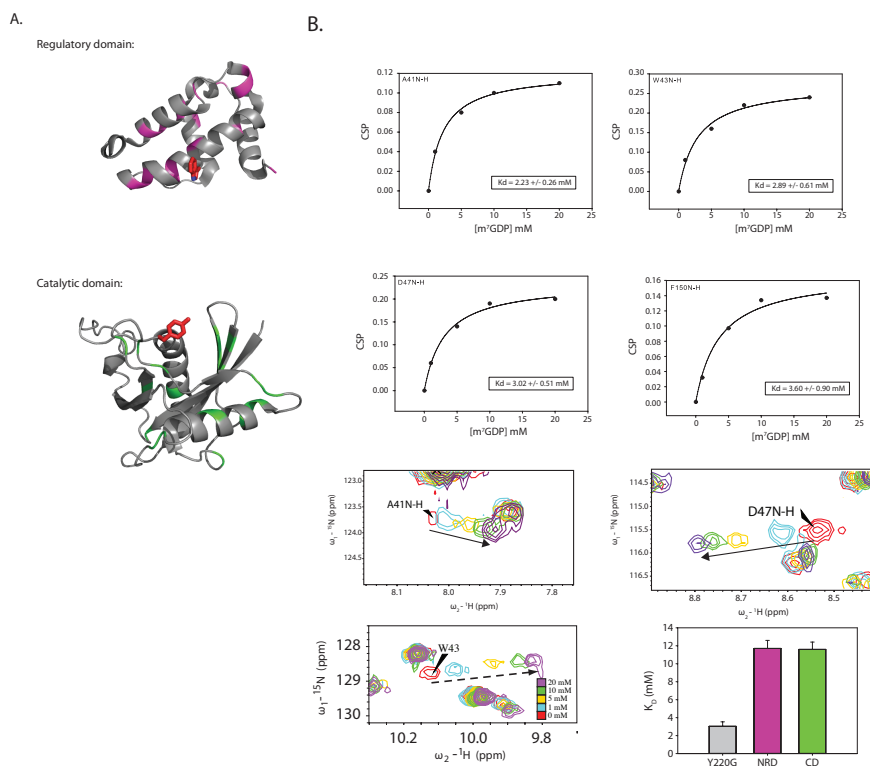


**Figure S2.4: W43 and Y220G mutations quench ms- $\mu$ s dynamics in Dcp2core and Y220G allows for observation of cap binding by NMR.** a, Common backbone amide resonances that reappear upon

mutation of either W43 or Y220 in Dcp2<sub>core</sub> as displayed on the individual RD and CD. **b**, Plots of CSP (ppm) versus m<sup>7</sup>GDP concentration from HSQC cap binding titration experiments. Residues used to determine cap binding affinity with corresponding fits and representative cross-peaks show shifts with increasing [m<sup>7</sup>GDP]. Lower right graph compares average K<sub>D</sub> (mM) observed for Dcp2<sub>core</sub> Y220G in comparison to the isolated NRD and CD of Dcp2.

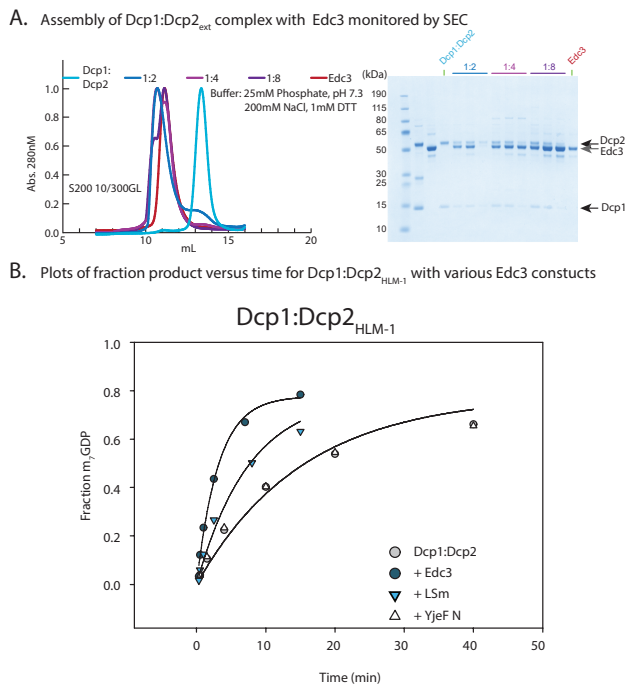


**Figure S2.5: Edc3 interaction with Dcp1:Dcp2<sub>ext</sub> and activity with Dcp1:Dcp2<sub>HLM-1</sub>.** **a**, Analytical S200 size-exclusion chromatograms of Dcp1:Dcp2<sub>ext</sub> or Edc3 alone or in complex with increasing excess of Edc3. SDS-PAGE of fractions from the center of the peaks from a given sizing chromatogram. **b**, Decapping activity of Dcp1:Dcp2<sub>ext</sub> incubated with excess Edc3, LSm domain or YjeF N domain.

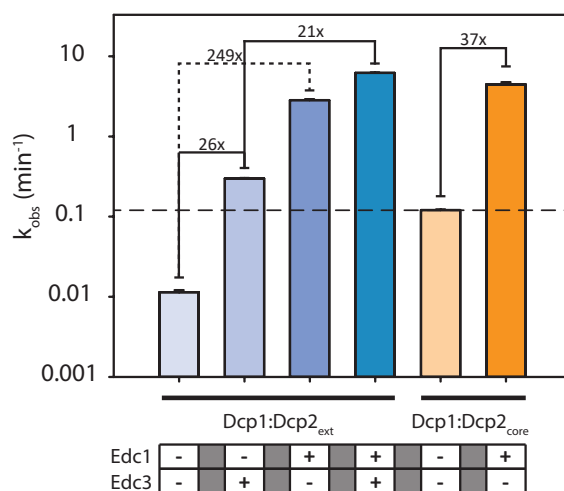
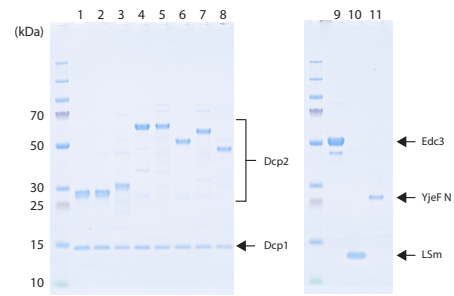


**Figure S2.6: Comparison of rates with Edc3 and Edc1 of Dcp1:Dcp2<sub>ext</sub> and Dcp1:Dcp2<sub>core</sub>.** Logscale comparison of the rates of Dcp1:Dcp2<sub>ext</sub> in complex with Edc1, Edc3 or both and Dcp1:Dcp2<sub>core</sub> in complex with Edc1.



1. Dcp1:Dcp2 (1-243)
2. Dcp1:Dcp2 (1-243) Y220G
3. Dcp1:Dcp2 (1-266)
4. Dcp1:Dcp2 (1-504)
5. Dcp1:Dcp2 (1-504) Y220G
6. Dcp1:Dcp2 (1-504)  $\Delta$ IM1
7. Dcp1:Dcp2 (1-504)  $\Delta$ IM2
8. Dcp1:Dcp2 (1-504)  $\Delta$ IM1/2
9. Edc3
10. LSm (1-94)
11. YjeF N (188-454)

**Figure S2.7: Coomassie stained SDS-PAGE of purified proteins used in this study.**

**Table S2.1: Table of constructs used in this study**

Protein Construct	Amino Acid Boundaries	Solubility/Purification Tags	Plasmid Backbone	Organism
Dcp1/Dcp2 <sub>core</sub>	Dcp1: 1-127 Dcp2: 1-243	Dcp1: N-terminal His <sub>6</sub> -GB1-TEV	pYACYC	<i>S. pombe</i>
Dcp1/Dcp2 <sub>core</sub> (Y220G)	Dcp1: 1-127 Dcp2: 1-243	Dcp1: N-His <sub>6</sub> -GB1-TEV	pYACYC	<i>S. pombe</i>
Dcp1/Dcp2 <sub>HLM1</sub>	Dcp1: 1-127 Dcp2: 1-266	Dcp1: N-His <sub>6</sub> -GB1-TEV	pYACYC	<i>S. pombe</i>
Dcp1/Dcp2 <sub>HLM1</sub> (Y220G)	Dcp1: 1-27 Dcp2: 1-266	Dcp1: N-His <sub>6</sub> -GB1-TEV	pRSF	<i>S. pombe</i>
Dcp1/Dcp2 <sub>ext</sub>	Dcp1: 1-127 Dcp2: 1-504	Dcp1: N-His <sub>6</sub> -GB1-TEV Dcp2: C-terminal StrepII	pRSF	<i>S. pombe</i>
Dcp1/Dcp2 <sub>ext</sub> (Y220G)	Dcp1: 1-127 Dcp2: 1-504	Dcp1: N-His <sub>6</sub> -GB1-TEV Dcp2: C-terminal StrepII	pRSF	<i>S. pombe</i>
Dcp1/Dcp2 <sub>ext</sub> (Δ267-350)	Dcp1: 1-127 Dcp2: 1-504 (Δ267-350)	Dcp1: N-His <sub>6</sub> -GB1-TEV Dcp2: C-terminal StrepII	pRSF	<i>S. pombe</i>
Dcp1/Dcp2 <sub>ext</sub> (ΔIM2)	Dcp1: 1-127 Dcp2: 1-504 (Δ399-434)	Dcp1: N-His <sub>6</sub> -GB1-TEV Dcp2: C-terminal StrepII	pRSF	<i>S. pombe</i>
Dcp1/Dcp2 <sub>ext</sub> (Δ267-350 & IM2)	Dcp1: 1-127 Dcp2: 1-504 (Δ267-350) & (Δ399-434)	Dcp1: N-His <sub>6</sub> -GB1-TEV Dcp2: C-terminal StrepII	pRSF	<i>S. pombe</i>
Dcp1/Dcp2 <sub>1-444</sub>	Dcp1: 1-127 Dcp2: 1-444	Dcp1: N-His <sub>6</sub> -GB1-TEV Dcp2: C-terminal StrepII	pRSF	<i>S. pombe</i>
Dcp1/Dcp2(Δ350-400)	Dcp1: 1-127 Dcp2: 1-504 (Δ350-400)	Dcp1: N-His <sub>6</sub> -GB1-TEV Dcp2: C-terminal StrepII	pRSF	<i>S. pombe</i>
Edc3	Edc3: 1-454	N-terminal His <sub>6</sub> -TEV	pET30b	<i>S. pombe</i>
Edc3 Lsm domain	Edc3: 1-94	N-terminal His <sub>6</sub> -TEV	pET30b	<i>S. pombe</i>
Edc3 YjeF N domain	Edc3: 188-454	N-terminal His <sub>6</sub> -TEV	pET30b	<i>S. pombe</i>
Edc1 Direct Activation Motif (DAM)	Edc1: 155-180	None (synthesized by Peptide2.0)	N/A	<i>S. pombe</i>

**Table S2.2: Dynamic Light Scattering (DLS) of Dcp1:Dcp2<sub>ext</sub> and Dcp1:Dcp2<sub>core</sub>**

Sample	Mean radius ± σ (nm)
Dcp1:Dcp2 <sub>core</sub>	6.326 ± 0.1541
Dcp1:Dcp2 <sub>ext</sub>	6.322 ± 0.1475

**Table S2.3: Mean  $k_{\text{obs}}$  of 1.5  $\mu\text{M}$  Dcp1:Dcp2 constructs**

<b>Complex</b>	<b>Mean <math>k_{\text{obs}} \pm \sigma</math> (<math>\text{min}^{-1}</math>)</b>	<b>Complex</b>	<b>Mean <math>k_{\text{obs}} \pm \sigma</math> (<math>\text{min}^{-1}</math>)</b>
Dcp1:Dcp2 <sub>core</sub>	$0.0892 \pm 0.01$	Dcp1:Dcp2 <sub>HLM-1</sub>	$0.2751 \pm 0.0435$
Dcp1:Dcp2 <sub>core</sub> (Y220G)	$0.1361 \pm 0.016$	Dcp1:Dcp2 <sub>HLM-1</sub>	$0.1141 \pm 0.0184$
Dcp1:Dcp2 <sub>HLM-1</sub>	$0.0658 \pm 0.0005$	Dcp1:Dcp2 <sub>HLM-1</sub>	$0.0578 \pm 0.0085$
Dcp1:Dcp2 <sub>ext</sub>	$0.0114 \pm 0.0007$	Dcp1:Dcp2 <sub>ext</sub> + Edc3	$0.4116 \pm 0.0476$
Dcp1:Dcp2 <sub>ext</sub> (Y220G)	$0.0722 \pm 0.0161$	Dcp1:Dcp2 <sub>ext</sub> + LSm	$0.1077 \pm 0.00765$
Dcp1:Dcp2 ( $\Delta 267-350$ )	$0.0508 \pm 0.0025$	Dcp1:Dcp2 <sub>ext</sub> (Y220G) + YjeF N	$0.0166 \pm 0.00055$
Dcp1:Dcp2 ( $\Delta$ IM2)	$0.0588 \pm 0.0007$	Dcp1:Dcp2 <sub>ext</sub> (Y220G) + Edc3	$0.2351 \pm 0.0035$
Dcp1:Dcp2 ( $\Delta 267-350$ /IM2)	$0.0812 \pm 0.005$		

## REFERENCES

1. Dunckley, T. and Parker, R. The DCP2 protein is required for mRNA decapping in *Saccharomyces cerevisiae* and contains a functional MutT motif. *EMBO J.* **18**, 5411–5422 (1999).
2. Wang, Z., Jiao, X., Carr-Schmid, A., Kiledjian, M. The hDcp2 protein is a mammalian mRNA decapping enzyme. *Proc. Natl. Acad. Sci. U. S. A.* **99**, 12663–8 (2002).
3. Grudzien-Nogalska, E., Kiledjian, M. New insights into decapping enzymes and selective mRNA decay. *Wiley Interdiscip. Rev. RNA* **8**, 1–11 (2017).
4. Song, M. G., Li, Y., Kiledjian, M. Multiple mRNA Decapping Enzymes in Mammalian Cells. *Mol. Cell* **40**, 423–432 (2010).
5. Konarska, M. M., Padgett, R. A., Sharp, P. A. Recognition of cap structure in splicing in vitro of mRNA precursors. *Cell* **38**, 731–736 (1984).
6. Izaurralde, E., Lewis, J., McGuigan, C., Jankowska, M., Darzynkiewicz, E., Mattaj, I. W. A nuclear cap binding protein complex involved in pre-mRNA splicing. *Cell*, **78**, 657–68 (1994).
7. Visa, N., Izaurralde, E., Ferreira, J., Daneholt, B., Mattaj, I. W. A nuclear cap-binding complex binds Balbiani ring pre-mRNA cotranscriptionally and accompanies the ribonucleoprotein particle during nuclear export. *J. Cell Biol.* **133**, 5–14 (1996).
8. Moore, M. J. From Birth to Death: The Complex Lives of Eukaryotic mRNAs. *Science* **309**, 1514–1518 (2005).
9. Topisirovic, I., Svitkin, Y. V., Sonenberg, N., Shatkin, A. J. Cap and cap-binding proteins in the control of gene expression. *Wiley Interdiscip. Rev. RNA* **2**, 277–298 (2011).
10. Xiang, S., Cooper-Morgan, A., Jiao, X., Kiledjian, M., Manley, J. L., Tong, L. (2009)

- Structure and function of the 5'→3' exoribonuclease Rat1 and its activating partner Rai1. *Nature* **458**, 784–788 (2009).
11. Chang, J. H., Jiao, X., Chiba, K., Oh, C., Martin, C. E., Kiledjian, M., Tong, L. Dxo1 is a new type of eukaryotic enzyme with both decapping and 5'-3' exoribonuclease activity. *Nat. Struct. Mol. Biol.* **19**, 1011–1017 (2012).
  12. Mauer, J., Luo, X., Blanjoie, A., Jiao, X., Grozhik, A. V., Patil, D. P., Linder, B., Pickering, B. F., Vasseur, J.-J., Chen, Q., *et al.* Reversible methylation of m6Am in the 5' cap controls mRNA stability. *Nature* **541**, 371–375 (2016).
  13. Newbury, S. and Woollard, A. The 5'-3' exoribonuclease xrn-1 is essential for ventral epithelial enclosure during *C. elegans* embryogenesis. *RNA* **10**, 59–65 (2004).
  14. Molleston, J. M. and Cherry, S. Attacked from all sides: RNA decay in antiviral defense. *Viruses* **9** (2017).
  15. Arribas-Layton, M., Wu, D., Lykke-Andersen, J., Song, H. Structural and functional control of the eukaryotic mRNA decapping machinery. *Biochim. Biophys. Acta - Gene Regul. Mech.* **1829**, 580–589 (2013).
  16. Borja, M. S., Piotukh, K., Freund, C., Gross, J. D. Dcp1 links coactivators of mRNA decapping to Dcp2 by proline recognition. *RNA* **17**, 278–290 (2011).
  17. Lai, T., Cho, H., Liu, Z., Bowler, M. W., Piao, S., Parker, R., Kim, Y. K., Song, H. Structural basis of the PNRC2-mediated link between mRNA surveillance and decapping. *Structure* **20**, 2025–2037 (2012).
  18. Wurm, J. P., Holdermann, I., Overbeck, J. H., Mayer, P. H. O., Sprangers, R. Changes in conformational equilibria regulate the activity of the Dcp2 decapping enzyme. *Proc. Natl. Acad. Sci.* **14**, 6034–6039 (2017).

19. Floor, S. N., Borja, M. S., Gross, J. D. Interdomain dynamics and coactivation of the mRNA decapping enzyme Dcp2 are mediated by a gatekeeper tryptophan. *Proc. Natl. Acad. Sci.* **109**, 2872–2877 (2012).
20. Fromm, S. A., Truffault, V., Kamenz, J., Braun, J. E., Hoffmann, N. A., Izaurralde, E., Sprangers, R. The structural basis of Edc3- and Scd6-mediated activation of the Dcp1:Dcp2 mRNA decapping complex. *EMBO J.* **31**, 279–290 (2012).
21. Decourty, L., Saveanu, C., Zemam, K., Hantraye, F., Frachon, E., Rousselle, J.-C., Fromont-Racine, M., Jacquier, A. Linking functionally related genes by sensitive and quantitative characterization of genetic interaction profiles. *Proc. Natl. Acad. Sci. U. S. A.* **105**, 5821–5826 (2008).
22. Badis, G., Saveanu, C., Fromont-Racine, M., Jacquier, A. Targeted mRNA degradation by deadenylation-independent decapping. *Mol. Cell* **15**, 5–15 (2004).
23. Dong, S., Li, C., Zenklusen, D., Singer, R. H., Jacobson, A., He, F. YRA1 Autoregulation Requires Nuclear Export and Cytoplasmic Edc3p-Mediated Degradation of Its Pre-mRNA. *Mol. Cell* **25**, 559–573 (2007).
24. Wang, C.-Y., Chen, W.-L., Wang, S.-W. Pdc1 Functions in the Assembly of P Bodies in *Schizosaccharomyces pombe*. *Mol. Cell. Biol.* **33**, 1244–1253 (2013).
25. Eulalio, A., Rehwinkel, J., Stricker, M., Huntzinger, E., Yang, S. F., Doerks, T., Dorner, S., Bork, P., Boutros, M, Izaurralde, E. Target-specific requirements for enhancers of decapping in miRNA-mediated gene silencing. *Genes Dev.* **21**, 2558–2570 (2007).
26. Ahmed, I., Buchert, R., Zhou, M., Jiao, X., Mittal, K., Sheikh, T. I., Scheller, U., Vasli, N., Rafiq, M. A., Qasim Brohi, M., *et al.* Mutations in DCPS and EDC3 in autosomal recessive intellectual disability indicate a crucial role for mRNA decapping in neurodevelopment. *Hum.*



- Mol. Genet.* **24**, 3172–3180 (2014).
27. Jonas, S. and Izaurralde, E. The role of disordered protein regions in the assembly of decapping complexes and RNP granules. *Genes Dev.* **27**, 2628–2641 (2013).
28. Charenton, C., Gaudon-Plesse, C., Fourati, Z., Taverniti, V., Black, R., Kolesnikova, O., Séraphin, B., Graille, M. A unique surface on Pat1 C-terminal domain directly interacts with Dcp2 decapping enzyme and Xrn1 5'-3' mRNA exonuclease in yeast. *Proc. Natl. Acad. Sci. U. S. A.* **114**, 9493–9501 (2017).
29. He, F. and Jacobson, A. Control of mRNA decapping by positive and negative regulatory elements in the Dcp2 C-terminal domain. *RNA* **21**, 1633-1647 (2015).
30. Fromm, S. A., Kamenz, J., Nöldeke, E. R., Neu, A., Zoher, G., Sprangers, R. In vitro reconstitution of a cellular phase-transition process that involves the mRNA decapping machinery. *Angew. Chemie - Int. Ed.* **53**, 7354–7359 (2014).
31. Schütz, S., Nöldeke, E. R., Sprangers, R. A synergistic network of interactions promotes the formation of in vitro processing bodies and protects mRNA against decapping. *Nucleic Acids Res.* **45**, 6911–6922 (2017).
32. Davey, N. E., Cyert, M. S., Moses, A. M. Short linear motifs – ex nihilo evolution of protein regulation. *Cell Commun. Signal.* **13**, 43 (2015).
33. Latysheva, N. S., Flock, T., Weatheritt, R. J., Chavali, S., Babu, M. M. How do disordered regions achieve comparable functions to structured domains? *Protein Sci.* **24**, 909–922 (2015).
34. Wurm, J. P., Overbeck, J., Sprangers, R. The *S. pombe* mRNA decapping complex recruits cofactors and an Edc1-like activator through a single dynamic surface. *RNA* **22**, 1360–1372 (2016).

35. Nagar, B., Hantschel, O., Young, M. A., Scheffzek, K., Veach, D., Bornmann, W., Clarkson, B., Superti-Furga, G., Kuriyan, J. Structural basis for the autoinhibition of c-Abl tyrosine kinase. *Cell* **112**, 859–871 (2003).
36. Floor, S. N., Jones, B. N., Hernandez, G., Gross, J. D. A split active site couples cap recognition by Dcp2 to activation. *Nat. Struct. Mol. Biol.* **17**, 1096–1101 (2010).
37. Charenton, C., Taverniti, V., Gaudon-Plesse, C., Back, R., Séraphin, B., Graille, M. Structure of the active form of Dcp1–Dcp2 decapping enzyme bound to m7GDP and its Edc3 activator. *Nat. Struct. Mol. Biol.* **23**, 982–986 (2016).
38. She, M., Decker, C. J., Svergun, D. I., Round, A., Chen, N., Muhlrads, D., Parker, R., Song, H. Structural Basis of Dcp2 Recognition and Activation by Dcp1. *Mol. Cell* **29**, 337–349 (2008).
39. Ling, S. H. M., Decker, C. J., Walsh, M. a, She, M., Parker, R., Song, H. Crystal structure of human Edc3 and its functional implications. *Mol. Cell. Biol.* **28**, 5965–76 (2008).
40. Valkov, E., Muthukumar, S., Chang, C.-T., Jonas, S., Weichenrieder, O., Izaurralde, E. Structure of the Dcp2–Dcp1 mRNA-decapping complex in the activated conformation. *Nat. Struct. Mol. Biol.* **23**, 574–579 (2016).
41. Mugridge, J. S., Ziemniak, M., Jemielity, J., Gross, J. D. Structural basis of mRNA-cap recognition by Dcp1–Dcp2. *Nat. Struct. Mol. Biol.* **23**, 987–994 (2016).
42. Deshmukh, M. V., Jones, B. N., Quang-Dang, D., Flinders, J., Floor, S. N., Kim, C., Jemielity, J., Kalek, M., Darzynkiewicz, E., Gross, J. D. mRNA decapping is promoted by an RNA-binding channel in Dcp2. *Mol. Cell* **29**, 324–336 (2008).
43. Huse, M. and Kuriyan, J. The conformational plasticity of protein kinases. *Cell* **109**, 275–282 (2002).
44. Collier, J. and Parker, R. General translational repression by activators of mRNA decapping.

- Cell* **122**, 875–886 (2005).
45. Pilkington, G. R. and Parker, R. Pat1 Contains Distinct Functional Domains That Promote P-Body Assembly and Activation of Decapping. *Mol. Cell. Biol.* **28**, 1298–1312 (2008).
  46. Bonnerot, C., Boeck, R., Lapeyre, B. The two proteins Pat1p (Mrt1p) and Spb8p interact in vivo, are required for mRNA decay, and are functionally linked to Pab1p. *Mol. Cell. Biol.* **20**, 5939–5946 (200).
  47. Tharun, S., He, W., Mayes, A. E., Lennertz, P., Beggs, J. D., Parker, R. Yeast Sm-like proteins function in mRNA decapping and decay. *Nature* **404**, 515–518 (2000).
  48. Sharif, H. and Conti, E. Architecture of the Lsm1-7-Pat1 Complex: A Conserved Assembly in Eukaryotic mRNA Turnover. *Cell Rep.* **5**, 283–291 (2013).
  49. Jones, B. N., Quang-Dang, D. U., Oku, Y., Gross, J. D. Chapter 2 A Kinetic Assay to Monitor RNA Decapping Under Single-Turnover Conditions 1st ed. Elsevier Inc (2008).
  50. Skrynnikov, N. R., Mulder, F. A. A., Hon, B., Dahlquist, F. W., Kay, L. E. Probing slow time scale dynamics at methyl-containing side chains in proteins by relaxation dispersion NMR measurements: Application to methionine residues in a cavity mutant of T4 lysozyme. *J. Am. Chem. Soc.* **123**, 4556–4566 (2001).
  51. Demers, J. P. and Mittermaier, A. Binding mechanism of an SH3 domain studied by NMR and ITC. *J. Am. Chem. Soc.* **131**, 4355–4367 (2009).
  52. Roehrl, M. H. A., Wang, J. Y., Wagner, G. A general framework for development and data analysis of competitive high-throughput screens for small-molecule inhibitors of protein-protein interactions by fluorescence polarization. *Biochemistry* **43**, 16056–16066 (2004).
  53. Dosztányi, Z., Csizmok, V., Tompa, P., Simon, I. IUPred: Web server for the prediction of intrinsically unstructured regions of proteins based on estimated energy content.

*Bioinformatics* **21**, 3433–3434 (2005).

54. Robert, X. and Gouet, P. Deciphering key features in protein structures with the new ENDscript server. *Nucleic Acids Res.* **42**, 320–324 (2014).

## CHAPTER 3

### **Biomolecular condensates amplify mRNA decapping by biasing enzyme conformation**

Ryan W. Tibble<sup>1,2</sup>, Anaïs Depaix<sup>3</sup>, Joanna Kowalska<sup>3</sup>, Jacek Jemielity<sup>4</sup>, John D. Gross<sup>1,2\*</sup>

#### **AUTHOR INFORMATION**

<sup>1</sup>Program in Chemistry and Chemical Biology, University of California, San Francisco, San Francisco, CA, 94158, USA

<sup>2</sup>Department of Pharmaceutical Chemistry, University of California, San Francisco, San Francisco, CA, 94158, USA

<sup>3</sup>Division of Biophysics, Institute of Experimental Physics, Faculty of Physics, University of Warsaw, 02-095, Warsaw, Poland

<sup>4</sup>Centre of New Technologies, University of Warsaw, 02-097, Warsaw, Poland

\*Correspondence: [jdgross@cgl.ucsf.edu](mailto:jdgross@cgl.ucsf.edu)

*This chapter adapted from:*

Tibble, R. W., Depaix, A., Kowalska, J., Jemielity, J. & Gross, J. D. Biomolecular condensates amplify mRNA decapping by biasing enzyme conformation. *Nat. Chem. Biol.* **17**, 615–623 (2021).

## ABSTRACT

Cells organize biochemical processes into biological condensates. P-bodies are cytoplasmic condensates enriched in enzymes important for mRNA degradation and have been identified as sites of both storage and decay. How these opposing outcomes can be achieved in condensates remains unresolved. mRNA decapping immediately precedes degradation and the Dcp1/Dcp2 decapping complex is enriched in P-bodies. Here, we show Dcp1/Dcp2 activity is modulated in condensates and depends on the interactions promoting phase separation. We find Dcp1/Dcp2 phase separation stabilizes an inactive conformation in Dcp2 to inhibit decapping. The activator Edc3 causes a conformational change in Dcp2 and rewires the protein-protein interactions to stimulate decapping in condensates. Disruption of the inactive conformation dysregulates decapping in condensates. Our results indicate regulation of enzymatic activity in condensates relies on a coupling across length scales ranging from microns to Ångstroms. We propose this regulatory mechanism may control the functional state of P-bodies and related phase-separated compartments.

## INTRODUCTION

Organizing cellular processes into biomolecular condensates is a mechanism to regulate biochemistry in distinct ways: altering molecular conformation and organization to promote specificity, increasing local concentration to accelerate enzymatic activity, and coupling interactions to enforce reaction directionality<sup>1-10</sup>. The emergent properties afforded by formation of extensive interaction networks in condensates can also enhance enzymatic activity beyond local concentration effects<sup>11,12</sup>. Such enhancements could arise from the coupling of enzyme allostery to interactions spanning the diameter of condensates. How the collective properties across length scales are coupled to enzyme catalysis is poorly understood.

Cellular mRNA is highly regulated through the assembly of messenger ribonucleoprotein (mRNP) complexes and many mRNPs accumulate in biomolecular condensates under normal

and stressed conditions<sup>13,14</sup>. P-bodies are a conserved class of biomolecular condensates enriched in proteins involved in 5'-3' mRNA decay<sup>15-17</sup>. Although the molecular composition and interactions within P-bodies is well studied, their biological function is controversial. Several studies suggest P-bodies are sites of decay because colocalized mRNA are cleared over time<sup>16,18-20</sup>. Alternatively, P-bodies may function as sites of mRNA storage due to the absence of decay intermediates in sequencing and live cell imaging data<sup>15,21,22</sup>. Moreover, mRNAs exhibit context-dependent degradation in P-bodies and can be restored to the translating pool upon recovery from cell stress<sup>23-26</sup>. Given their heterotypic and dynamic nature, isolating and studying P-bodies is challenging and presents a hurdle in understanding their function.

Like other biomolecular condensates, P-body assembly relies on a network of redundant multivalent interactions between resident proteins mediated by intrinsically disordered regions (IDRs)<sup>27</sup>. Many 5'-3' decay proteins contain structured domains flanked by IDRs important for interaction with RNA and protein cofactors<sup>28</sup>. This includes the conserved decapping complex—comprised of the catalytic subunit Dcp2 and its obligate activator Dcp1—responsible for removing the 7-methylguanosine (m7G) cap from mRNA, committing the transcript to degradation<sup>29-31</sup>. Excision of disordered regions in the eukaryotic decapping complex inhibit its localization to P-bodies and leads to transcript dysregulation and conditional lethality<sup>32-34</sup>.

The localization and regulation imparted by IDRs in the decapping complex are mediated through conserved short-linear interaction motifs<sup>28,32,33</sup>. Recently, positive and negative regulatory motifs were identified in the C-terminal IDR of yeast Dcp2 that affect decapping *in vitro* and *in vivo*<sup>35,36</sup>. This established a model where Dcp2 is autoinhibited and coactivators alleviate autoinhibition to increase mRNA binding and catalysis<sup>36,37</sup>. However, the molecular mechanisms for regulation of autoinhibition are not well understood.

Edc3 is an activator of decapping responsible for regulating specific mRNAs and deadenylation-independent 5'-3' decay in budding yeast<sup>34,38</sup>. Edc3 interacts with positive regulatory motifs in the C-terminus of Dcp2 to alleviate autoinhibition<sup>35,36,39,40</sup>. Edc3 localizes to

P-bodies and forms multivalent interactions with RNA and the Dcp-2 C-terminus to promote liquid-liquid phase separation<sup>33,41,42</sup>. Initial studies suggested Edc3-mediated phase separation of Dcp1/Dcp2 inhibited decapping<sup>42</sup>. These studies indirectly measured Dcp1/Dcp2 activity in condensates as monitoring decapping in condensates is challenging. It remains unclear how phase separation regulates decapping.

In this study, we address the relationship between molecular organization and function in minimal decapping condensates containing Dcp1/Dcp2 and Edc3. Using a dual-labeled fluorescent RNA to simultaneously monitor the 5'-cap and RNA body, we measure rates of decapping in condensates. We find Dcp1/Dcp2 is inactive in condensates and addition of Edc3 reorganizes the underlying network of interactions to activate Dcp1/Dcp2 90-fold. Activation in condensates is greater than in solution because of increased repression of Dcp1/Dcp2 activity in the absence of Edc3, not because enzyme turnover is accelerated. We show Edc3 promotes a Dcp1/Dcp2 conformational change to enhance decapping and suggest the condensate environment biases an equilibrium in Dcp1/Dcp2 that represses enzyme activity. Our findings suggest condensate composition tunes enzyme conformational dynamics to affect activity, which may be an emergent property of biomolecular condensates used for controlling RNA degradation and other biochemical reactions in cells.

## RESULTS

### Phase separation of Dcp1/Dcp2 is potentiated by Edc3

We recently reconstituted the decapping complex from *S. pombe* that includes a C-terminal boundary at residue 504 in Dcp2 optimized for expression and necessary for regulation of activity (Dcp2<sub>ext</sub>, **Fig. 3.1a** and **Table S3.1**)<sup>36</sup>. Dcp2<sub>ext</sub> contains structured, N-terminal regulatory (NRD) and catalytic (CD) domains and regulatory motifs in a C-terminal IDR. In the absence of activators, Dcp1/Dcp2<sub>ext</sub> is autoinhibited by inhibitory motifs (IMs) and Edc3 interacts with flanking helical leucine rich motifs (HLMs) to promote decapping (**Fig. 3.1a,b**).



Dcp1/Dcp2<sub>ext</sub> undergoes phase separation at higher concentrations (**Fig. 3.1c**). Because prior studies examined Dcp1/Dcp2 condensates using a construct lacking IMs, we characterized how these elements contribute to phase separation of Dcp1/Dcp2<sub>ext</sub> in parallel with those formed in complex with Edc3<sup>33,42</sup>.

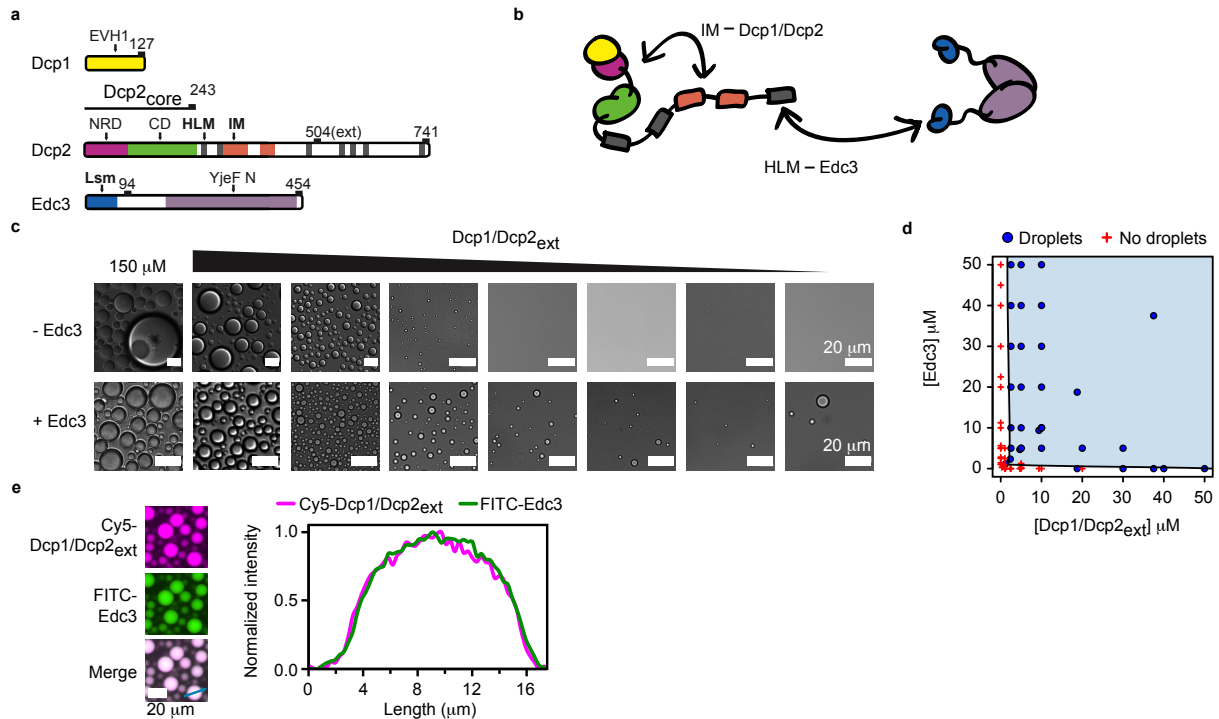


**Figure 3.1: Edc3 enhances Dcp1/Dcp2<sub>ext</sub> phase separation.** **a**, Schematic for Dcp1, Dcp2, and Edc3. Domains and motifs are labeled and white space is indicative of disordered regions. Dcp2 contains structured core domains, Dcp2<sub>core</sub>, and the construct used in this study, Dcp2<sub>ext</sub>, contains regulatory elements in the C-terminal IDR. **b**, Cartoon of Dcp1/Dcp2<sub>ext</sub> and Edc3 highlighting interactions between IMs and core domains of Dcp1/Dcp2<sub>ext</sub> and between HLMs and Edc3. Cartoons are colored as shown in **a**. **c**, Dcp1/Dcp2<sub>ext</sub> undergoes liquid-liquid phase separation and addition of stoichiometric Edc3 reduces the critical concentration for phase separation twenty-fold. Each sequential micrograph is a two-fold dilution of the preceding. **d**, Phase diagram of Dcp1/Dcp2<sub>ext</sub> and Edc3 *in vitro*. **e**, Dcp1/Dcp2<sub>ext</sub> and Edc3 are equally enriched and homogeneously distributed in droplets. Protein concentration is 50 μM. Representative micrographs are shown from three independent experiments with similar results.

Droplets containing Dcp1/Dcp2<sub>ext</sub> underwent fusion and varied in size from <math><50 \mu\text{m}^2</math> to >math>500 \mu\text{m}^2</math>, indicative of a liquid-like biomolecular condensate (**Fig. S3.1a,b**). The low-complexity regions of the Dcp2 C-terminus (residues 274-504) are sufficient to promote phase separation, however the structured NRD and CD may antagonize this behavior in the absence of Dcp1 (**Fig. S3.1c,d**). Dcp1/Dcp2<sub>ext</sub> droplets are able to recruit RNA (**Fig. S3.1e**). Our data demonstrate Dcp1/Dcp2<sub>ext</sub> can form large, microscopic condensates mediated by the C-terminus.

Because Edc3 forms multivalent interactions with HLMs in the Dcp2 C-terminus, we tested how Edc3 influenced the critical concentration for phase separation. Edc3 reduced the critical concentration of Dcp1/Dcp2<sub>ext</sub> phase separation 20-fold (**Fig. 3.1c,d**). Dcp1/Dcp2<sub>ext</sub> and Edc3 colocalized to droplets, were homogeneously distributed, undergo fusion and recruit RNA (**Fig. 3.1e** and **Fig. S3.1a,e**). Droplets containing Edc3 did not exceed 100  $\mu\text{m}^2$ , in contrast to the numerous  $>100 \mu\text{m}^2$  droplets observed for Dcp1/Dcp2<sub>ext</sub> (**Fig. 3.1c** and **Fig. S3.1b**). Edc3 altered Dcp1/Dcp2<sub>ext</sub> exchange in condensates in a concentration-dependent manner (**Fig. S3.2a,b** and **Table S3.2**). These data indicate the properties of Dcp1/Dcp2<sub>ext</sub> condensates change upon addition of Edc3, raising the possibility that protein interactions promoting droplet formation differ.

### **Edc3 alters interactions driving Dcp1/Dcp2 condensation**

Short-linear interaction motifs typically mediate phase separation and we hypothesized IMs and HLMs in the C-terminus of Dcp2 may differentially contribute to Dcp1/Dcp2<sub>ext</sub> condensation in the absence or presence of Edc3 (**Fig. 3.2a**). To test this, we developed a series of truncations in Dcp2 and Edc3 and looked for the presence of droplets using microscopy (**Fig. 3.2b**).

If Dcp1/Dcp2<sub>ext</sub> phase separation is driven by interactions between IMs and the structured regions of Dcp1/Dcp2<sub>ext</sub> *in trans*, then their removal should abrogate phase separation. However, if Edc3 results in a molecular reorganization of droplets to favor interactions between Edc3 and HLMs, then phase separation of Dcp1/Dcp2/Edc3 should be independent of IMs (**Fig. 3.2a**). In support, a construct lacking IMs, Dcp2<sub>HLM1/2</sub>, abolished phase separation of Dcp1/Dcp2 but not Dcp1/Dcp2/Edc3 (**Fig. 3.2c**).

Dcp1 can interact with an IM and a region of the Dcp2 C-terminus and may function as an interface for the multivalency required for Dcp1/Dcp2<sub>ext</sub> phase separation (**Fig. 3.2a**)<sup>36,43</sup>. This predicts excess Dcp1 would outcompete intermolecular Dcp1—Dcp2 interactions to prevent

phase separation of Dcp1/Dcp2<sub>ext</sub>, but not affect Edc3-driven phase separation because Edc3—HLM interactions are independent of Dcp1. Indeed, four-fold molar excess Dcp1 prevented Dcp1/Dcp2<sub>ext</sub> phase separation while addition of Edc3 resulted in droplet formation (**Fig. 3.2d**). Moreover, Edc3-dependent phase separation required Edc3 dimerization (**Fig. 3.2e**). Thus, Dcp2 IMs and Dcp1 are crucial for Dcp1/Dcp2<sub>ext</sub> phase separation while Dcp2 HLMs and Edc3 promote Dcp1/Dcp2<sub>ext</sub>/Edc3 droplet formation. This suggests molecular composition changes the network of interactions critical for condensate formation.

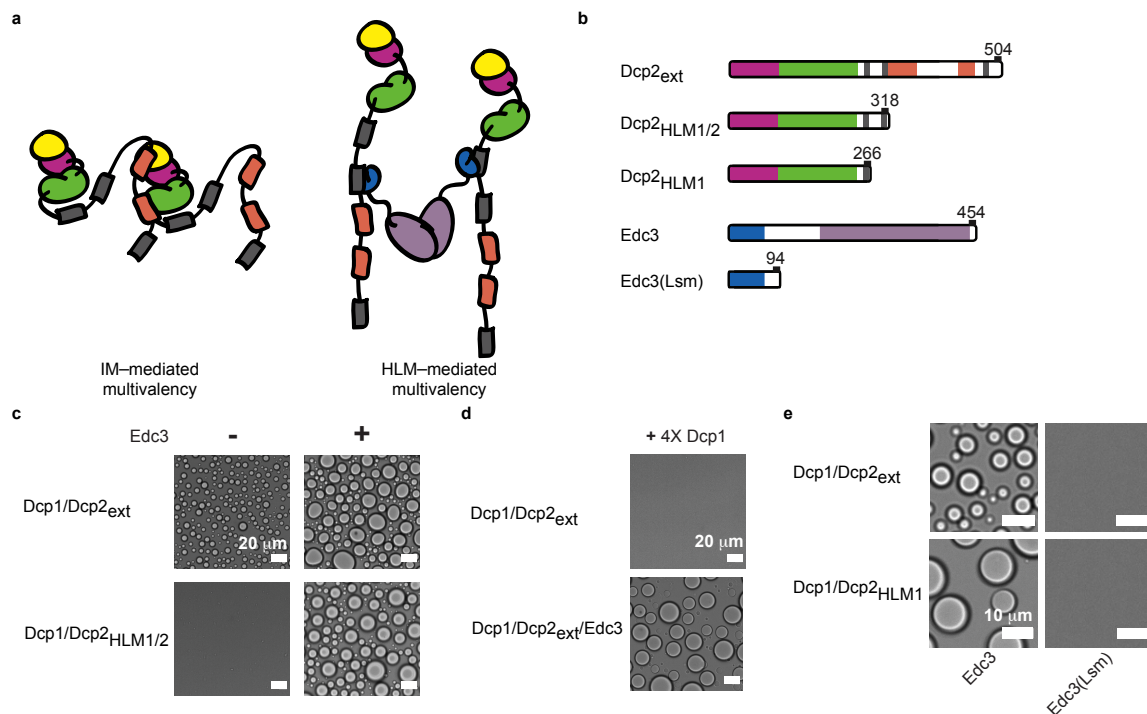


**Figure 3.2: Interactions underlying Dcp1/Dcp2<sub>ext</sub> and Dcp1/Dcp2<sub>ext</sub>/Edc3 phase separation differ. a**, Interaction between IMs of one Dcp2 molecule and a neighboring Dcp1/Dcp2<sub>ext</sub> *in trans* mediates Dcp1/Dcp2<sub>ext</sub> phase separation whereas Edc3 interacts with HLMs to bridge across Dcp2 molecules. **b**, Dcp2 and Edc3 truncations used to determine interactions important for phase separation. **c**, Removal of inhibitory motifs in the C-terminus of Dcp2 ablates phase separation of the decapping complex but Dcp1/Dcp2<sub>HLM1/2</sub> can still undergo phase separation when Edc3 is added. Concentration of Dcp1/Dcp2<sub>HLM1/2</sub> is 300  $\mu$ M, Dcp1/Dcp2<sub>ext</sub> is 100  $\mu$ M, Dcp1/Dcp2<sub>HLM1/2</sub>/Edc3 and Dcp1/Dcp2<sub>ext</sub>/Edc3 are at 50  $\mu$ M. **d**, Addition of four-fold molar excess Dcp1 disrupts Dcp1/Dcp2<sub>ext</sub> phase separation but not Dcp1/Dcp2<sub>ext</sub>/Edc3 droplet formation. Concentration of Dcp1 is 200  $\mu$ M, Dcp1/Dcp2<sub>ext</sub> and Dcp1/Dcp2<sub>ext</sub>/Edc3 is 50  $\mu$ M. **e**, Dimerization of Edc3 is necessary to promote phase separation of Dcp1/Dcp2 containing a single or multiple HLMs. Dcp1/Dcp2<sub>HLM1</sub> and Edc3 were stoichiometrically mixed at 150  $\mu$ M. Dcp1/Dcp2<sub>ext</sub> and Edc3 were mixed at 50  $\mu$ M. Representative micrographs are shown from three independent experiments with similar results.

### **Edc3 activates decapping in droplets**

Since the molecular organization of Dcp1/Dcp2<sub>ext</sub> and Dcp1/Dcp2<sub>ext</sub>/Edc3 droplets involves interactions important for autoinhibition and activation, we asked whether condensates exhibit different decapping activity. To directly quantify Dcp1/Dcp2<sub>ext</sub> decapping in droplets, we synthesized a 38mer-RNA substrate containing a 5'-m<sup>7</sup>GDP conjugated to fluorescein and 3' adenosine conjugated to Cy5, allowing for simultaneous monitoring of the 5'-cap and RNA body by microscopy (**Fig. 3.3a** and **Fig. S3.3a-d**). We mixed this substrate with a concentration of Dcp1/Dcp2<sub>ext</sub> above its critical concentration and did not observe appreciable loss in fluorescence intensity after 20 minutes, suggesting RNA is decapped at less than 0.006 min<sup>-1</sup> (**Fig. 3.3b,c**). However, droplet formation with excess Edc3 resulted in a decrease in m<sup>7</sup>GDP from droplets at a rate of 0.56 min<sup>-1</sup> (**Fig. 3.3d,e**). Thus, Edc3 enhanced Dcp1/Dcp2<sub>ext</sub> in droplets 90-fold and m<sup>7</sup>GDP loss from droplets is dependent on enzyme catalysis (**Fig. S3.3e,f**). Addition of substoichiometric Edc3 to pre-formed Dcp1/Dcp2<sub>ext</sub> droplets caused a dose-dependent loss of m<sup>7</sup>GDP signal from droplets at rates up to 22-fold greater than Dcp1/Dcp2<sub>ext</sub> droplets (**Fig. 3.3f,g**). Localization of the RNA body did not change, suggesting it is retained within condensates (**Fig. 3.3c,e**). Changes in RNA abundance from limiting amounts to excess relative to Dcp1/Dcp2<sub>ext</sub> had a two-fold effect on initial decapping rates in Dcp1/Dcp2<sub>ext</sub>/Edc3 droplets (**Fig. S3.3g**). We conclude decapping can occur within droplets but critically depends on Edc3.

Edc3 activates decapping 90-fold in droplets, suggesting Dcp1/Dcp2<sub>ext</sub>/Edc3 condensates increase decapping activity relative to the surrounding solution. Alternatively, Dcp1/Dcp2<sub>ext</sub> condensates may repress activity. To distinguish these possibilities, we measured the maximal rate of decapping of dual-labeled substrate using Dcp1/Dcp2<sub>core</sub>, which is not autoinhibited and does not undergo phase separation<sup>36</sup>. The rate observed in Dcp1/Dcp2<sub>ext</sub>/Edc3 droplets does not greatly differ from that observed for Dcp1/Dcp2<sub>core</sub> in solution (**Fig. S3.4a,b**). However, the rate of decapping determined in Dcp1/Dcp2<sub>ext</sub> droplets is

30-fold slower than Dcp1/Dcp2<sub>core</sub>. Thus, we conclude the droplet environment leads to repression of Dcp1/Dcp2<sub>ext</sub> in the absence of Edc3 and does not favor enhanced decapping activity by Edc3. Furthermore, our results suggest a high concentration of Dcp1/Dcp2<sub>ext</sub> in droplets is not sufficient for active decapping but requires interaction with Edc3.

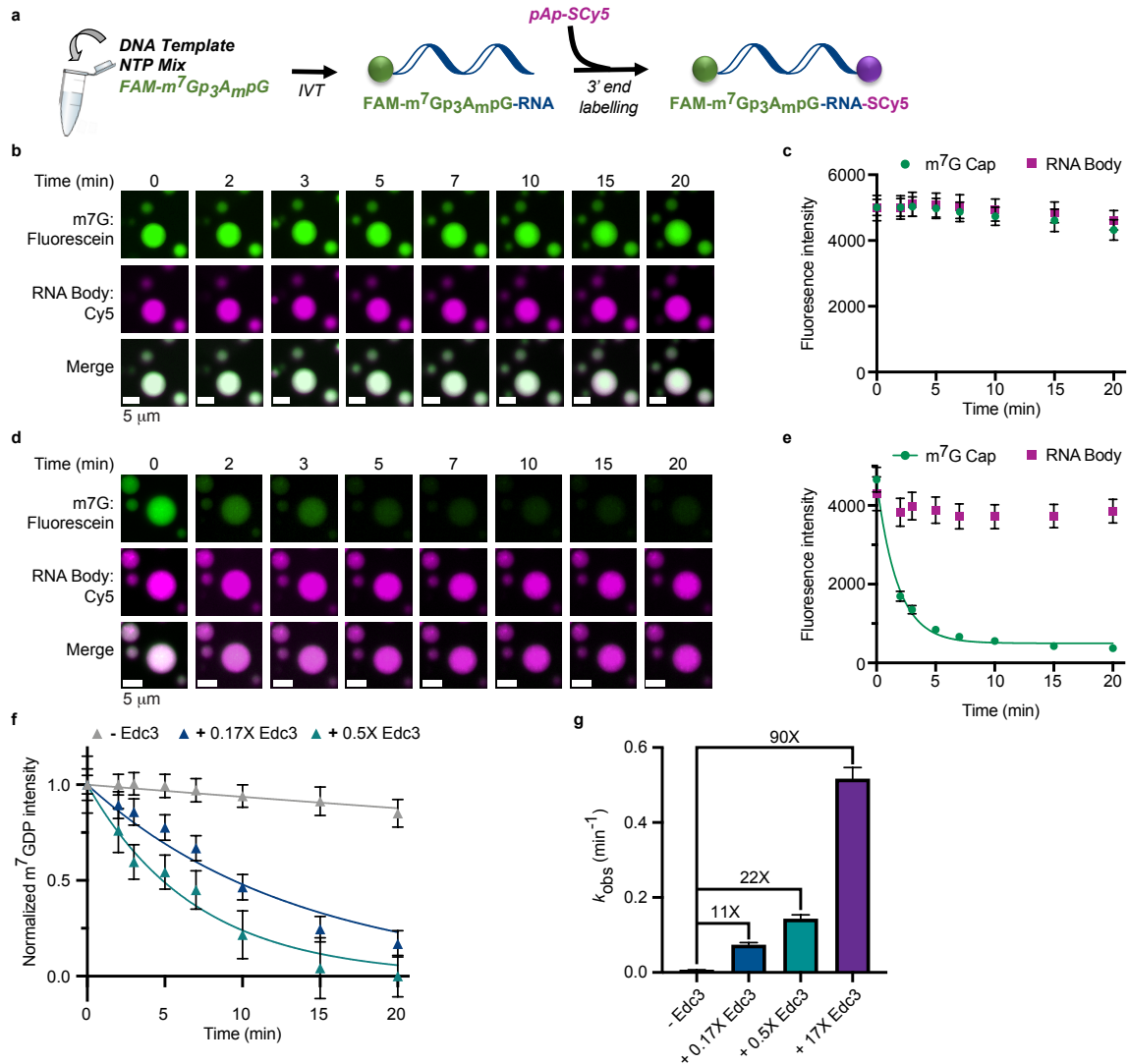


**Figure 3.3: The ability of phase-separated Dcp1/Dcp2<sub>ext</sub> to decap RNA is modulated by Edc3.** **a**, Synthesis scheme for two-color fluorescent 38mer RNA capped with fluorescein m<sup>7</sup>G cap (FAM-m<sup>7</sup>GDP) and labeled at the 3' end with Cy5-adenosine. **b, c**, Addition of dual-labeled RNA to Dcp1/Dcp2<sub>ext</sub> (60 μM total protein concentration) droplets shows minimal signal loss in both FAM-m<sup>7</sup>GDP and Cy5-RNA over twenty minutes. **d, e**, Time-dependent loss of FAM-m<sup>7</sup>GDP and Cy5-RNA signal from droplets formed by 5 μM Dcp1/Dcp2<sub>ext</sub> and 80 μM Edc3. **f**, Addition of substoichiometric Edc3 to preformed Dcp1/Dcp2<sub>ext</sub> droplets (60 μM total Dcp1/Dcp2<sub>ext</sub> concentration) results in dose-dependent loss of FAM-m<sup>7</sup>GDP signal from droplets. m<sup>7</sup>GDP intensity is normalized to initial fluorescence signal. **g**, Edc3 activates Dcp1/Dcp2<sub>ext</sub> up to 90-fold in condensates. Representative micrographs and data are from twenty droplets examined over two independent experiments with similar results. Data are presented as mean ± s.e.m.

### **Edc3 couples activation of decapping to phase separation**

To differentiate between Dcp1/Dcp2<sub>ext</sub> activity inside and outside condensates, we performed two single-turnover decapping experiments using capped, radiolabeled RNA (**Fig. 3.4a**). First, we measured decapping in a mixture containing Dcp1/Dcp2<sub>ext</sub> inside (dense phase) and outside (dilute phase) droplets after addition of capped RNA (bulk decapping). Second, we separated the dilute and dense phases by centrifugation, added capped substrate to the dilute phase, and monitored product formation (dilute phase decapping). Differences in decapping activity between the two samples can be attributed to contributions from Dcp1/Dcp2<sub>ext</sub> sequestered in droplets.

We used this activity partitioning assay to determine the contribution of Dcp1/Dcp2<sub>ext</sub> phase separation to overall activity in the absence or presence of Edc3. Decapping rates were comparable in Dcp1/Dcp2<sub>ext</sub> dilute and bulk phases, demonstrating Dcp1/Dcp2<sub>ext</sub> in droplets does not significantly contribute to overall activity and confirms Dcp1/Dcp2<sub>ext</sub> droplets are inactive (**Fig. 3.4b** and **Table S3.3**). Enhanced repression is not observed using this assay because it is masked by Dcp1/Dcp2<sub>ext</sub> decapping in the dilute phase. This is in contrast to droplets containing Edc3 and Dcp1/Dcp2<sub>ext</sub>, whereby activity in bulk solution is three-fold greater than the dilute phase (**Fig. 3.4b** and **Table S3.3**). Because Dcp1/Dcp2<sub>ext</sub> activity in the dilute phase is relatively insensitive to Edc3, we conclude regulation of decapping activity predominantly occurs in condensates.

To examine Edc3 activation and phase separation more closely, we performed activity partitioning experiments at increasing Edc3 concentrations and monitored for the appearance of droplets using microscopy. Cooperative activation of decapping by Edc3 correlated with phase separation, is dependent on Edc3 dimerization, and requires interaction with HLMs (**Fig. 3.4c**, **Fig. S3.5a,b**, **Tables S3.4** and **S3.5**). In contrast to bulk solution, increasing Edc3 concentration did not change rates of decapping in the dilute phase, indicating Edc3 strongly activates Dcp1/Dcp2<sub>ext</sub> through condensate formation (**Fig. 3.4c**).

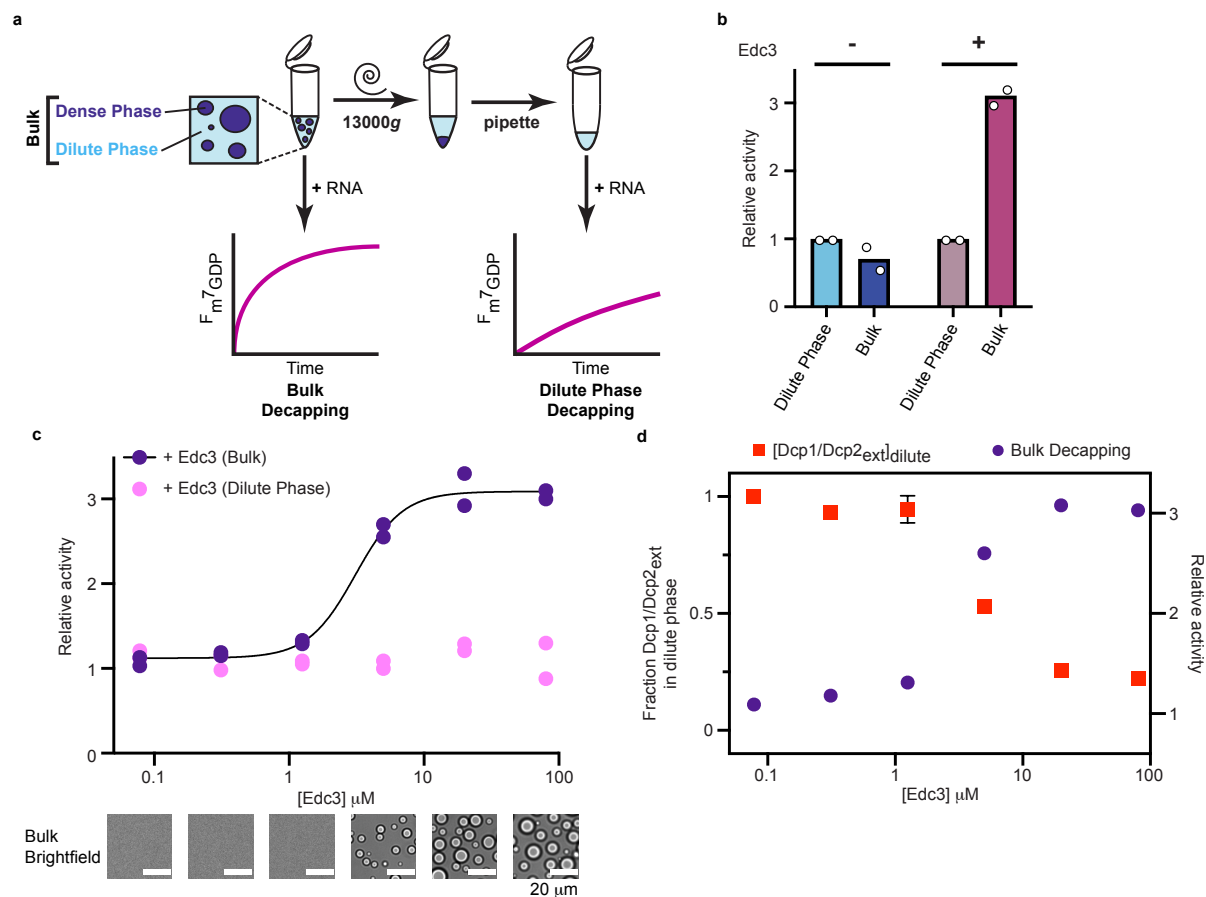


**Figure 3.4: Edc3 couples activation of decapping to phase separation.** **a**, Schematic of *in vitro* decapping assay to determine contribution of decapping activity from Dcp1/Dcp2<sub>ext</sub> in droplets (Dense Phase) and outside droplets (Dilute Phase). **b**, Dcp1/Dcp2<sub>ext</sub> localized in droplets does not strongly contribute to overall activity (blue bars) but removal of Dcp1/Dcp2<sub>ext</sub>/Edc3 droplets strongly diminishes activity (pink bars). Concentration of Dcp1/Dcp2<sub>ext</sub> is 100  $\mu\text{M}$  and 5  $\mu\text{M}$  in absence or presence of 80  $\mu\text{M}$  Edc3, respectively. Relative activity refers to ratio of observed rate to dilute phase. **c**, Activation of decapping by Edc3 is concomitant with formation of microscopically visible droplets. Removal of droplets abrogates activation by Edc3. **d**, Edc3 activation coincides with depletion of Dcp1/Dcp2<sub>ext</sub> (red squares) from solution. Curve showing mean Edc3 activation is reproduced from **c** for purposes of comparison. Relative activity refers to ratio of observed rate to Dcp1/Dcp2<sub>ext</sub> in dilute phase without Edc3. Decapping data are from two independent experiments. Pelleting data are presented as mean  $\pm$  s.e.m. for three independent experiments. Representative micrographs are from three independent experiments with similar results.

We characterized the ability of Edc3 to enrich Dcp1/Dcp2<sub>ext</sub> and RNA in droplets using a pelleting assay in conjunction with fluorescence microscopy. A decrease in Dcp1/Dcp2<sub>ext</sub> from dilute phase occurred at Edc3 concentrations coinciding with condensate formation (**Fig. 3.4d** and **Fig. S3.5c,d**). The  $K_{1/2}$  of Dcp1/Dcp2<sub>ext</sub> depletion (4.3  $\mu\text{M}$ ) agrees with the  $K_{1/2}$  of Edc3 activation (3.3  $\mu\text{M}$ ), indicating decapping activation and phase separation are coupled. Depletion of Edc3 from the dilute phase was not responsible for the differential activity observed

because Edc3 accumulated in the dilute phase (**Fig. S3.5c**). Edc3 did not affect RNA partitioning but did increase RNA mobility in condensates and enhance Dcp1/Dcp2<sub>ext</sub> partitioning with RNA (**Fig. S3.6a-c**). Our results suggest Edc3 reorganizes interactions in condensates and couples catalytic activation to phase separation to compartmentalize decapping activity.

### **Edc3 shifts a conformational equilibrium in Dcp1/Dcp2**

Dcp1/Dcp2 is dynamic and exists in multiple states preceding formation of a catalytically active complex (**Fig. 3.5a**)<sup>44</sup>. In the absence of activators and substrate, Dcp1/Dcp2<sub>core</sub> is in equilibrium between an inactive form where the cap binding site and RNA binding channel are occluded and a precatalytic form that can bind RNA and is on-pathway to decapping<sup>45–48</sup>. We used NMR spectroscopy to understand how the Dcp2 C-terminus and Edc3 affect the Dcp1/Dcp2 equilibrium to inhibit and activate decapping under conditions where Dcp1/Dcp2<sub>ext</sub> does not phase separate and then asked if a similar mechanism is responsible for activation in condensates.

Studying conformational dynamics in proteins containing large IDRs is challenging due to significant overlap of crosspeaks in the NMR spectra. To overcome this, we prepared a segmentally-labelled Dcp1/Dcp2<sub>ext</sub> that retains activity and gives a well-dispersed spectrum, allowing for transfer of assignments from Dcp1/Dcp2<sub>core</sub> (**Fig. S3.7a-c** and **S3.8a**). The Dcp2 C-terminus caused global chemical shift perturbations in Dcp1/Dcp2<sub>core</sub>, suggesting it interacts with or reorganizes Dcp1/Dcp2<sub>core</sub> (**Fig. S3.9a,b**). While perturbations caused by the C-terminus indicate an equilibrium involving more than two states, chemical shifts in the CD are largely colinear with those caused by the Dcp2 NRD and Dcp1, suggesting the C-terminus influences the inactive—precatalytic equilibrium (**Fig. 5b** and **Fig. S3.10a**). Because this equilibrium is fast on the NMR chemical shift timescale, resonance positions report on the population-weighted average of the two states. Assuming the magnetic environment of the isolated CD approximates



the precatalytic state, we conclude the C-terminus increases the population of the inactive form (Fig. 3.5c)<sup>45,49</sup>. Additionally, Dcp1/Dcp2<sub>ext</sub> interaction with RNA is disfavored relative to Dcp1/Dcp2<sub>core</sub> as shown by a ten-fold increase in the  $K_d$  (Fig. 3.5c, Fig. S3.11a, and Table S3.6). Together, these results implicate stabilization of the inactive state as the mechanism for autoinhibition.

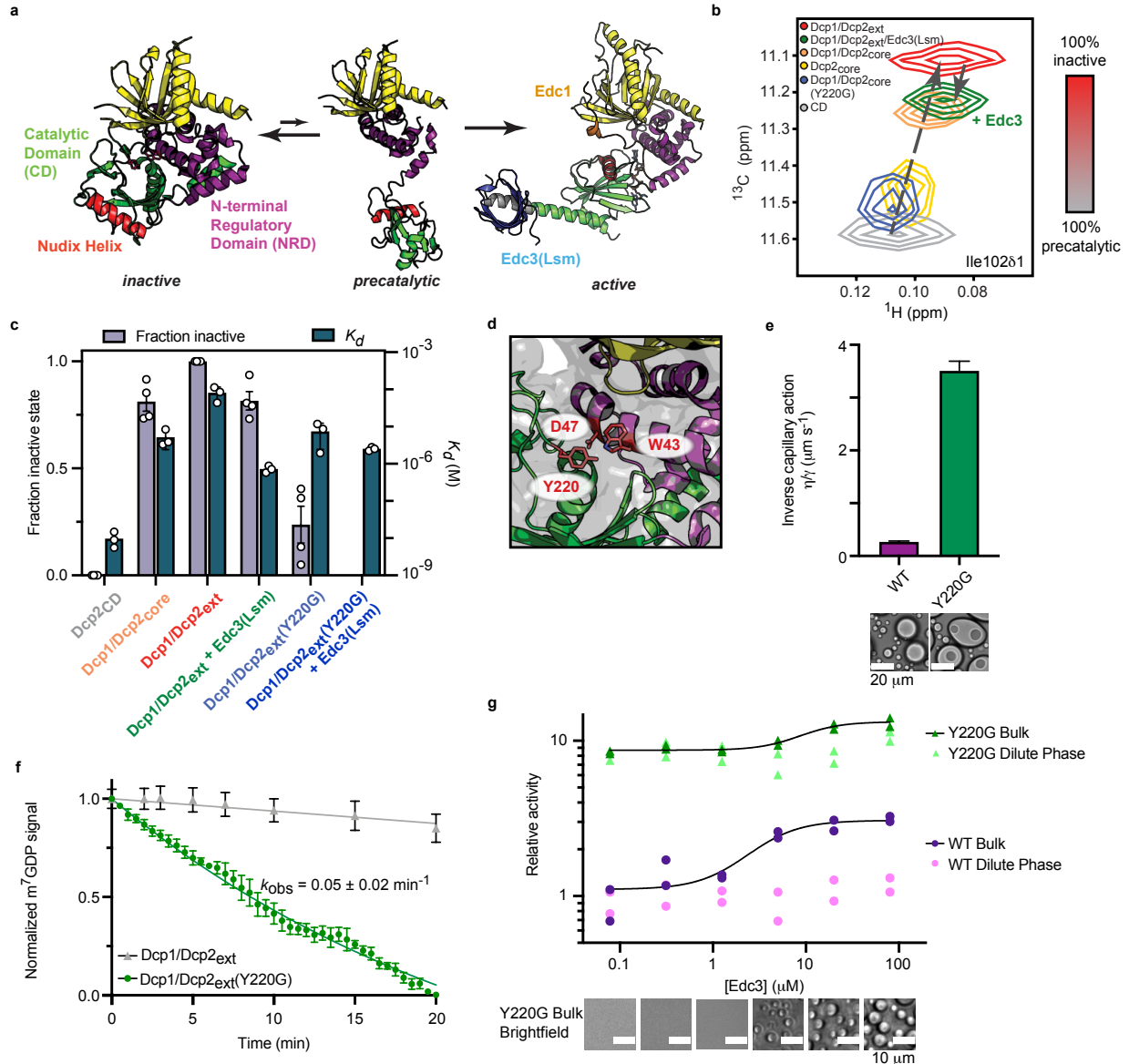


**Figure 3.5: The Dcp2 C-terminus stabilizes an autoinhibited conformation required for regulation of decapping in condensates.** **a**, Dcp2 conformation is in a fast equilibrium between inactive and precatalytic states (PDB: 2QKM). Activators Edc1 and Edc3 stabilize the active state (PDB: 6AM0). Dcp1/Dcp2<sub>core</sub> is colored as in Figure 1a and the Nudix Helix, which contains catalytic residues is colored red. **b**,  $^1\text{H}/^{13}\text{C}$ -HSQC of methyl group in Ile102 undergoes linear chemical shift changes toward the inactive state when the Dcp2 regulatory domain, Dcp1, and the Dcp2 C-terminus are added. Edc3 and Y220G mutation in the Dcp2 catalytic domain revert the chemical shift toward the precatalytic state. **c**,

The population of the inactive state correlates with weakened RNA binding by Dcp1/Dcp2. Data from four NMR resonances and three independent RNA binding experiments are presented as mean  $\pm$  s.e.m. **d**, Y220 residue in the Dcp2 catalytic domain occludes residues critical for m<sup>7</sup>G recognition (W43 and D47) in the inactive state. **e**, Dcp1/Dcp2<sub>ext</sub>(Y220G) droplets do not relax to a spherical state after fusion, contain subcompartments, and exhibit a ten-fold greater viscosity-to-surface tension ratio relative to wild-type Dcp1/Dcp2<sub>ext</sub> droplets. Protein concentration is 100  $\mu$ M. Reported error is standard error of the fit to data in Extended Data Fig. 5c. **f**, Dcp1/Dcp2<sub>ext</sub>(Y220G) increases decapping of dual-labeled RNA substrate 10-fold in droplets. Wild-type Dcp1/Dcp2<sub>ext</sub> data from Fig. 3.3g is reproduced for comparison. m<sup>7</sup>GDP intensity is normalized to initial fluorescence signal. Data are presented as mean  $\pm$  s.e.m for twenty droplets examined over two independent experiments. **g**, The Y220G mutation activates decapping and minimizes contribution from decapping in condensates. Data presented are from two independent experiments and relative activity is determined by ratio of observed rates to wild-type Dcp1/Dcp2<sub>ext</sub> in absence of Edc3. Representative micrographs are from three independent experiments with similar results.

We next asked if Edc3 alleviates autoinhibition by shifting the conformational equilibrium of Dcp1/Dcp2<sub>ext</sub> to the precatalytic form. To prevent NMR resonance broadening, we assayed activation using the Edc3 Lsm domain, Edc3(Lsm), which is sufficient to enhance Dcp2 catalysis and abrogates phase separation (**Fig. 3.2c**)<sup>36</sup>. Globally, Edc3(Lsm) reduced the perturbations observed in Dcp1/Dcp2<sub>ext</sub> to more closely resemble Dcp1/Dcp2<sub>core</sub>, indicating fewer interactions or rearrangements between the Dcp2 C-terminus and core domains (**Fig. S3.9a,b**). In addition, Edc3(Lsm) caused migration of Dcp1/Dcp2<sub>ext</sub> resonances along the linear trajectory toward Dcp1/Dcp2<sub>core</sub>, suggesting an increase in the fraction of precatalytic Dcp1/Dcp2<sub>ext</sub> complex (**Fig. 3.5b,c** and **Fig. S3.10a**). Edc3(Lsm) also decreased Dcp1/Dcp2<sub>ext</sub>  $K_d$  for RNA 100-fold (**Fig. 3.5c**, **Fig. S3.11a**, and **Table S3.6**). We conclude Edc3 activates decapping by favoring the precatalytic conformation and enabling RNA recognition and hydrolysis.

### Conformational changes control decapping in condensates

We previously predicted a conserved aromatic residue in the Dcp2 catalytic domain (Y220) stabilizes the inactive state by contacting residues critical for m<sup>7</sup>G recognition (W43 and D47) (**Fig. 3.5d**)<sup>36</sup>. Supporting this, mutating Y220 to glycine (Y220G) alleviates autoinhibition and bypasses Edc3 activation<sup>36</sup>. We evaluated whether this gain-of-function arises from changes in the precatalytic—inactive equilibrium in Dcp1/Dcp2. Chemical shifts reporting on this equilibrium underwent significant perturbations toward the precatalytic state, indicating Y220G disrupts formation of the inactive conformation (**Fig. 3.5b,c** and **Fig. S3.10a**). In addition, the

Y220G mutation increased RNA binding in Dcp1/Dcp2<sub>ext</sub>, making it largely insensitive to Edc3 (**Fig. 3.5c**, **Fig. S3.11a**, and **Table S3.6**). These observations confirm Edc3 favors the precatalytic conformation of Dcp1/Dcp2 and demonstrates how the Y220G mutation bypasses Edc3 activation.

Interactions important for autoinhibition are also crucial for Dcp1/Dcp2<sub>ext</sub> droplet formation (**Fig. 3.2c,d**). We next used the Y220G mutation to ask if Dcp1/Dcp2<sub>ext</sub> phase separation and conformational equilibrium are coupled. Dcp1/Dcp2<sub>ext</sub>(Y220G) forms droplets with altered physicochemical properties that contain substructures and fail to properly relax after fusion, with a 10-fold increase in inverse capillary action relative to wild-type (**Fig. 3.5e**, **Fig. S3.11b**). This suggests the conformational equilibrium of Dcp1/Dcp2 is coupled to the liquid-like properties of condensates and Y220 may be required for interactions promoting phase separation.

The Y220G mutation destabilizes the inactive state of Dcp1/Dcp2 and alters Dcp1/Dcp2<sub>ext</sub> droplets. These observations predict the Y220G mutation may activate decapping in condensates because interactions important for Dcp1/Dcp2<sub>ext</sub> droplet formation promote the inactive state. Dcp1/Dcp2<sub>ext</sub>(Y220G) decaps the dual-labeled RNA in droplets at 0.05 min<sup>-1</sup>, 10-fold faster than wild-type (**Fig. 3.5f**, **Fig. S3.11c**). We conclude the formation of the inactive state is crucial for repressing decapping activity in Dcp1/Dcp2<sub>ext</sub> condensates.

Similar to Edc3, the Y220G mutation promotes the precatalytic conformation. If Edc3 cannot conformationally regulate Dcp1/Dcp2, then its ability to couple activation and phase separation may be impaired. Activity partitioning experiments show Dcp1/Dcp2<sub>ext</sub>(Y220G) enhanced decapping 8-fold and Edc3 minimally activated decapping (**Fig. 3.5g** and **Table S3.7**). In addition, Edc3-mediated activation and phase separation were no longer correlated (**Fig. S3.11d**). Thus, the Y220G mutant decouples activation from phase separation to stimulate Dcp2 catalysis inside or outside condensates. We conclude Dcp2 conformation is crucial for proper regulation and compartmentalization of mRNA decapping activity in condensates.

### **Strong activation of Dcp2 requires condensate rewiring**

Edc1 promotes the active conformation of Dcp2 through a mechanism distinct from Edc3 and activates decapping to a greater extent than Edc3 in solution (**Fig. 3.5a**)<sup>36,45</sup>. Because Edc1 disrupts the inactive state, we hypothesized it acts similar to the Y220G mutation and activates decapping in both the bulk and dilute phases. We found Edc1 activated decapping >10-fold and Edc3 did not further enhance catalysis (**Fig. 3.6a** and **Table S3.8**). Additionally, Edc1 increases the critical concentration of Dcp1/Dcp2<sub>ext</sub> and Edc3 phase separation. While Edc1 increased the rate of Dcp1/Dcp2<sub>ext</sub> catalysis in condensates, full activation required both Edc1 and Edc3 (**Fig. 3.6b**). Thus, Edc3-mediated rearrangements are necessary to overcome the repressed catalytic environment of Dcp1/Dcp2<sub>ext</sub> condensates to promote maximal activation.

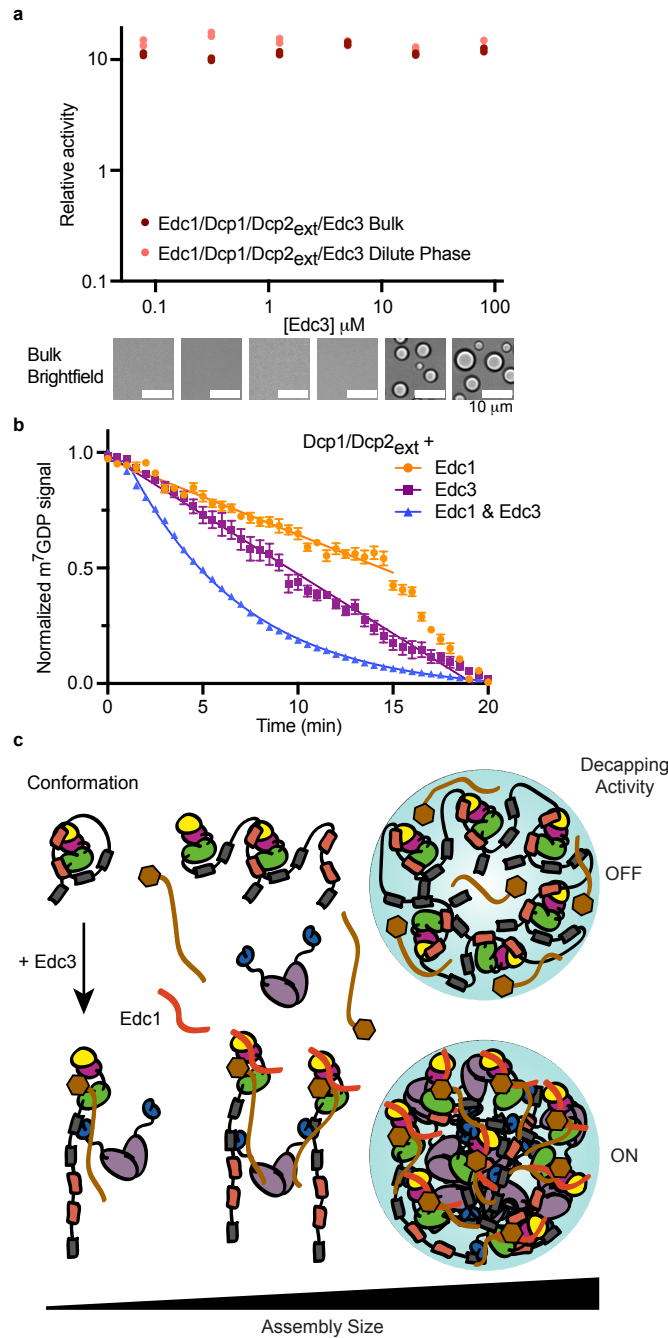


**Figure 3.6: Maximum activation of Dcp1/Dcp2<sub>ext</sub> in condensates requires Edc3.** **a**, Edc1 activates Dcp1/Dcp2<sub>ext</sub> independent of Edc3-mediated phase separation and abrogates contribution of decapping in condensates. Data from two independent experiments are shown and relative activity reflects ratio between observed rates and rates for Dcp1/Dcp2<sub>ext</sub> in absence of Edc1 and Edc3. Representative micrographs are from three independent experiments with similar results. **b**, Edc1 activates Dcp1/Dcp2<sub>ext</sub> in droplets but requires Edc3 for maximal activation. Data represents mean  $\pm$  s.e.m from twenty droplets examined over two independent experiments. **c**, Model showing how Edc3 mediates a conformational change in Dcp1/Dcp2 that is coupled to an alteration of the protein-protein interactions promoting higher-order assemblies found in condensates. These changes in interactions switch decapping activity from an off to on state. Edc1 stabilizes the active conformation to activate Dcp1/Dcp2 inside and outside condensates.

## DISCUSSION

We addressed the influence of phase separation on RNA decapping by Dcp1/Dcp2. We found decapping can be both repressed and activated in condensates (**Fig. 3.6c**). We explain this differential activity by demonstrating changes in Dcp1/Dcp2 conformation are coupled to alterations in the protein network underlying condensate formation. IMs in Dcp2 stabilize an autoinhibited conformation and drive self-association into condensates repressed in decapping activity. The activator Edc3 rectifies this inhibited environment to promote mRNA decapping in condensates by rewiring interactions and causing a conformational change in Dcp1/Dcp2 important for substrate recognition. Edc1 and a mutation in Dcp2 destabilize the inactive conformation of Dcp1/Dcp2 to activate decapping inside and outside condensates. Our work suggest IDRs of enzymes can couple phase separation to conformational control of activity.

Edc3 activates decapping 90-fold in droplets, which is in contrast to the three-fold stimulation determined in bulk experiments (**Fig. 3.3** and **3.4**). The amplification of decapping activation in condensates is greater than in the surrounding solution because phase separation strongly inhibits Dcp1/Dcp2 activity. Our results demonstrate the C-terminus of Dcp2 favors an inactive state and it is possible this equilibrium is further shifted in condensates to repress enzyme activity. Consistent with this view, a mutation in Dcp2 (Y220G) disfavors the autoinhibited state to activate decapping and alters the material properties of Dcp1/Dcp2 condensates (**Fig. 3.5**). These observations suggest active site conformation is coupled to long-range interactions in condensates to directly regulate activity. Evaluating enzyme dynamics in condensates is an exciting challenge for the future.

Macromolecular composition and conformation are important for regulating specificity in biochemical processes in condensates<sup>1,6,7,9</sup>. We propose composition and the underlying interactions serve as a mechanism to allosterically inhibit or activate enzymatic activity. In the framework of 5'-3' mRNA decay, cells may leverage this feature to minimize aberrant degradation events that would result from widely distributed decay mRNPs. In support, the

Y220G mutation and Edc1 decouple activation from phase separation to cause rapid decapping with rates indistinguishable inside or outside condensates. The widespread, accelerated decapping could explain the conditional lethality observed for both the Y220 mutation and removal of the Dcp2 C-terminus in yeast<sup>47</sup>. Furthermore, Edc1-like activators may co-opt this allosteric regulation under conditions of cellular stress to target mRNA for degradation independent of phase separation. Future examination of the cooperation between cofactors will be critical to understanding how enzymatic activity is regulated in biochemical pathways enriched in condensates.

Our reconstitution of condensates containing the eukaryotic decapping machinery largely recapitulates the micromolar concentrations observed in P-bodies<sup>32</sup>. Previous *in vitro* analysis indicated decapping activity in bulk solution was two-fold inhibited in the presence of Dcp1/Dcp2/Edc3 condensates and excess RNA<sup>42</sup>. We observed similar inhibition of initial decapping rates in condensates when RNA is in excess, however decapping was still activated 25-fold relative to Dcp1/Dcp2<sub>ext</sub> condensates (**Fig. S3.3g**). This activation arises from the presence of inhibitory motifs in Dcp2 that increase repression of activity in condensates, which was not observed in prior studies that lacked these motifs<sup>42</sup>. The data presented here underscore the complementarity of monitoring both the phase-separated environment and bulk solution to uncover mechanistic insights into the regulation of enzymatic activity in condensates. Furthermore, the fluorescent probes developed here can be used to examine molecular mechanisms in other condensates important for RNA biology.

Phase separation is important for regulating numerous enzymatic processes. We demonstrate the importance of mesoscale phase-separated assemblies in regulating mRNA decapping. The interplay between composition, molecular interactions, and active site conformation in Dcp2 condensates underscore the complexity of phase separation in cellular processes. The emergent properties afforded by phase separation equip cells with highly

regulatable sites of enzyme activity that may explain why P-bodies and other biomolecular condensates can give rise to multiple biochemical outcomes.

## METHODS

### Protein Expression and Purification

See **Table S1** for protein constructs, solubility tags, and expression vectors used in this study. Dcp1/Dcp2 constructs were expressed in *E. coli* BL21(DE3) (New England Biolabs) grown in LB medium. Cells were grown at 37°C until OD<sub>600</sub> = 0.6–0.8 and transferred to 4°C for 30 min before induction with 0.75 mM IPTG. Cells were induced for 16–18 hours at 20–25°C. Cells were harvested at 5000g, resuspended in lysis buffer (25 mM HEPES pH 7.5, 400 mM NaCl, 10 mM 2-mercaptoethanol, 0.1% Triton X-100) supplemented with lysozyme and protease inhibitor cocktail (Roche), lysed by sonication (50% duty cycle, 4 × 1 min), and clarified at 16,000g. Clarified lysate was loaded onto a StrepTrap column (GE Healthcare), washed with 10 column volumes (CV) lysis buffer without detergent followed by a second wash with 10 CV 25 mM HEPES pH 7.5, 100 mM NaCl, 10 mM 2-mercaptoethanol. Step elution of target proteins was performed with 25 mM HEPES pH 7.5, 100 mM NaCl, 1 mM DTT, 5 mM desthiobiotin. For Edc3 and Dcp1/Dcp2 constructs lacking a C-terminal StrepII tag, a HisTrap column (GE Healthcare) was used in place of the StrepTrap. For purification by HisTrap, the lysis and wash buffers described above were supplemented with 10 mM imidazole and contained 10 mM 2-mercaptoethanol in place of DTT. Proteins were eluted from the HisTrap column in 10CV wash buffer supplemented with 250 mM imidazole and incubated overnight with TEV protease. Following Strep purification or TEV digestion, target proteins were loaded onto a HiTrap Heparin column (GE Healthcare) and washed with 10CV low salt buffer (25 mM HEPES pH 7.5, 100 mM NaCl, 1 mM DTT). Protein elution then occurred over a 10CV gradient to 100% high salt buffer (25 mM HEPES pH 7.5, 1 M NaCl, 1 mM DTT). Proteins were purified with a final size-exclusion chromatography step using a Superdex75 or 200 16/60 column (GE Healthcare) equilibrated in



25 mM HEPES pH 7.5, 150 mM NaCl, 1 mM DTT. Proteins were analyzed by SDS-PAGE, concentrated, and flash frozen in liquid nitrogen for storage at -80°C.

A pET29 plasmid encoding a pentamutant SortaseA( $\Delta$ 59) construct from *S. aureus* with improved activity (eSrtA) was obtained from Addgene (plasmid #75144) and expressed in LB medium at 18°C for 16 hours<sup>50</sup>. Cells were pelleted at 5000g and resuspended in lysis buffer containing 50 mM Tris pH 8, 300 mM NaCl, 10 mM imidazole, 1 mM MgCl<sub>2</sub>, and protease inhibitors (Roche). Following sonication (50% duty cycle, 4 × 1 min) the lysate was clarified at 16000g. Clarified lysate was passed over a HisTrap Nickel affinity purification column, and eSrtA was eluted in 25 mM HEPES pH 7.5, 150 mM NaCl, 250 mM imidazole. A final dialysis against 25 mM HEPES pH 7.5, 150 mM NaCl was performed overnight at 4°C. Dialyzed eSrtA was concentrated to 1 mM final concentration and flash frozen for storage and later use.

### **Fluorescent-labeling of purified proteins and RNAs**

Fluorescent Dcp1/Dcp2<sub>ext</sub> and Edc3 were generated by diluting the protein to 0.5 mg/mL and dialyzing at 4°C for four hours in size exclusion buffer without DTT. Cy5 or Fluorescein maleimide (Thermo-Fisher) was added to the protein solution in 5-fold molar excess and incubated for one hour at room temperature. The reaction was quenched with 10 mM  $\beta$ -ME and free dye was separated from labelled protein by Illustra NICK columns (GE Healthcare). Labelled protein was exchanged back into size exclusion buffer containing DTT by concentrating and diluting 10-fold three times. Labelling efficiency and concentrations were calculated by UV-Vis spectroscopy. Labelled oligonucleotides were purchased from Integrated DNA Technologies with a 5' 6-FAM modification.

### **Brightfield and Fluorescence Microscopy**

Microscopy images were collected on an inverted widefield fluorescence Nikon Ti-E microscope equipped with a Hamamatsu Flash4.0 camera using PlanApo 20x or 40x air objectives. Samples were imaged in a Greiner Bio-One 384-well glass bottom plate PEGylated

using 20 mg/mL PEG-Silane (Laysan Bio, MPEG-SIL-5000) and passivated with 100 mg/mL BSA as described<sup>51</sup>. Prior to addition of samples, the wells were washed 3x with 25 mM HEPES pH 7.5, 150 mM NaCl, 1 mM DTT. Dcp1/Dcp2 constructs assayed for phase separation by microscopy were prepared by initiating removal of the N-terminal MBP solubility tag with 1:40 molar equivalent TEV:Dcp1/Dcp2. Dcp1/Dcp2/Edc3 droplets were prepared by incubating Dcp1/Dcp2 and Edc3 prior to removal of the N-terminal MBP tag from Dcp1/Dcp2<sub>ext</sub>. Imaging was performed after 30 minutes to ensure TEV cleavage and droplet. Image analysis was performed using ImageJ<sup>52</sup>. For localization and enrichment of Dcp1/Dcp2<sub>ext</sub>, Edc3, or RNA in droplets, 1%-5% protein concentration was fluorescently labelled. Enrichment was estimated from the average ratio of intensity in at least twenty droplets ( $I_{\text{droplet}}$ ) to average intensity in surrounding solution ( $I_{\text{dilute}}$ ).

### **Fluorescence recovery after photobleaching (FRAP) assays**

For experiments examining Dcp1/Dcp2<sub>ext</sub> recovery, condensates were formed with 40  $\mu\text{M}$  Dcp1/Dcp2<sub>ext</sub>. Experiments monitoring the effects of Edc3 were performed with 5  $\mu\text{M}$  Dcp1/Dcp2 and 5  $\mu\text{M}$  or 80  $\mu\text{M}$  Edc3. For analysis of RNA recovery, condensates were formed with 40  $\mu\text{M}$  Dcp1/Dcp2<sub>ext</sub> with or without Edc3 and FITC-29mer RNA was added. The concentration of labeled protein or RNA was 250 nM across all samples. Samples were imaged in a passivated glass bottom 384-well plate (Greiner Bio-One). Imaging was performed at room temperature using an inverted Nikon Ti microscope equipped with an Andor Borealis CSU-W1 spinning disk confocal, Plan Apo VC 100x/1.4 oil objective and Andor iXon Ultra DU888 EMCCD camera. For each photobleaching experiment, a rectangular region of interest (ROI) was drawn around single condensates and irradiated for 1.5s with 7mW power at 473 nm with a Vortran laser between the fifth and sixth acquired frame. For analysis, three ROIs were used corresponding to the bleached droplet, an unbleached droplet, and background. Analysis was performed using ImageJ. Recovery traces were obtained by performing a double normalization

to account for photobleaching during image acquisition<sup>53</sup>. Recovery  $t_{1/2}$  and immobile fractions were determined from fits of single exponentials using Prism 8/9 (GraphPad) and are reported in Supplementary Table 2.

### **Synthesis of dually labelled RNA probe**

The reagents for RNA labelling, FAM-m<sup>7</sup>Gp<sub>3</sub>A<sub>m</sub>pG and pAp-SCy5, were synthesized by modifications of previously reported methods<sup>54,55</sup>. FAM-m<sup>7</sup>G-capped RNA was generated on the template of annealed oligonucleotides, which contained a T7 A $\phi$ 2.5 promoter sequence (CAGTAATACGACTCACTATT) and encoded a 35-nt-long sequence (AGG GAAGCG GGCATG CGGCCA GCCATA GCCGAT CA). Typical *in vitro* transcription reaction (100  $\mu$ L) was carried out at 37 °C for 4 h and contained RNA Pol buffer (40 mM Tris-HCl pH 7.9, 6 mM MgCl<sub>2</sub>, 1 mM DTT, 2 mM spermidine), 10 U/ $\mu$ L T7 polymerase (ThermoFisher Scientific), 1 U/ $\mu$ L RiboLock RNase Inhibitor (ThermoFisher Scientific), 0.5 mM CTP/GTP/UTP, 0.125 mM ATP, 0.625 mM FAM-m<sup>7</sup>Gp<sub>3</sub>A<sub>m</sub>pG cap and 0.1  $\mu$ M annealed oligonucleotides as a template. Following 4 h incubation, the template was removed by treatment with 1 U/ $\mu$ L DNase I (ThermoFisher Scientific) for 30 min at 37 °C. The crude RNAs were purified using RNA Clean & Concentrator-5 (Zymo Research). Transcripts quality was checked on 15% acrylamide/7 M urea gels, whereas the concentration was determined spectrophotometrically.

The obtained transcripts were directly used in the ligation step with a Sulfo-Cy5 (SCy5) labelled pAp analogue. A typical ligation reaction (30  $\mu$ L) was carried out at 16 °C overnight and contained 5' capped RNA (1  $\mu$ M), 1 U/ $\mu$ L T4 RNA ligase 1 (New England Biolabs), 1.3 U/ $\mu$ L Ribolock RNase inhibitor (ThermoFisher Scientific), 100  $\mu$ M pAp-SCy5 analogue, 0.1 volumes of DMSO (3  $\mu$ L), 0.03 volumes of 0.1 M DTT (1  $\mu$ L) and 0.1 volumes of 10 mM ATP (3  $\mu$ L). The resulting dually labelled RNA was first purified using RNA Clean & Concentrator-5 (Zymo Research) followed by the final HPLC purification (Clarity® 3  $\mu$ M Oligo-RP phenomenex column, linear gradient from 5% to 35% ACN in 50 mM TEAAc pH 7 over 15 min at 50 °C, Agilent

Technologies Series 1200 HPLC). The collected fractions were freeze dried 3 times. RNA quality, before and after each purification step, was checked on 15% acrylamide/7 M urea gels (**Fig. S3**), whereas the concentration was determined spectrophotometrically.

### **Visualization of Decapping by Microscopy**

60  $\mu\text{M}$  Dcp1/Dcp2<sub>ext</sub> and Dcp1/Dcp2<sub>ext</sub>(Y220G) droplets were prepared in 25 mM HEPES pH 7.5, 150 mM NaCl, 1 mM DTT, 1 mM EDTA, and 4U RNase inhibitor. To these reactions, 100 nM dual-labeled RNA and initial images were collected in passivated glass bottom wells to observe droplet localization. Decapping was initiated with 5 mM MgCl<sub>2</sub> and control reactions were performed without addition of metal. To study the effects of Edc3, condensates were formed with 5  $\mu\text{M}$  Dcp1/Dcp2<sub>ext</sub> and 80  $\mu\text{M}$  Edc3. For experiments visualizing Edc3 activation in pre-formed Dcp1/Dcp2 condensates, 60  $\mu\text{M}$  Dcp1/Dcp2<sub>ext</sub> and 100 nM RNA were incubated with TEV for 30 minutes at room temperature. Next, Edc3 was added 10 minutes prior to reaction initiation described above. To monitor the effects of RNA abundance on condensate decapping, experiments were performed at substoichiometric and superstoichiometric ratios RNA:Dcp1/Dcp2<sub>ext</sub>. For RNA limiting experiments, 1  $\mu\text{M}$  Dcp1/Dcp2 and 15  $\mu\text{M}$  Edc3 were mixed together and 100 nM dual-labeled 35mer RNA was added. For experiments with excess RNA, the RNA probe was supplemented with 19.9  $\mu\text{M}$  capped, unlabeled 35mer. Experiments evaluating Edc1 and Edc3 coactivation were performed at pH 6.5 to slow catalysis, which allowed for adequate image acquisition. Dcp1/Dcp2<sub>ext</sub> was kept at 40  $\mu\text{M}$  and 80  $\mu\text{M}$  Edc1 and Edc3 were added individually or in combination prior to initiation of decapping with 5 mM MgCl<sub>2</sub>. For all experiments, images were collected in both the fluorescein and Cy5 channels and the mean droplet intensity was background corrected and calculated in ImageJ. Mean intensity was plotted as function of time and fit to a first-order exponential decay function (GraphPad Prism 8/9) except in experiments examining the effects of RNA abundance, which were fit to a second-order exponential.

## Monitoring of decapping using fluorescence polarization

Serially-diluted Dcp1/Dcp2<sub>core</sub> in 25 mM Hepes pH 7.5, 150 mM NaCl, 1 mM DTT was incubated with 5 nM RNA probe in a low volume, low binding 384 well plate (Greiner Bio-One) for 10 minutes. Reactions were monitored using a SpectraMax plate reader (Molecular Dynamics). An initial FP reading was taken to represent time '0' just prior to addition of 5 mM MgCl<sub>2</sub> and rapid mixing. Time-dependent changes in signal were monitored for 30 minutes and curves were fit to the equation:

$$\text{mP} = (Y_o - Y_{\text{min,cap}})e^{-k_1t} + (Y_{\text{min,obs}} - Y_{\text{min,cap}})(1 - e^{-k_2t}) + Y_{\text{min,cap}} \quad (1)$$

where  $Y_o$  is the mP value at time zero,  $Y_{\text{min,cap}}$  is the background mP from free FAM-m<sup>7</sup>GDP,  $Y_{\text{min,obs}}$  is the minimum observed mP observed during the course of the experiment, and  $k_1$ ,  $k_2$  are constants free to vary in fitting. We assume a decrease in mP is a consequence of decapping, which results in release of product FAM-m<sup>7</sup>GDP with rate  $k_1$ . However, m<sup>7</sup>GDP product can also interact with Dcp1/Dcp2 with an observed rate of  $k_2$  to cause a concentration-dependent elevation in the endpoint mP. Determined  $k_1$  values at each concentration were plotted and fit to a single turnover Michaelis-Menten model to determine  $k_{\text{max}}$ .

## In Vitro Decapping Assays

Synthetic 5'-triphosphate 29mer RNA (TriLink BioTechnologies) derived from the MFA2 gene of *S. cerevisiae* was enzymatically capped with GTP[ $\alpha$ -<sup>32</sup>P] and S-adenosylmethionine (SAM) as previously described<sup>56</sup>. Reactions were carried out in 25 mM HEPES pH 7.5, 150 mM NaCl, 5 mM MgCl<sub>2</sub>, 0.1 mg/mL acetylated BSA with 4U RNase inhibitor. For monitoring decapping in Dcp1/Dcp2<sub>ext</sub> condensates, 100  $\mu$ M total concentration was used. Prior to assays monitoring Edc3 activation, the MBP tag was removed from Dcp1/Dcp2<sub>ext</sub> using TEV and separated using Amylose resin. For reactions monitoring Edc3 activation, Dcp1/Dcp2<sub>ext</sub> was kept constant at 5  $\mu$ M while Edc3 was varied from 78.1 nM to 80  $\mu$ M. For reactions examining coordinated activation of decapping by Edc1 and Edc3, Edc1 was kept constant at 150  $\mu$ M.

Dcp1/Dcp2<sub>ext</sub> concentrations were always at least 10-fold excess over RNA to prevent product inhibition. 1.5x protein and 3x RNA solutions were equilibrated separately for 30 minutes at room temperature to allow formation of liquid droplets. To evaluate Dcp1/Dcp2<sub>ext</sub> activity in dilute phase, the bulk solution was centrifuged for 10 minutes at 13000g after incubation to pellet droplets and the supernatant was removed for subsequent assays. Reactions were initiated by mixing 15 μL 1.5x protein and 7.5 μL 3x RNA solutions. Time points were taken by quenching the reaction with excess EDTA and TLC was used to resolve m<sup>7</sup>GDP product from capped RNA. The formation of product was quantified using a GE Healthcare Typhoon 9410 scanner and ImageQuant 7 software. Observed rates,  $k_{obs}$ , were determined by fitting to a first-order exponential. Relative activity was determined by normalizing the observed rates to the dilute phase (**Fig. 3.4b**) or to 5 μM Dcp1/Dcp2 in solution (**Fig. 3.4c, 3.5g, 3.6a, Fig. S3.8a**). To examine Edc3 activation,  $k_{obs}$  versus Edc3 concentration was fit to the model:

$$k_{obs} = \frac{k_{max}[E]^n}{K_{1/2}^n + [E]^n} \quad (2)$$

in order to obtain  $k_{max}$ ,  $K_{1/2}$ , and  $n$ . See Tables **S3-5**, and **S7-8** for absolute decapping rates.

### **Dcp1/Dcp2<sub>ext</sub> pelleting assay**

Loss of Dcp1/Dcp2<sub>ext</sub> from solution due to phase separation as a function of Edc3 concentration was monitored by loss of fluorescent Dcp1/Dcp2<sub>ext</sub> signal. Briefly, 5 μM Dcp1/Dcp2<sub>ext</sub> (250 nM Cy5-labeled) was incubated with Edc3 concentrations used in the *in vitro* decapping assay experiments. Following a 30-minute incubation at room temperature, droplets were pelleted by centrifugation at 13000g for 10 minutes. The supernatant was removed and placed in a Greiner Bio-One 384-well low volume, low binding plate. Fluorescence intensity was measured on a BioTek Synergy H4 plate reader and normalized to give a fractional amount remaining in solution. In addition, the supernatant was analyzed using denaturing 4-12% Tris-glycine SDS-PAGE. Disappearance of Dcp2 was quantified using a region of interest of the same size in ImageJ and subtracting background signal.

### **Expression of labeled Dcp1/Dcp2 for NMR**

ILVMA methyl labeling of Dcp2 or Dcp1/Dcp2 constructs was carried out in D<sub>2</sub>O M9 minimal media with <sup>15</sup>NH<sub>4</sub>Cl and <sup>2</sup>H/<sup>12</sup>C-glucose as the sole nitrogen and carbon sources, respectively. Labeled precursors (Ile: 50 mg L<sup>-1</sup>, Leu/Val: 100 mg L<sup>-1</sup>, Met: 100 mg L<sup>-1</sup>, Ala: 100 mg L<sup>-1</sup>) were added 40 minutes prior to induction with 1 mM IPTG. Following overnight incubation at 20-25°C, cells were lysed and purified using nickel affinity purification, TEV digestion, heparin, and size exclusion chromatography as described above.

### **SortaseA Ligation of segmentally-labeled Dcp1/Dcp2 for NMR**

Dcp1/Dcp2(1-266) containing a C-terminal LPETGGH *S. aureus* SortaseA recognition site and labeled at ILVMA terminal methyl groups was expressed and purified as described above. Purified protein was then mixed with at least five-fold molar excess His<sub>6</sub>-MBP-G<sub>3</sub>-Dcp2(274-504)-StrepII expressed in LB medium and purified using GE StrepTrap and Q ion exchange columns. eSrtA equal to 0.5 molar equivalent of Dcp1/Dcp2(1-266) and 2 mM CaCl<sub>2</sub> were added to the solution prior to initiation of the reaction with TEV protease, which cleaves the His<sub>6</sub>-MBP tag from G<sub>3</sub>-Dcp2(274-504)-StrepII to expose the required N-terminal glycine for ligation. The reaction was dialyzed against 25mM HEPES pH 7.5, 150 mM NaCl, 2 mM CaCl<sub>2</sub> overnight at 4°C<sup>57</sup>. Ligated Dcp1/Dcp2<sub>ext</sub>, containing a mutational scar from (267STAPSDL<sub>273</sub> in wild-type to 267LPETGGG<sub>273</sub>), was purified by heparin and StrepTrap chromatography as described. A final dialysis in 25 mM HEPES pH 7.5, 150 mM NaCl, 2 mM DTT was performed overnight at 4°C prior to NMR experiments.

### **NMR Experiments**

NMR samples were exchanged into a buffered D<sub>2</sub>O solution containing 25 mM HEPES pD 7.1, 150 mM NaCl, and 2 mM DTT using either dialysis or a centrifugal concentrator. Note the concentration of Dcp1/Dcp2<sub>ext</sub> was kept below its critical concentration and the Edc3 Lsm domain was used to prevent confounding effects from phase separation. NMR experiments

were performed on an 800 MHz Bruker Avance III or Avance NEO spectrometer equipped with a cryoprobe and Topspin3. Spectra were recorded at 298K, processed using NMRPipe, and analyzed using NMRFAM-Sparky<sup>58</sup>. Chemical shift perturbations ( $\Delta\delta$ , ppm) between Dcp1/Dcp2<sub>ext</sub> or Dcp1/Dcp2<sub>ext</sub>/Edc3(Lsm) and Dcp1/Dcp2<sub>core</sub> were calculated from the Euclidian equation:

$$\sqrt{(\delta H_{ext} - \delta H_{core})^2 + (0.2(\delta C_{ext} - \delta C_{core}))^2} \quad (3)$$

where 0.2 is a scaling factor for the carbon spectral width. CSPs were depicted on the inactive structure of Dcp1/Dcp2<sub>core</sub> using PyMOL. For calculation of the inactive state population ( $p_{inactive}$ ), we focused on resonances undergoing linear perturbations indicative of fast exchange and suggest a two-state equilibrium. The observed chemical shift was taken as the weighted average of the resonances corresponding to the precatalytic and inactive states: the catalytic domain (CD) of Dcp2 and Dcp1/Dcp2<sub>ext</sub>, respectively:

$$\Omega_{obs} = p_{precatalytic}\Omega_{CD} + p_{inactive}\Omega_{Dcp1/Dcp2ext} \quad (4)$$

From this relationship, the population of the inactive state can be calculated as:

$$p_{inactive} = \frac{\Omega_x - \Omega_{CD}}{\Omega_{Dcp1/Dcp2ext} - \Omega_{CD}} \quad (5)$$

where  $\Omega_x$  is the chemical shift for a given construct of Dcp1/Dcp2 (in ppm).

## Fluorescence Polarization

Fluorescence polarization (FP) was performed in Greiner Bio-One 384-well low volume, low binding plates. Conditions for all binding assays was 25 mM HEPES pH 7.5, 100 mM NaCl, 5 mM MgCl<sub>2</sub>, 0.02% Triton X-100, 0.1 mg/mL acetylated BSA and 4U RNase inhibitor with 5 nM 5'-phosphorylated oligo 30U RNA with 3' 6-FAM (IDT). Reactions were incubated for ten minutes before measuring polarization on a LJL Biosystems Analyst AD plate reader. Equilibrium dissociation constants ( $K_d$ ) were fit to the Hill equation for single-site binding:

$$mP = Y_0 + \frac{Y_{max}[X]^n}{K_d^n + [X]^n} \quad (6)$$



where  $[X]$  represents the concentration of protein,  $Y_0$  is the mP for the probe alone,  $Y_{\max}$  is the mP value at saturation, and  $n$  is the Hill coefficient. To prevent scattering effects from phase separation, the MBP tag was not cleaved from Dcp1/Dcp2<sub>ext</sub> and Edc3 Lsm domain was used.

### Condensate Fusion Experiments

Brightfield images were collected on a Nikon Ti-E inverted microscope equipped with a PlanApo 40x air objective and Hamamatsu Flash4.0 camera. For wild-type Dcp1/Dcp2<sub>ext</sub>, time lapse images were collected every one second while images for Dcp1/Dcp2<sub>ext</sub>(Y220G) were collected at either one second or 15 second intervals. Fusion events were analyzed in ImageJ by drawing an ellipse around droplets of similar size at each time point and measuring the long and short axis. The aspect ratio (long/short axis) was plotted as a function of time in Prism 9 (GraphPad) to determine the time of fusion,  $\tau$ . Plotting  $\tau$  as a function of initial length  $((l_{\text{long}} - l_{\text{short}}) \cdot l_{\text{short}})^{1/2}$  gives a linear relationship where the slope represents the inverse capillary action—the ratio of condensate viscosity to surface tension  $(\eta/\gamma)^{59}$ .

## SUPPLEMENTAL FIGURES

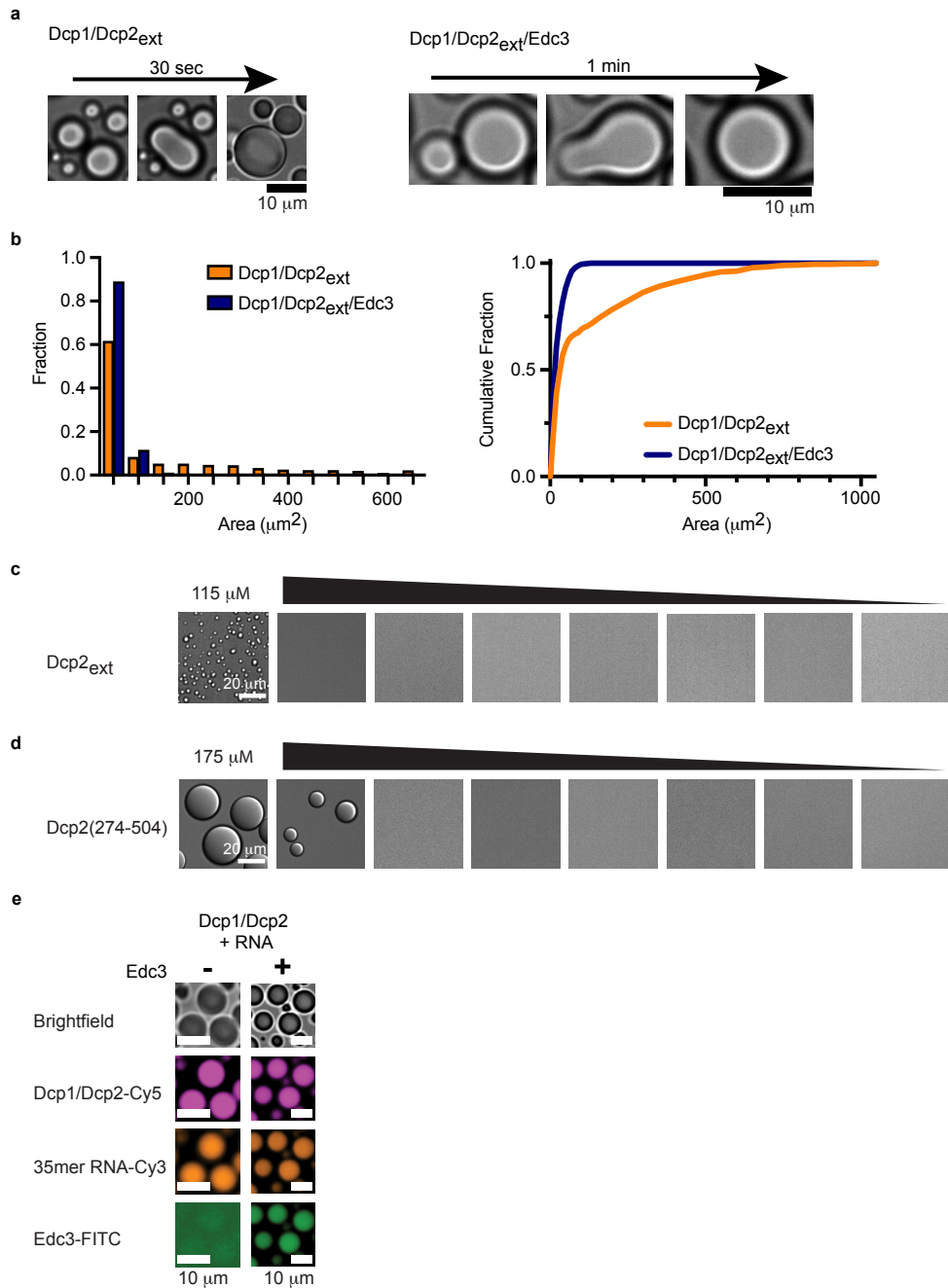


**Figure. S3.1: Edc3 alters physical properties of Dcp1/Dcp2<sub>ext</sub> liquid droplets.** **a**, (Left) Fusion of Dcp1/Dcp2<sub>ext</sub> (Left) and Dcp1/Dcp2<sub>ext</sub>/Edc3 (Right) droplets demonstrate liquid behavior. **b**, (Left) Histogram of droplet area (in μm<sup>2</sup>) observed for Dcp1/Dcp2<sub>ext</sub> and stoichiometric Dcp1/Dcp2<sub>ext</sub>/Edc3 droplets at concentrations 10-fold greater than  $c_{sat}$ , the concentration at which phase separation occurs. (Right) Cumulative Distribution Function of the data presented on the left demonstrates Dcp1/Dcp2<sub>ext</sub> droplets exhibit a wider distribution of sizes and cannot be adequately explained by only droplets  $\leq 100$  μm<sup>2</sup>. **c**, Brightfield images of serial two-fold diluted Dcp2<sub>ext</sub> show it forms small liquid droplets at high concentrations. **d**, Brightfield images show the disordered C-terminus is sufficient to undergo phase separation in a concentration-dependent manner. **e**, Dcp1/Dcp2<sub>ext</sub>, Edc3, and RNA all colocalize to droplets. Dcp1/Dcp2<sub>ext</sub> concentration is 60 μM and 5 μM in absence and presence of 80 μM Edc3,

respectively. RNA concentration is 100 nM. Micrographs shown in **a**, **c-e** are representative images from three independent experiments with similar results.

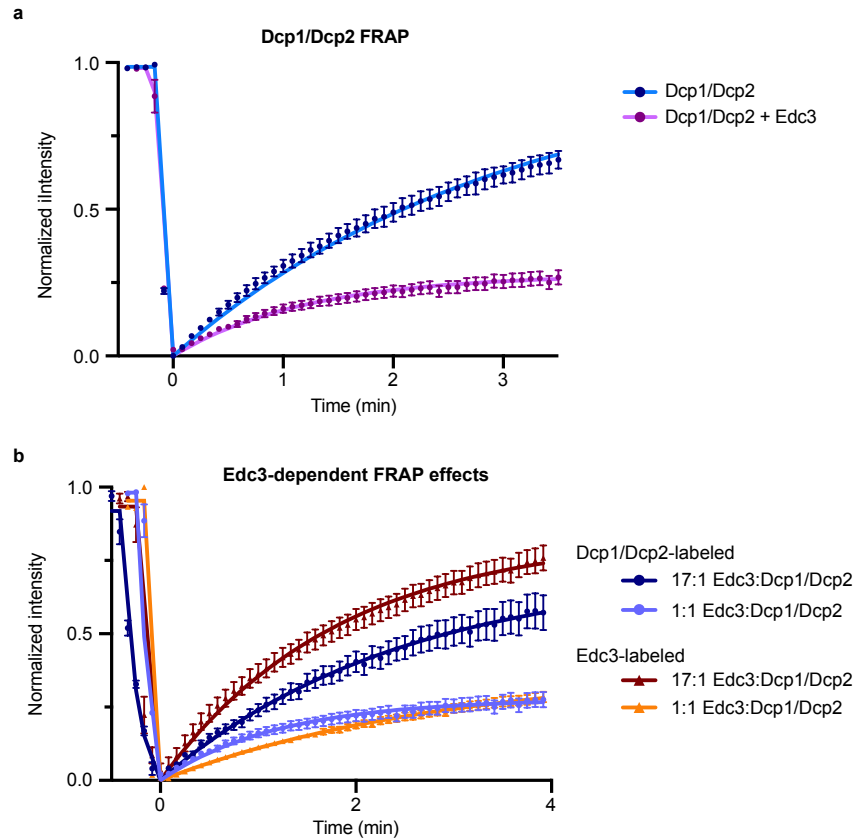


**Figure S3.2: Edc3 alters Dcp1/Dcp2<sub>ext</sub> mobility in droplets.** **a**, Edc3 reduces the mobility of Dcp1/Dcp2 in in vitro droplets as demonstrated by reduced fraction recovery after photobleaching (FRAP). **b**, Increasing the ratio of Edc3 increases the exchange of Dcp1/Dcp2<sub>ext</sub> and Edc3 in droplets. Data are reported as mean  $\pm$  s.e.m. for twenty recovery profiles collected over two independent experiments.

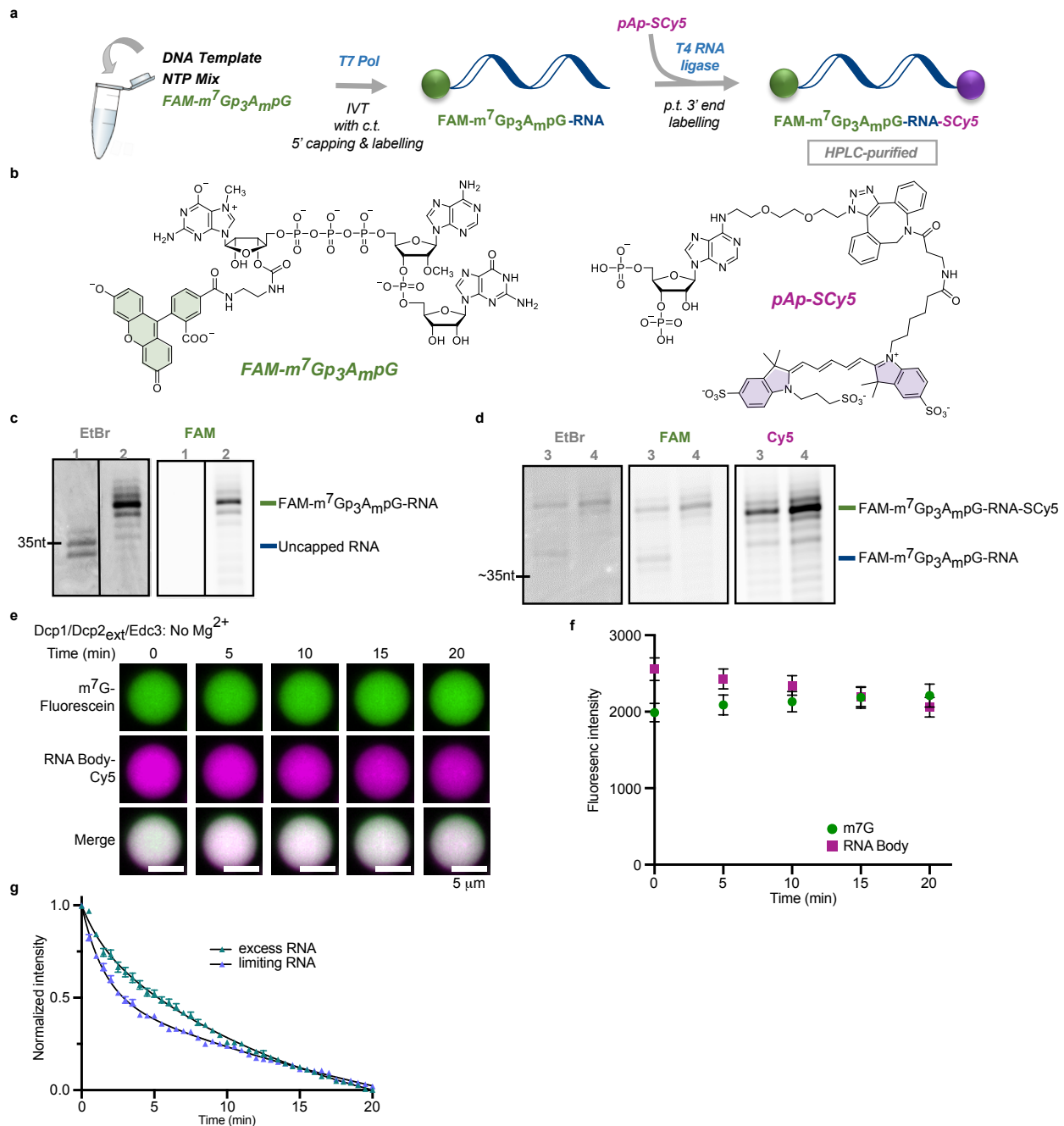


**Figure S3.3: Synthesis and decapping of dually labelled 5' capped 35 nt RNA probe.** **a**, Overview of the labelling procedure, IVT – in vitro transcription, c.t. – co-transcriptional, p.t. – post-transcriptional; **b**, structures of the reagents used for the 5' and 3' end labelling; **c**, Analysis of purified 5' capped & labelled RNA after IVT: lane 1 – reference uncapped RNA, lane 2 – RNA capped co-transcriptionally with fluorescent cap analog (FAM- $m^7Gp_3AmpG$ ). **d**, Labelling of the 3' end of FAM- $m^7Gp_3AmpG$ -RNA with pAp-SCy5 to yield dually labelled RNA after purification; lane 3 – crude dually labelled RNA after purification; lane 4 – HPLC-purified RNA probe. **e**, **f**, Co-localization of m7G cap (fluorescein) and RNA body (Cy5) in Dcp1/Dcp2<sub>ext</sub>/Edc3 condensates over twenty minutes demonstrates decapping does not occur in the absence of Mg<sup>2+</sup>, which is required for catalysis. **g**, Excess RNA slows initial rate of decapping two-fold in droplets formed with 1  $\mu$ M Dcp1/Dcp2<sub>ext</sub> and 15  $\mu$ M Edc3. Total RNA concentration is 100 nM when limiting and 20  $\mu$ M when in excess. Representative micrographs and data in **f**, **g** are presented as mean  $\pm$

s.e.m. for twenty droplets examined in two independent experiments with similar results. Error bars are not depicted when smaller than the data points.

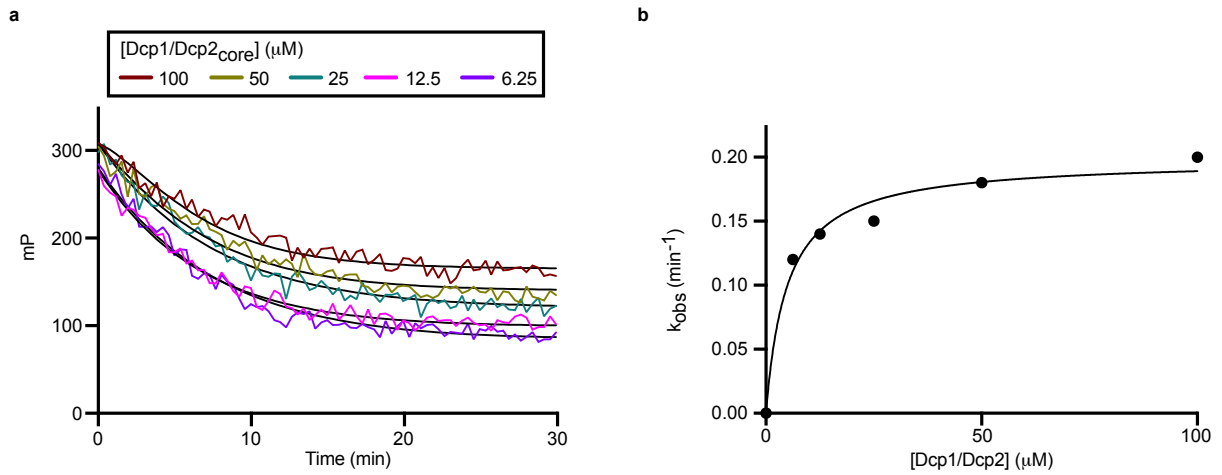


**Figure S3.4: Monitoring decapping of dual-labeled 35mer RNA using fluorescence polarization. a,** Decrease in mP over time as a result of more rapid tumbling of released FAM-m7GDP demonstrates RNA decapping by Dcp1/Dcp2<sub>core</sub>. **b,** Observed rates of decapping determined from a demonstrate Dcp1/Dcp2<sub>core</sub> is able to hydrolyze dual-labeled substrate at maximal rate of 0.2 min<sup>-1</sup>.

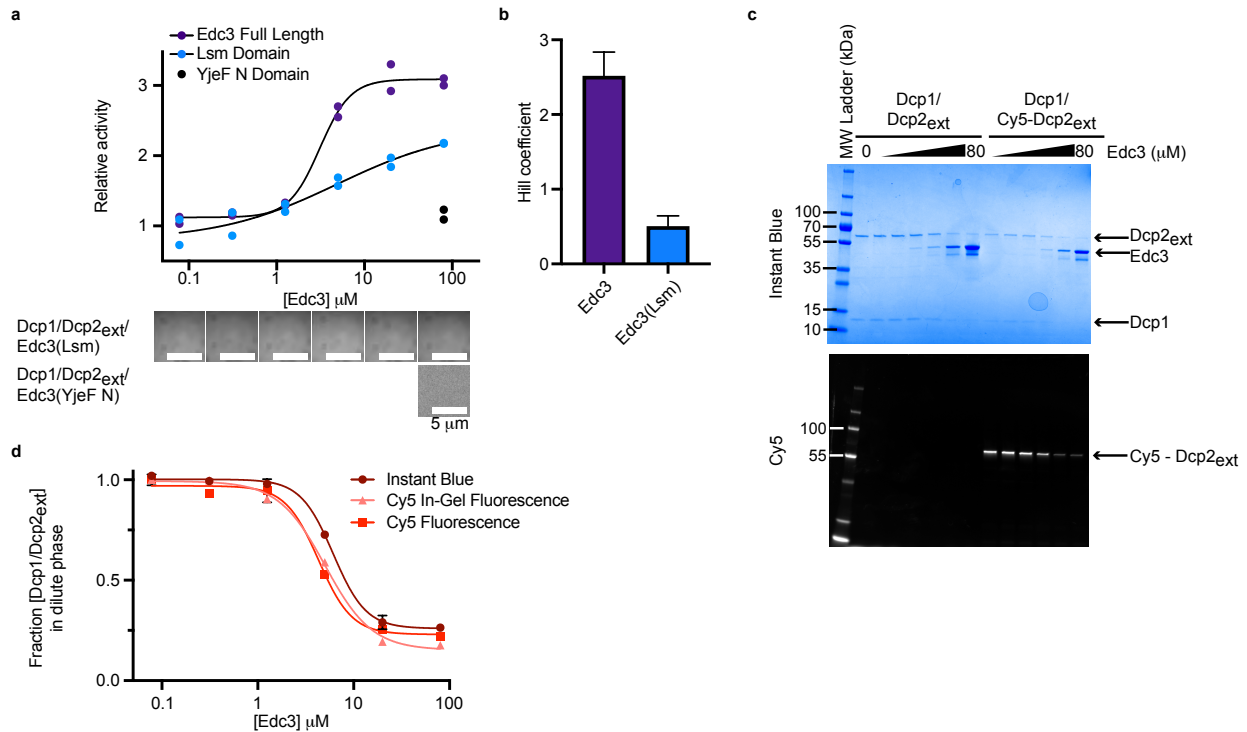


**Figure S3.5: Edc3 sequesters Dcp1/Dcp2<sub>ext</sub> in condensates to cooperatively activate decapping. a,** Enhancement of decapping by Edc3 Lsm domain occurs in the absence of condensates. C-terminal Edc3 YjeF N domain does not stimulate Dcp1/Dcp2<sub>ext</sub> activity or cause phase separation. Activation by full-length Edc3 is reproduced from Fig. 4c for comparison. Two independent experiments are shown. Representative micrographs are from three independent experiments with similar results. **b,** Cooperativity of activation by dimeric Edc3 is five-fold greater than the Lsm domain. Hill coefficients are reported as mean ± standard error from fitting two independent experiments shown in **a**. **c,** Depletion of Dcp1/Dcp2<sub>ext</sub> from the dilute phase at increasing concentrations of Edc3 visualized by SDS-PAGE. (Top) Instant Blue

staining reveals total protein remaining in dilute phase following pelleting of liquid droplets. (Bottom) In-gel fluorescence of Cy5-labelled Dcp2 shows its Edc3-dependent disappearance from the solution. **d**, Quantification of Dcp1/Dcp2<sub>ext</sub> from analysis of Dcp2 stained with Instant Blue or measured by in-gel Cy5 emission. Cy5 fluorescence is reproduced from Figure 3d for comparison. Representative SDS-PAGE and quantification are from two independent experiments with data presented as mean  $\pm$  s.e.m. Error bars are not shown when smaller than the data points.

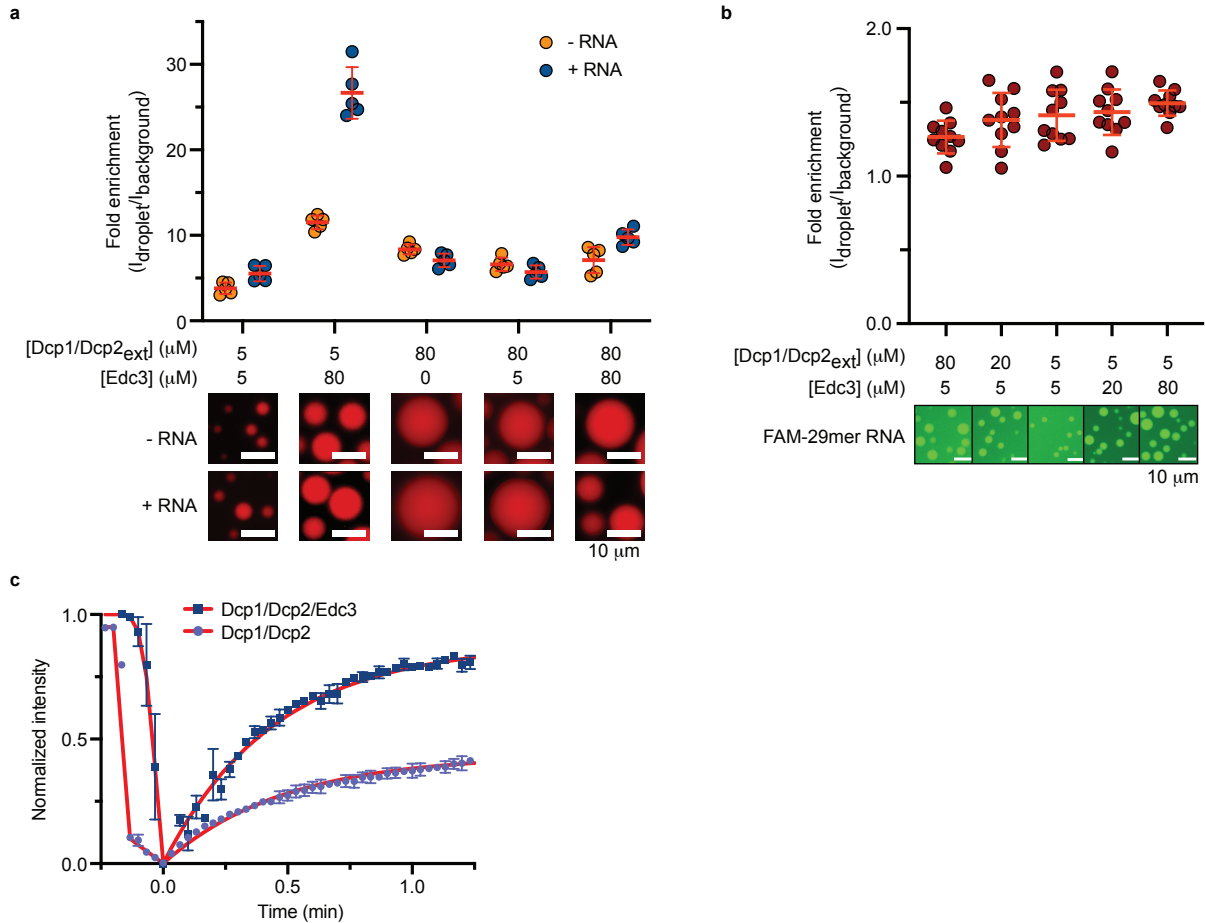


**Figure S3.6: Edc3 alters Dcp1/Dcp2<sub>ext</sub> enrichment and RNA mobility in liquid droplets. a**, Superstoichiometric Edc3 enriches Dcp1/Dcp2<sub>ext</sub> in droplets and causes causes droplets to be more sensitive to presence of RNA. Images below graph correspond to representative Cy5-labelled Dcp1/Dcp2<sub>ext</sub> micrographs and data presented are mean  $\pm$  s.e.m. for five independent experiments with similar results. **b**, Enrichment of FAM-29mer RNA in droplets of varying Dcp1/Dcp2<sub>ext</sub> and Edc3 concentrations. Representative micrographs and data presented are mean  $\pm$  s.e.m. for ten independent experiments with similar results. **c**, Edc3 increases the mobile fraction of RNA in droplets. Dcp1/Dcp2<sub>ext</sub> concentration is 40  $\mu$ M in absence and 5  $\mu$ M in presence of 80  $\mu$ M Edc3. Data presented are mean  $\pm$  s.e.m. for twenty recovery profiles collected over two independent experiments. Error bars are not depicted when smaller than the data point.

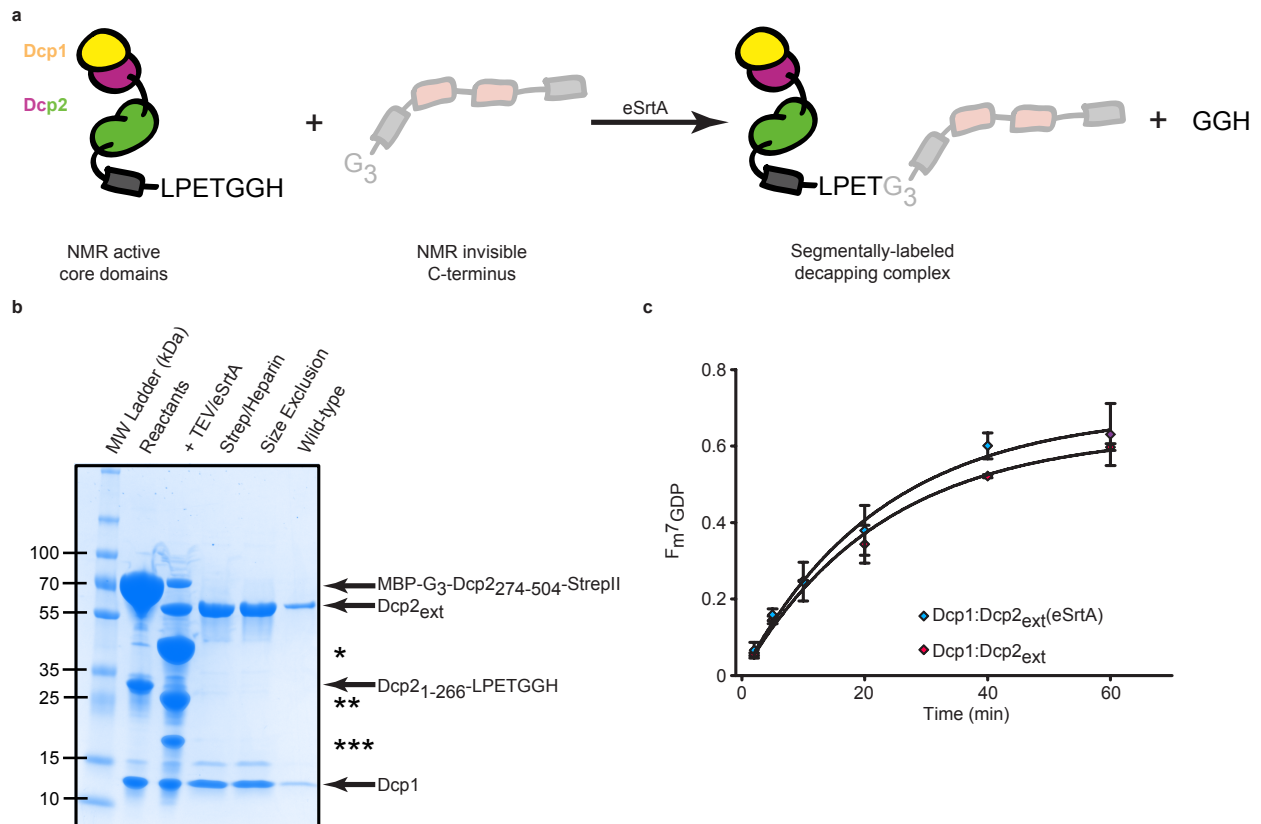


**Figure S3.7: Generation of segmentally-labeled Dcp1/Dcp2<sub>ext</sub> for NMR.** **a**, Reaction scheme for ligation of ILVMA-labeled, NMR active Dcp1/Dcp2 core domains with NMR invisible C-terminus using an enhanced SortaseA (eSrtA, See Methods). **b**, SDS-PAGE for the ligation reaction. The left gel corresponds to the reaction and purification of ligation product while wild-type Dcp1/Dcp2<sub>ext</sub> is shown on the right gel image. \*Indicates N-terminal MBP tag generated upon incubation with TEV. \*\*Indicates unreacted C-terminus generated upon incubation with TEV. \*\*\*Indicates eSrtA band. **c**, Ligation product and wild-type Dcp1/Dcp2<sub>ext</sub> exhibit similar decapping activity on a capped 29mer RNA substrate. Data presented are mean  $\pm$  s.e.m. for two independent experiments.





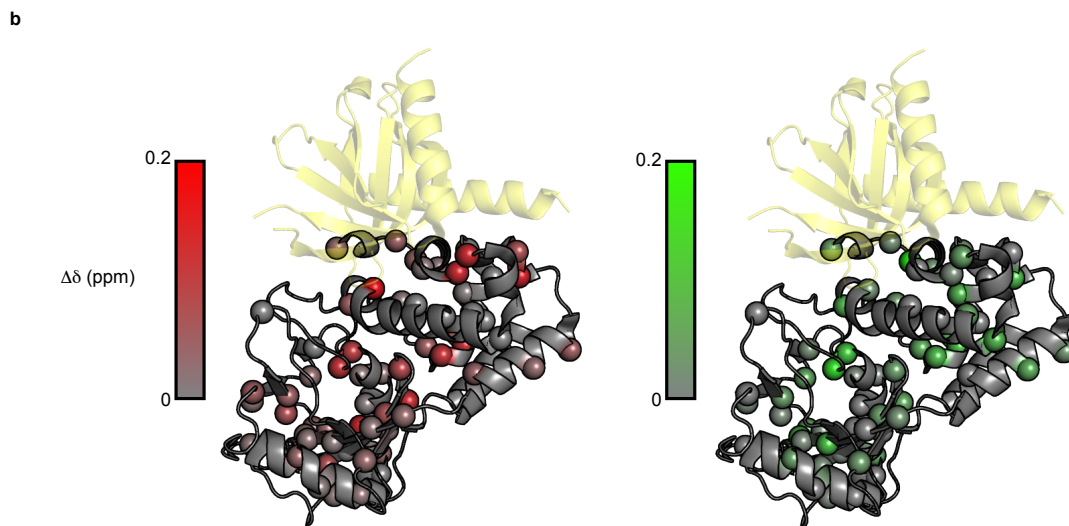
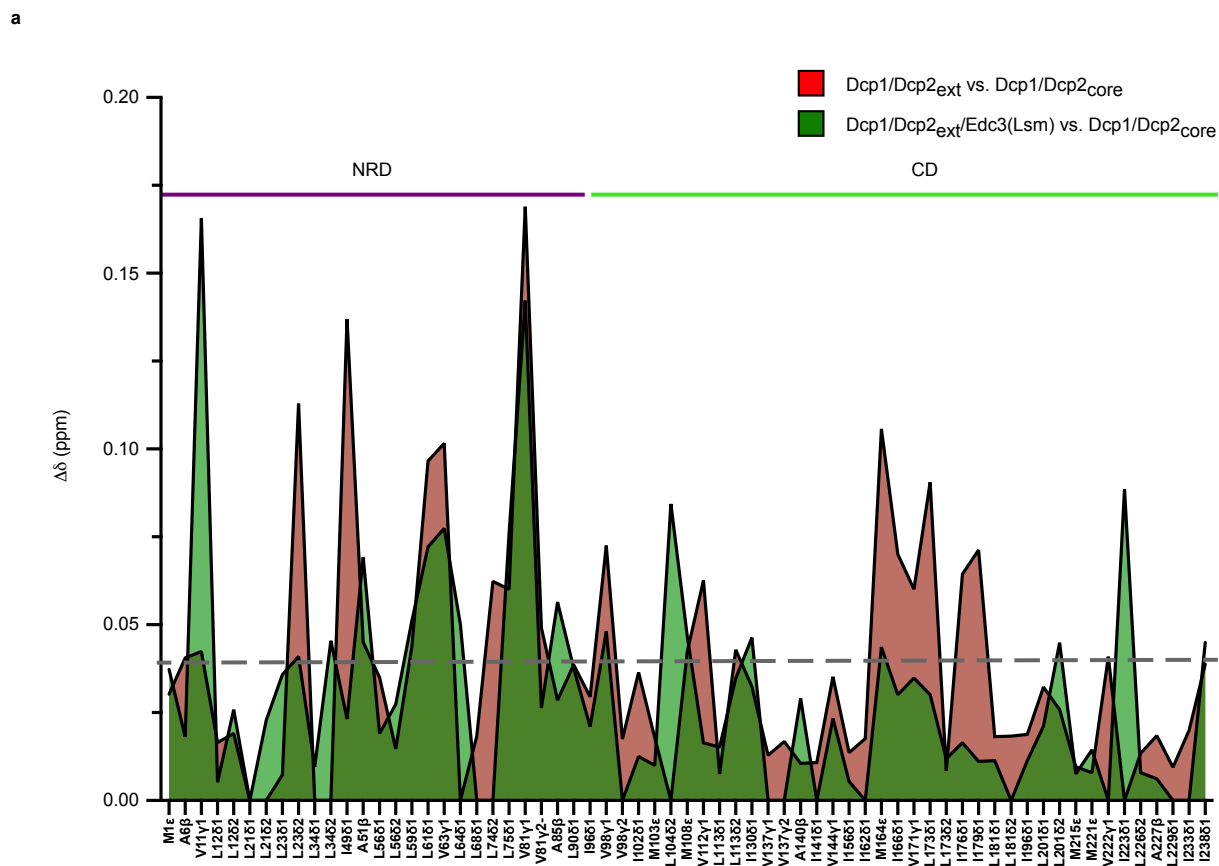


**Figure S3.9: Edc3(Lsm) reduces chemical shift perturbations (CSPs) of Dcp1/Dcp2<sub>ext</sub> to more closely resemble the chemical shifts of Dcp1/Dcp2<sub>core</sub>.** **a**, CSPs of Dcp1/Dcp2<sub>ext</sub> containing the C-terminus in the absence (red) and presence (green) of Edc3 for ILVMA terminal methyl resonances in the structured catalytic core of Dcp2. CSPs are calculated relative to Dcp1/Dcp2<sub>core</sub>, which lacks the disordered C-terminus. The reduction in CSPs upon the addition of Edc3 indicates the structure of the core domains more closely resembles that of the uninhibited Dcp1/Dcp2<sub>core</sub> complex. The dotted line represents the standard deviation of observed CSPs plotted in the graph. **b**, CSPs for Dcp1/Dcp2<sub>ext</sub> (Left) and Dcp1/Dcp2<sub>ext</sub>/Edc3 (Right) mapped onto the inactive state of Dcp1/Dcp2 (PDB: 2QKM). ILVMA residues are shown as spheres. Dcp1 is shown as yellow ribbon structure.

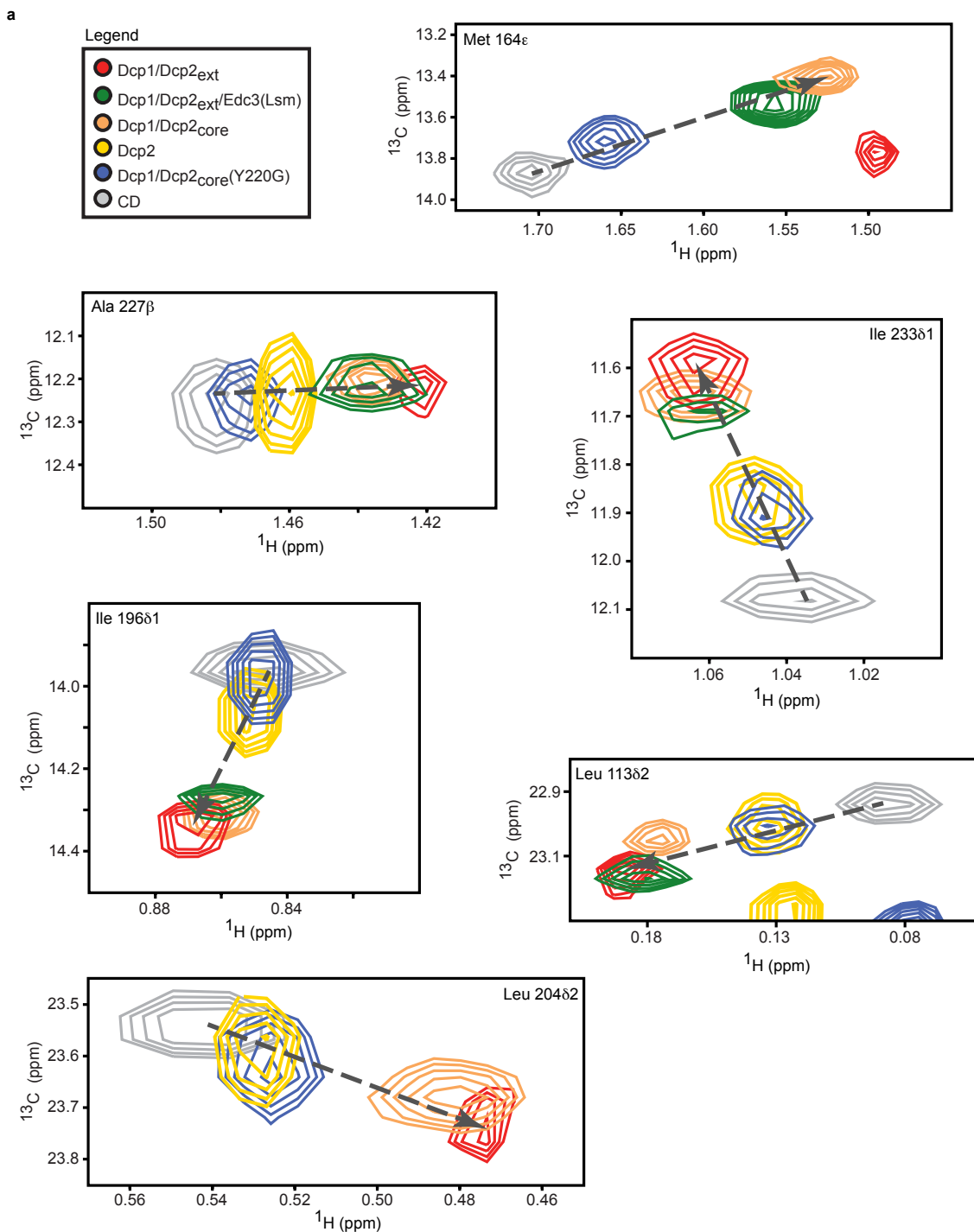


**Figure S3.10: Several resonances in the catalytic domain of Dcp2 report on the inactive—precatalytic equilibrium. a,**  $^1\text{H}/^{13}\text{C}$ -methyl resonances in Dcp2 constructs predominantly fall along a linear trajectory (dotted line), indicative of fast interconversion between the inactive and precatalytic states on the NMR timescale. Resonances for Ala 227 $\beta$ , Ile 223 $\delta$ 1, and Ile 196 $\delta$ 1 were used in addition to Ile 102 $\delta$ 1 (**Fig. 3.5b**) to calculate the relative population of the inactive state due to the observance of resonances for all constructs strictly lying along a linear trajectory.

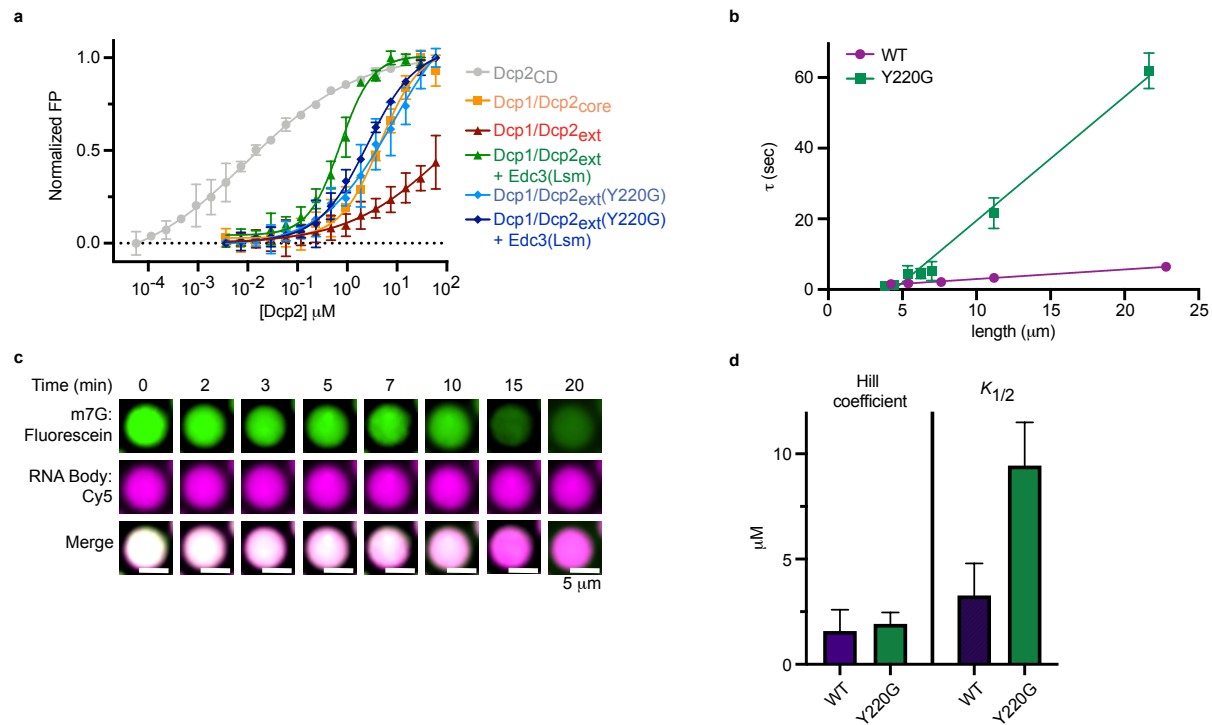


**Figure S3.11: Dcp1/Dcp2<sub>ext</sub> conformational equilibria is important for substrate recognition, liquid-like behavior, and proper regulation of decapping in condensates.** **a**, FP curves for various Dcp2 constructs binding to U30mer RNA. Data are normalized to the span between minimum and maximum mP values for each protein tested. Dcp1/Dcp2<sub>ext</sub> was normalized to span between its minimum and average maximum for all proteins tested. Data are presented as mean  $\pm$  s.e.m. for three independent experiments and error bars are not shown when smaller than the data point. **b**, Fusion of Dcp1/Dcp2<sub>ext</sub>(Y220G) condensates occurs slower than wild-type droplets of similar size. Time ( $\tau$ ) data presented are from fits of exponential decrease in droplet length following initial fusion event and error represents standard error of the fit and are not depicted when smaller than the data point. Representative micrographs are from three independent experiments with similar results. **c**, Decapping of dual-labeled RNA substrate by Dcp1/Dcp2<sub>ext</sub>(Y220G) by fluorescence microscopy. Representative micrographs are from twenty droplets collected over two independent experiments with similar results. **d**, The Y220G mutation does not affect the cooperativity of activation by Edc3 but increases the  $K_{1/2}$  of activation three-fold. Hill coefficients and  $K_{1/2}$  are presented as mean  $\pm$  s.e.m. for experimental fits from two independent experiments shown in **Fig. 3.5g**.

## SUPPLEMENTAL TABLES

Table S3.1: Protein constructs used in this study

Protein Construct	Amino Acid Boundaries	Solubility/Purification Tags	Plasmid Backbone	Organism
Dcp1/Dcp2 <sub>ext</sub>	Dcp1: 1-127 Dcp2: 1-504	Dcp1: N-terminal His <sub>6</sub> -MBP-TEV Dcp2: C-terminal StrepII	pRSF	<i>S. pombe</i>
Dcp1/Dcp2 <sub>ext</sub> (Y220G)	Dcp1: 1-127 Dcp2: 1-504	Dcp1: N-terminal His <sub>6</sub> -MBP-TEV Dcp2: C-terminal StrepII	pRSF	<i>S. pombe</i>
Dcp1/Dcp2 <sub>core</sub>	Dcp1: 1-127 Dcp2: 1-243	Dcp1: N-terminal His <sub>6</sub> -MBP-TEV	pRSF	<i>S. pombe</i>
Dcp1/Dcp2 <sub>core</sub> (Y220G)	Dcp1: 1-127 Dcp2: 1-243	Dcp1: N-terminal His <sub>6</sub> -MBP-TEV	pRSF	<i>S. pombe</i>
Dcp1/Dcp2 <sub>HLM1/2</sub>	Dcp1: 1-127 Dcp2: 1-318	Dcp1: N-terminal His <sub>6</sub> -MBP-TEV Dcp2: C-terminal StrepII	pRSF	<i>S. pombe</i>
Dcp1/Dcp2 <sub>HLM1</sub>	Dcp1: 1-127 Dcp2: 1-266	Dcp1: N-terminal His <sub>6</sub> -MBP-TEV	pRSF	<i>S. pombe</i>
Dcp1/Dcp2 <sub>(eSrtA)</sub>	Dcp1: 1-27 Dcp2: 1-266 + LPETGGH	Dcp1: N-terminal His <sub>6</sub> -MBP-TEV	pRSF	<i>S. pombe</i>
Dcp1	Dcp1: 1-127	Dcp1: N-terminal His <sub>6</sub> -MBP-TEV	pRSF	<i>S. pombe</i>
Dcp2 <sub>ext</sub>	Dcp2: 1-504	Dcp2: N-terminal His <sub>6</sub> -MBP-TEV; C-terminal StrepII	pRSF	<i>S. pombe</i>
Dcp2 <sub>core</sub>	Dcp2: 1-243	Dcp2: N-terminal His <sub>6</sub> -MBP-TEV	pRSF	<i>S. pombe</i>
Dcp2 <sub>CD</sub> (Catalytic Domain)	Dcp2: 96-243	Dcp2: N-terminal His <sub>6</sub> -MBP-TEV	pRSF	<i>S. pombe</i>
Dcp2 C-terminus	Dcp2: 244-504	Dcp2: N-terminal His <sub>6</sub> -MBP-TEV; C-terminal StrepII	pRSF	<i>S. pombe</i>
Dcp2 C-terminus eSrtA	Dcp2: G <sub>3</sub> + 274-504	Dcp2: N-terminal His <sub>6</sub> -MBP-TEV; C-terminal StrepII	pRSF	<i>S. pombe</i>
Edc3	Edc3: 1-454	N-terminal His <sub>6</sub> -TEV	pET30b	<i>S. pombe</i>
Edc3 Lsm domain	Edc3: 1-94	N-terminal His <sub>6</sub> -TEV	pET30b	<i>S. pombe</i>
Edc3 YjeF N domain	Edc3: 188-454	N-terminal His <sub>6</sub> -TEV	pET30b	<i>S. pombe</i>
Edc1 Direct Activation Motif (DAM)	Edc1: 155-180	None (synthesized by Peptide2.0)	N/A	<i>S. pombe</i>

**Table S3.2: Values for half-time of recovery and the fraction of mobile molecules obtained from fitting to FRAP curves**

	$t_{1/2}$ (min)	Mobile Fraction
<b>Dcp1/Dcp2 FRAP</b>		
Dcp1/Dcp2	0.91 ± 0.06	0.28 ± 0.01
Dcp1/Dcp2 + Edc3	1.62 ± 0.05	0.85 ± 0.01
<b>1:1 Edc3:Dcp1/Dcp2</b>		
Dcp1/Dcp2	0.95 ± 0.07	0.28 ± 0.01
Edc3	2.15 ± 0.04	0.39 ± 0.01
<b>17:1 Edc3:Dcp1/Dcp2</b>		
Dcp1/Dcp2	1.9 ± 0.12	0.65 ± 0.02
Edc3	1.4 ± 0.05	0.87 ± 0.02
<b>RNA FRAP</b>		
Dcp1/Dcp2	0.40 ± 0.04	0.45 ± 0.01
Dcp1/Dcp2/Edc3	0.29 ± 0.03	0.87 ± 0.02

**Table S3.3: Dcp1/Dcp2<sub>ext</sub> decapping rates in Bulk and Dilute phases**

Protein	Bulk $k_{obs}$ (min <sup>-1</sup> )	Supernatant $k_{obs}$ (min <sup>-1</sup> )
Dcp1/Dcp2 <sub>ext</sub>	0.36 ± 0.14	0.51 ± 0.04
Dcp1/Dcp2 <sub>ext</sub> /Edc3	1.37 ± 0.13	0.43 ± 0.08

**Table S3.4: Dcp1/Dcp2<sub>ext</sub> decapping rates in Bulk and Dilute Phase with variable Edc3**

[Edc3] (μM)	Bulk $k_{obs}$ (min <sup>-1</sup> )	Supernatant $k_{obs}$ (min <sup>-1</sup> )
80	1.06 ± 0.10	0.52 ± 0.03
20	1.08 ± 0.06	0.62 ± 0.10
5	0.91 ± 0.08	0.53 ± 0.08
1.25	0.46 ± 0.06	0.53 ± 0.03
0.3125	0.41 ± 0.04	0.58 ± 0.06
0.078125	0.38 ± 0.06	0.52 ± 0.04
0	0.35 ± 0.04	0.49 ± 0.06

**Table S3.5: Dcp1/Dcp2<sub>ext</sub> decapping rates with addition of Edc3 Lsm and YjeF N domains**

[Edc3] (μM)	Lsm $k_{obs}$ (min <sup>-1</sup> )	YjeF N $k_{obs}$ (min <sup>-1</sup> )
80	0.93 ± 0.14	0.43 ± 0.04
20	0.79 ± 0.10	
5	0.68 ± 0.09	
1.25	0.53 ± 0.07	
0.3125	0.43 ± 0.01	
0.078125	0.37 ± 0.01	
0	0.37 ± 0.02	

**Table S3.6: Equilibrium dissociation constants ( $K_D$ ) for various Dcp2 constructs determined by fluorescence polarization**

Protein	$K_D$ (μM)
Dcp2 <sub>CD</sub>	0.0097 ± 0.0031
Dcp1/Dcp2 <sub>core</sub>	4.57 ± 1.04
Dcp1/Dcp2 <sub>ext</sub>	84.1 ± 62.5
Dcp1/Dcp2 <sub>ext</sub> + Edc3(Lsm)	0.837 ± 0.121
Dcp1/Dcp2 <sub>ext</sub> (Y220G)	8.58 ± 3.69
Dcp1/Dcp2 <sub>ext</sub> (Y220G) + Edc3(Lsm)	2.53 ± 0.24

**Table S3.7: Dcp1/Dcp2<sub>ext</sub>(Y220G) and Dcp1/Dcp2<sub>ext</sub> WT decapping rates in Bulk and Dilute Phase at variable Edc3 concentrations**

[Edc3] ( $\mu\text{M}$ )	Y220G Bulk $k_{obs}$ ( $\text{min}^{-1}$ )	Y220G Supernatant $k_{obs}$ ( $\text{min}^{-1}$ )	WT Bulk $k_{obs}$ ( $\text{min}^{-1}$ )	WT Supernatant $k_{obs}$ ( $\text{min}^{-1}$ )
80	$4.68 \pm 0.37$	$3.74 \pm 0.26$	$1.10 \pm 0.04$	$0.49 \pm 0.03$
20	$4.39 \pm 0.24$	$3.01 \pm 0.00$	$1.00 \pm 0.08$	$0.47 \pm 0.15$
5	$3.45 \pm 0.17$	$2.88 \pm 0.34$	$0.87 \pm 0.04$	$0.38 \pm 0.14$
1.25	$3.06 \pm 0.02$	$3.25 \pm 0.15$	$0.47 \pm 0.01$	$0.42 \pm 0.10$
0.3125	$3.18 \pm 0.10$	$3.43 \pm 0.11$	$0.51 \pm 0.09$	$0.44 \pm 0.14$
0.078125	$2.97 \pm 0.40$	$3.02 \pm 0.12$	$0.31 \pm 0.07$	$0.40 \pm 0.12$
0	$2.81 \pm 0.16$	$2.93 \pm 0.20$	$0.35 \pm 0.01$	$0.42 \pm 0.07$

**Table S3.8: Edc1/Dcp1/Dcp2 decapping rates in Bulk and Dilute Phase at variable Edc3 concentrations**

[Edc3] ( $\mu\text{M}$ )	Bulk $k_{obs}$ ( $\text{min}^{-1}$ )	Supernatant $k_{obs}$ ( $\text{min}^{-1}$ )
80	$5.09 \pm 0.25$	$5.69 \pm 0.57$
20	$4.65 \pm 0.15$	$5.23 \pm 0.23$
5	$5.81 \pm 0.24$	$5.85 \pm 0.36$
1.25	$4.75 \pm 0.20$	$6.15 \pm 0.36$
0.3125	$4.19 \pm 0.15$	$7.04 \pm 0.35$
0.078125	$4.65 \pm 0.18$	$5.90 \pm 0.40$

## REFERENCES

1. Banani, S. F. *et al.* Compositional Control of Phase-Separated Cellular Bodies. *Cell* **166**, 651–663 (2016).
2. Gallego, L. D. *et al.* Phase separation directs ubiquitination of gene-body nucleosomes. *Nature* **579**, 592–597 (2020).
3. Hnisz, D., Shrinivas, K., Young, R. A., Chakraborty, A. K. & Sharp, P. A. A Phase Separation Model for Transcriptional Control. *Cell* **169**, 13–23 (2017).
4. Riback, J. A. *et al.* Composition-dependent thermodynamics of intracellular phase separation. *Nature* 1–6 (2020) doi:10.1038/s41586-020-2256-2.
5. Sheu-Gruttadauria, J. & MacRae, I. J. Phase Transitions in the Assembly and Function of Human miRISC. *Cell* **173**, 946-957.e16 (2018).
6. Langdon, E. M. *et al.* mRNA structure determines specificity of a polyQ-driven phase separation. *Science* **360**, 922–927 (2018).
7. Kim, T. H. *et al.* Phospho-dependent phase separation of FMRP and CAPRIN1 recapitulates regulation of translation and deadenylation. *Science* **365**, 825–829 (2019).
8. Hondele, M. *et al.* DEAD-box ATPases are global regulators of phase-separated organelles. *Nature* **573**, 144–148 (2019).
9. Brady, J. P. *et al.* Structural and hydrodynamic properties of an intrinsically disordered region of a germ cell-specific protein on phase separation. *Proc. Natl. Acad. Sci.* **114**, E8194–E8203 (2017).
10. Peebles, W. & Rosen, M. K. Mechanistic dissection of increased enzymatic rate in a phase-separated compartment. *Nat. Chem. Biol.* **17**, 693–702 (2021).
11. Banani, S. F., Lee, H. O., Hyman, A. A. & Rosen, M. K. Biomolecular condensates: organizers of cellular biochemistry. *Nat. Rev. Mol. Cell Biol.* **18**, 285–298 (2017).
12. Zhang, Y., Narlikar, G. J. & Kutateladze, T. G. Enzymatic Reactions inside Biological Condensates. *J. Mol. Biol.* **433**, 166624 (2021).

13. Mitrea, D. M. & Kriwacki, R. W. Phase separation in biology; functional organization of a higher order. *Cell Commun. Signal.* **14**, 1 (2016).
14. Moore, M. J. From Birth to Death: The Complex Lives of Eukaryotic mRNAs. *Science* **309**, 1514–1518 (2005).
15. Hubstenberger, A. *et al.* P-Body Purification Reveals the Condensation of Repressed mRNA Regulons. *Mol. Cell* **68**, 144-157.e5 (2017).
16. Sheth, U. & Parker, R. Decapping and Decay of Messenger RNA Occur in Cytoplasmic Processing Bodies. *Science* **300**, 805–808 (2003).
17. Luo, Y., Na, Z. & Slavoff, S. A. P-Bodies: Composition, Properties, and Functions. *Biochemistry* **57**, 2424–2431 (2018).
18. Chan, L. Y., Mugler, C. F., Heinrich, S., Vallotton, P. & Weis, K. Non-invasive measurement of mRNA decay reveals translation initiation as the major determinant of mRNA stability. *eLife* **7**, e32536 (2018).
19. Mugler, C. F. *et al.* ATPase activity of the DEAD-box protein Dhh1 controls processing body formation. *eLife* **5**, e18746 (2016).
20. Hutchins, E. J., Piacentino, M. L. & Bronner, M. E. P-bodies are sites of rapid RNA decay during the neural crest epithelial—mesenchymal transition. *bioRxiv* 2020.07.31.231860 (2020) doi:10.1101/2020.07.31.231860.
21. Horvathova, I. *et al.* The Dynamics of mRNA Turnover Revealed by Single-Molecule Imaging in Single Cells. *Mol. Cell* **68**, 615-625.e9 (2017).
22. Tutucci, E. *et al.* An improved MS2 system for accurate reporting of the mRNA life cycle. *Nat. Methods* **15**, 81–89 (2018).
23. Aizer, A. *et al.* Quantifying mRNA targeting to P-bodies in living human cells reveals their dual role in mRNA decay and storage. *J. Cell Sci.* **127**, 4443–4456 (2014).
24. Brengues, M., Teixeira, D. & Parker, R. Movement of Eukaryotic mRNAs Between Polysomes and Cytoplasmic Processing Bodies. *Science* **310**, 486–489 (2005).



25. Wang, C. *et al.* Context-dependent deposition and regulation of mRNAs in P-bodies. *eLife* **7**, e29815 (2018).
26. Pitchiaya, S. *et al.* Dynamic Recruitment of Single RNAs to Processing Bodies Depends on RNA Functionality. *Mol. Cell* **74**, 521-533.e6 (2019).
27. Boeynaems, S. *et al.* Protein Phase Separation: A New Phase in Cell Biology. *Trends Cell Biol.* **28**, 420–435 (2018).
28. Jonas, S. & Izaurralde, E. The role of disordered protein regions in the assembly of decapping complexes and RNP granules. *Genes Dev.* **27**, 2628–2641 (2013).
29. Beelman, C. A. *et al.* An essential component of the decapping enzyme required for normal rates of mRNA turnover. *Nature* **382**, 642–646 (1996).
30. Dunckley, T. & Parker, R. The DCP2 protein is required for mRNA decapping in *Saccharomyces cerevisiae* and contains a functional MutT motif. *EMBO J.* **18**, 5411–5422 (1999).
31. Wang, Z., Jiao, X., Carr-Schmid, A. & Kiledjian, M. The hDcp2 protein is a mammalian mRNA decapping enzyme. *Proc. Natl. Acad. Sci.* **99**, 12663–12668 (2002).
32. Xing, W., Muhlrads, D., Parker, R. & Rosen, M. K. A quantitative inventory of yeast P body proteins reveals principles of composition and specificity. *eLife* **9**, e56525 (2020).
33. Fromm, S. A. *et al.* In Vitro Reconstitution of a Cellular Phase-Transition Process that Involves the mRNA Decapping Machinery. *Angew. Chem. Int. Ed.* **53**, 7354–7359 (2014).
34. He, F., Celik, A., Wu, C. & Jacobson, A. General decapping activators target different subsets of inefficiently translated mRNAs. *eLife* **7**, e34409 (2018).
35. He, F. & Jacobson, A. Control of mRNA decapping by positive and negative regulatory elements in the Dcp2 C-terminal domain. *RNA* **21**, 1633–1647 (2015).
36. Paquette, D. R., Tibble, R. W., Daifuku, T. S. & Gross, J. D. Control of mRNA decapping by autoinhibition. *Nucleic Acids Res.* **46**, 6318–6329 (2018).

37. Lobel, J. H., Tibble, R. W. & Gross, J. D. Pat1 activates late steps in mRNA decay by multiple mechanisms. *Proc. Natl. Acad. Sci.* **116**, 23512–23517 (2019).
38. Badis, G., Saveanu, C., Fromont-Racine, M. & Jacquier, A. Targeted mRNA Degradation by Deadenylation-Independent Decapping. *Mol. Cell* **15**, 5–15 (2004).
39. Fromm, S. A. *et al.* The structural basis of Edc3- and Scd6-mediated activation of the Dcp1:Dcp2 mRNA decapping complex. *EMBO J.* **31**, 279–290 (2012).
40. Harigaya, Y., Jones, B. N., Muhlrاد, D., Gross, J. D. & Parker, R. Identification and Analysis of the Interaction between Edc3 and Dcp2 in *Saccharomyces cerevisiae*. *Mol. Cell. Biol.* **30**, 1446–1456 (2010).
41. Damman, R. *et al.* Atomic-level insight into mRNA processing bodies by combining solid and solution-state NMR spectroscopy. *Nat. Commun.* **10**, 1–11 (2019).
42. Schütz, S., Nöldeke, E. R. & Sprangers, R. A synergistic network of interactions promotes the formation of in vitro processing bodies and protects mRNA against decapping. *Nucleic Acids Res.* **45**, 6911–6922 (2017).
43. Wurm, J. P., Overbeck, J. & Sprangers, R. The *S. pombe* mRNA decapping complex recruits cofactors and an Edc1-like activator through a single dynamic surface. *RNA* **22**, 1360–1372 (2016).
44. Mugridge, J. S., Collier, J. & Gross, J. D. Structural and molecular mechanisms for the control of eukaryotic 5'–3' mRNA decay. *Nat. Struct. Mol. Biol.* **25**, 1077–1085 (2018).
45. Wurm, J. P., Holdermann, I., Overbeck, J. H., Mayer, P. H. O. & Sprangers, R. Changes in conformational equilibria regulate the activity of the Dcp2 decapping enzyme. *Proc. Natl. Acad. Sci.* **114**, 6034–6039 (2017).
46. She, M. *et al.* Structural Basis of Dcp2 Recognition and Activation by Dcp1. *Mol. Cell* **29**, 337–349 (2008).
47. Deshmukh, M. V. *et al.* mRNA Decapping Is Promoted by an RNA-Binding Channel in Dcp2. *Mol. Cell* **29**, 324–336 (2008).

48. Mugridge, J. S., Tibble, R. W., Ziemniak, M., Jemielity, J. & Gross, J. D. Structure of the activated Edc1-Dcp1-Dcp2-Edc3 mRNA decapping complex with substrate analog poised for catalysis. *Nat. Commun.* **9**, 1–10 (2018).
49. Floor, S. N., Borja, M. S. & Gross, J. D. Interdomain dynamics and coactivation of the mRNA decapping enzyme Dcp2 are mediated by a gatekeeper tryptophan. *Proc. Natl. Acad. Sci.* **109**, 2872–2877 (2012).
50. Chen, I., Dorr, B. M. & Liu, D. R. A general strategy for the evolution of bond-forming enzymes using yeast display. *Proc. Natl. Acad. Sci.* **108**, 11399–11404 (2011).
51. Keenen, M. M., Larson, A. G. & Narlikar, G. J. Chapter Three - Visualization and Quantitation of Phase-Separated Droplet Formation by Human HP1 $\alpha$ . in *Methods in Enzymology* (ed. Rhoades, E.) vol. 611 51–66 (Academic Press, 2018).
52. Schindelin, J. *et al.* Fiji: an open-source platform for biological-image analysis. *Nat. Methods* **9**, 676–682 (2012).
54. Kowalska, J., Osowniak, A., Zuberek, J. & Jemielity, J. Synthesis of nucleoside phosphosulfates. *Bioorg. Med. Chem. Lett.* **22**, 3661–3664 (2012).
55. Warminski, M. *et al.* Amino-Functionalized 5' Cap Analogs as Tools for Site-Specific Sequence-Independent Labeling of mRNA. *Bioconjug. Chem.* **28**, 1978–1992 (2017).
56. Jones, B. N., Quang-Dang, D.-U., Oku, Y. & Gross, J. D. Chapter 2 A Kinetic Assay to Monitor RNA Decapping Under Single-Turnover Conditions. in *Methods in Enzymology* vol. 448 23–40 (Academic Press, 2008).
57. Refaei, M. A. *et al.* Observing selected domains in multi-domain proteins via sortase-mediated ligation and NMR spectroscopy. *J. Biomol. NMR* **49**, 3–7 (2011).
58. Lee, W., Tonelli, M. & Markley, J. L. NMRFAM-SPARKY: enhanced software for biomolecular NMR spectroscopy. *Bioinformatics* **31**, 1325–1327 (2015).

## **CHAPTER 4**

**Additional biochemical and biophysical studies of the decapping complex at  
ångstrom and mesoscopic scales**

## Aromatic residues in Dcp2 have different roles mRNA decapping

The catalytic core of Dcp2 contains several surface-exposed aromatic residues that may be important for RNA recognition. Previously, Trp43 (W43) in the Dcp2 N-terminal regulatory domain (NRD) was identified as essential for decapping activity because it recognizes the m<sup>7</sup>G cap through pi-stacking interactions and ensures specificity for the methyl mark<sup>1,2</sup>. Additional structures of the Dcp1/Dcp2 decapping complex made use of non-hydrolyzable cap analogs that would mimic the cap and first-transcribed nucleotide of mRNA<sup>3,4</sup>. These analogs could provide information on other aromatic residues in Dcp2 that contact mRNA. Two crystal structures of the decapping complex were solved containing two m<sup>7</sup>G moieties linked by a tetraphosphate group (m<sup>7</sup>Gp<sub>s</sub>ppp<sub>s</sub>m<sup>7</sup>G). In addition to W43, m<sup>7</sup>G groups interacted with Tyr92 (Y92), Trp117 (W117), and Tyr220 (Y220) (**Fig. 4.1a**). W117 and Y220 are in the catalytic domain (CD) of Dcp2 and may be important for substrate positioning. To determine whether these interactions are important for mRNA decapping, we individually mutated these residues to alanine and assayed decapping activity on both m<sup>7</sup>GpppRNA and GpppRNA.

Wild-type Dcp1/Dcp2 exhibited four-fold specificity for the methylated, capped RNA and as expected, the W43A mutation reduced decapping activity 100-fold and abolished specificity for the methyl mark (**Fig. 4.1b, Table 4.1**). Mutation of Y92 and Y220 did not lead to defects in decapping or loss in specificity for m<sup>7</sup>GpppRNA (**Fig. 4.1b, Table 4.1**). Y92 has been shown to make contacts with the activator Edc1 and its mutation only slightly reduces Edc1 activation of decapping, suggesting it has a minor role in decapping<sup>5</sup>. While Y220 has a limited effect on decapping in the context of the structured domains, earlier chapters have demonstrated its role in stabilizing an autoinhibited conformation of Dcp2 and another study has shown it may play a role in specificity for the first-transcribed nucleotide<sup>5-7</sup>. Finally, the W117A mutation inhibited decapping of m<sup>7</sup>GpppRNA four-fold, eliminating Dcp2 specificity for methylated cap (**Fig. 4.1b, Table 4.1**).

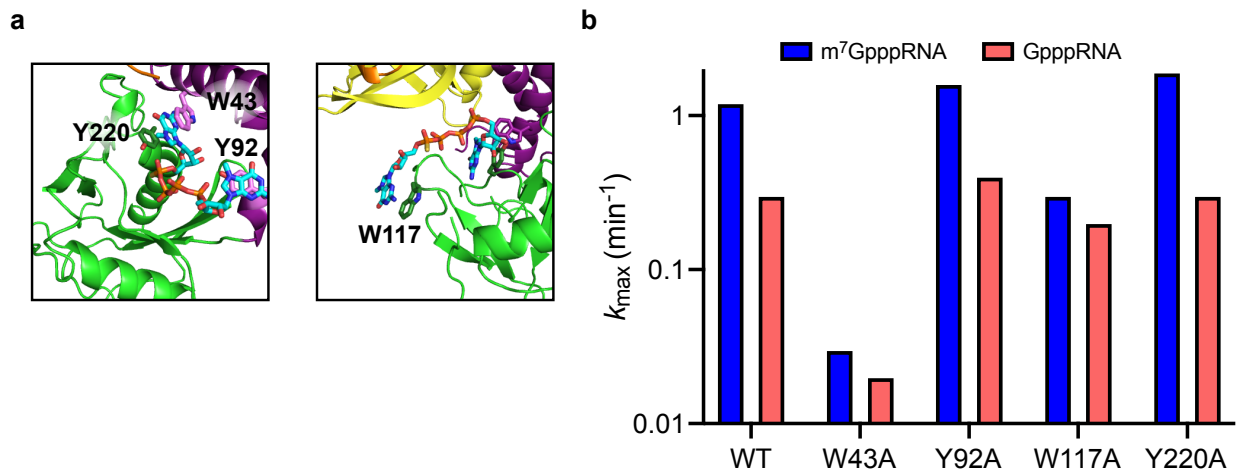


**Figure 4.1: Aromatic residues in Dcp2 that interact with m<sup>7</sup>G have different effects on activity and specificity.** **a**, Interactions between mRNA substrate analog and Dcp2 with key aromatic residues contacting the m<sup>7</sup>G cap labeled (PDB: 5KQ4). W43 and Y92 are in the N-terminal Regulatory Domain (NRD) and W117 and Y220 are in the Catalytic Domain (CD) of Dcp2. **b**, Single-turnover decapping rates of RNA containing methylated (blue) and unmethylated (salmon) cap structures by Dcp1/Dcp2 complexes with point mutations to aromatic residues shown to be interacting with m<sup>7</sup>G moieties in **a**.

The reason for this observed effect on decapping is difficult to explain. W117 is adjacent to the 190s loop in the CD, which contains residues important for Mg<sup>2+</sup> coordination essential for catalysis and interacts with the m<sup>7</sup>G cap in the active state<sup>5,8-10</sup>. This predicts W117 may have a structural role in proper positioning of the 190s loop. In addition, the interaction between W117 and m<sup>7</sup>G may represent an intermediate step that immediately precedes catalysis and ensures specific recognition of the methylated cap. While this intermediate step may be difficult to capture by structural methods, molecular dynamics simulations may provide useful information regarding the local structural rearrangements occurring during the Dcp2 catalytic cycle.

### Interdomain dynamics in Dcp2 are mediated through a regulatory helix

Dcp2 has a bipartite active site formed by the Dcp2 NRD and CD. More specifically, there is contains a helix in the NRD (regulatory helix, residues 31-50) that contains residues Trp43 and Asp47 (W43 and D47) that are critical for cap recognition during catalysis<sup>1,2,11</sup>. In addition, different conformational states of Dcp2 have been structurally characterized showing W43 and D47 can interact with Y220 in the CD (**Fig. 4.2a**)<sup>3,9,12</sup>. This interdomain interaction results in burial of W43 and D47 and is incompatible with cap recognition. In order to adopt the

active state, the CD needs to be displaced to allow  $m^7G$  interaction with W43 and D47 (**Fig. 4.2a**). As a result, Dcp2 undergoes interdomain motions on the ms- $\mu$ s timescale ( $\sim 2000 \text{ s}^{-1}$ )<sup>9,13</sup>. Dynamic NMR studies revealed mutation of W43 quenched these interdomain motions and uncoupled Dcp1 activation of decapping, indicating this residue mediates the conformational switch necessary for catalysis<sup>13</sup>. Mutation of Y220 in the CD also quenches ms- $\mu$ s motions and enhances enzymatic activity, demonstrating that interdomain motions are important for formation of the inactive state<sup>6,7</sup>.

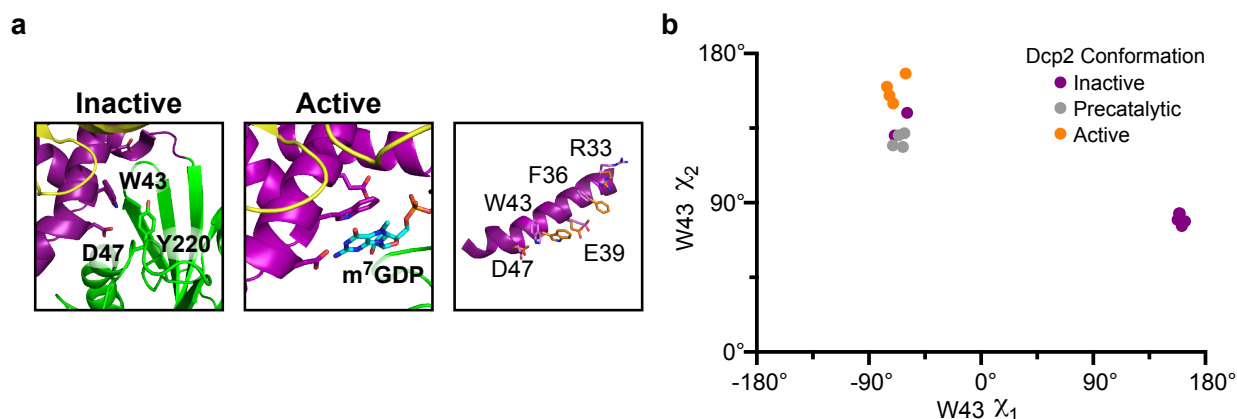


**Figure 4.2: Residues along the interfacial helix of the Dcp2 NRD undergo coordinated movements that enable  $m^7G$  recognition by W43.** **a**, W43 and D47 residues in the interfacial helix of the Dcp2 NRD are occluded by Y220 in the Dcp2 CD in the inactive state (Left) but become accessible for cap binding in the active state (Middle). (Right) Sidechain rotameric changes are propagated along the regulatory helix in the inactive (light purple) and active (orange) states. **b**, W43 sidechain  $\chi_1$  and  $\chi_2$  dihedral angles determined from different Dcp2 conformations observed in published crystal structures.

Closer inspection of the regulatory helix reveals that residues lining the interface between the NRD and CD adopt different states in the inactive and active states of Dcp2 (**Fig. 4.2a**). These concerted motions led us to hypothesize additional mutations may abrogate ms- $\mu$ s dynamics. In agreement, D47 reduced interdomain motions to the same extent as W43 and Y220 as indicated by the observance of additional crosspeaks in their  $^1H$ - $^{15}N$  HSQC NMR spectra (**Table 4.2**). Mutation of E39 also abrogated dynamics, albeit to a lesser extent than D47. Mutation of an aromatic residue at the NRD-CD interface but outside the regulatory helix, Y92, also quenched ms- $\mu$ s motions. Y92 is part of the interdomain linker and may serve to allosterically enforce the CD in the precatalytic or active states. Finally, mutation of W117, which

is distal to the interface does not affect Dcp2 dynamics. Thus, there are several interfacial residues in the Dcp2 NRD that act in a coordinated way to regulate conformational changes in Dcp2.

For W43 to engage with the cap, its sidechain must undergo a large rotational change as Dcp2 adopts the active conformation (**Fig. 4.2a**). This sidechain rotation establishes pi-pi interactions with m<sup>7</sup>G and promotes Watson-Crick-like base-pairing between the cap and D47 (**Fig. 4.2a**). Intriguingly, despite the existence of multiple Dcp2 conformations, the sidechain dihedral angles of W43 can be classified into two orientations (**Fig. 4.2b**). While the dihedral angles for the precatalytic and active states are clustered, they are distinct from those observed for the inactive state. This suggests interdomain dynamics in Dcp2 are required to permit rotation of the W43 indole into the cap-binding state. Dcp1 alters the rate of exchange between the NRD and CD to stabilize the inactive state in solution and activate decapping<sup>9,13</sup>. This counterintuitive activation mechanism could be explained if Dcp1 serves to limit the rotameric states sampled by W43, thus increasing the likelihood of proper cap recognition. This biasing could be accomplished by the NR-loop of Dcp1 that contacts the Dcp2 regulatory helix and, when mutated, prevents activation<sup>14</sup>. In addition, Y220 makes edge-edge interactions with W43 to stabilize the inactive rotamer and mutation of Y220 could activate decapping by permitting W43 to adopt its active rotamer even in the inactive state. NMR presents a useful method to test these predictions because the two states of the W43 sidechain would be distinguishable by their respective J-coupling constants. The results of this proposed work would lead to a more fundamental understanding of the mechanism of activation used by Dcp1, which has been poorly understood.

### **Examining the conformation of the mRNA decapping complex in condensates**

Dcp1/Dcp2 sequestered in condensates has a 10-fold greater catalytic range than in solution due to enhanced repression of activity<sup>7</sup>. In solution, the Dcp2 C-terminus promotes formation of an inactive state, and it is possible this interaction is stabilized or kinetically trapped



due to the higher local concentration in condensates. Another possibility is that at these higher concentrations Dcp1/Dcp2 adopts structures and conformations that would otherwise not be observed. Similar emergent interactions have been observed for *in vitro* condensates consisting of proteins involved in mRNA translation and deadenylation<sup>15,16</sup>. Studying the structures of molecules in droplets is challenging because of their liquid-like properties and the lack of tertiary structure in many phase-separating proteins. Recent applications of NMR and XL-MS offer a promising method for studying interactions that occur specifically in condensates as well as time-resolved information on how these interactions may change over time or in the presence of additional factors<sup>17,18</sup>. Moreover, working with more well-behaved constructs of proteins at the concentrations observed in droplets but in the absence of phase separation provides an alternative approach that may still provide valuable hypotheses that can ultimately be tested in the context of condensate formation.

The structured domains of Dcp1/Dcp2 do not undergo phase separation but can be purified to millimolar concentrations, which is predicted to be at or above what is observed in Dcp1/Dcp2 condensates *in vitro*. Thus, studying the biophysical properties of Dcp1/Dcp2 at these high concentrations could provide insights into what is occurring in condensates. Crystallization of proteins results in high local concentrations similar to phase separation and has led to the observation of two different Dcp1/Dcp2 dimers<sup>11</sup>. In one case, there are numerous intermolecular Dcp1—Dcp1, NRD—NRD and CD—CD interactions of adjacent Dcp2 molecules (**Fig. 4.3a**). However, this dimer is asymmetric because Dcp2 is in different conformations: one molecule is in the inactive state while the other is in the precatalytic state. In contrast, the second observed dimer is symmetric and involves fewer contacts between the RNA binding and HLM-1 helices of interacting monomers (**Fig. 4.3b**). Interestingly, dimerization results in stabilization of states incompatible with catalysis and we hypothesize they may structurally explain the enhanced repression observed in condensates.

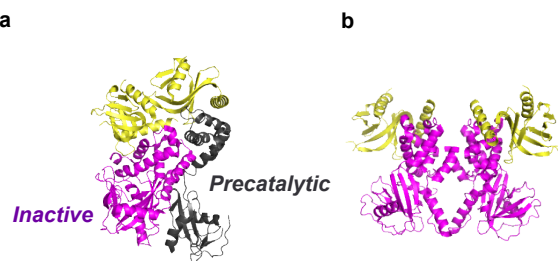


**Figure 4.3: Dcp1/Dcp2 dimers observed in solved crystal structure 2QKM.** **a**, One molecule of Dcp2 is in the closed, inactive conformation (purple) and the other is in the extended, precatalytic conformation (dark grey). Contacts are dominated by intermolecular NRD-NRD and CD-CD interactions. **b**, Both molecules of Dcp2 are in the inactive state and dimerization contacts are mediated by intermolecular B-Box (RNA binding) and HLM interactions.

To determine whether these dimers exist in condensates, we first needed to see if dimerization occurs in solution. Analytical ultracentrifugation (AUC) of proteins is a powerful method to biophysically interrogate the oligomeric state of proteins and we employed it to look for dimerization of Dcp1/Dcp2. At concentrations below phase separation, we observed a single species for Dcp1/Dcp2<sub>ext</sub> that best matches to the monomer and confirms AUC as a viable method for studying Dcp1/Dcp2 (**Fig. 4.4a**).

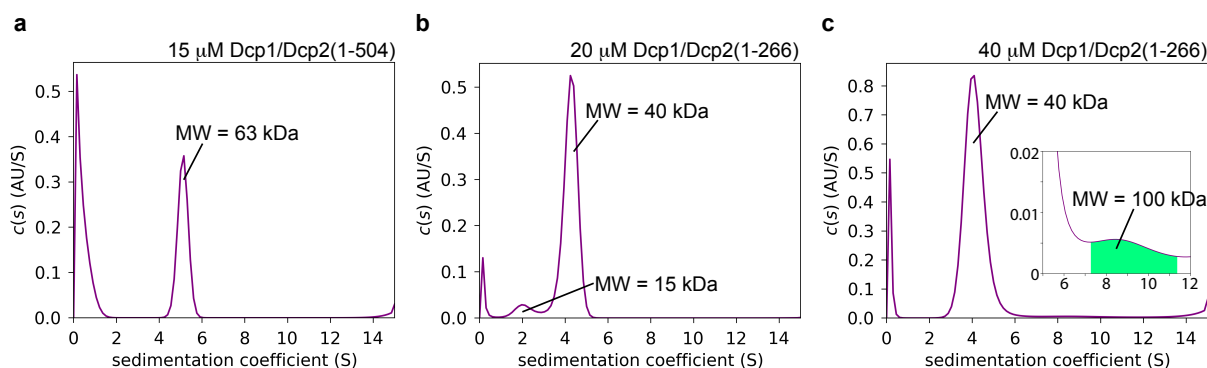


**Figure 4.4: Analytical ultracentrifugation (AUC) of Dcp1/Dcp2(1-504) and Dcp1/Dcp2(1-266).** **a**, Plot of sedimentation coefficient for 15  $\mu\text{M}$  Dcp1/Dcp2(1-504) is indicative of monomeric species (expected  $\text{MW}_{\text{monomer}} \sim 72\text{kDa}$ ). **b**, Two peaks are observed for AUC of 20  $\mu\text{M}$  Dcp1/Dcp2(1-266), with the species at lower sedimentation coefficient corresponding to unbound Dcp1 ( $\text{MW}_{\text{monomer}} \sim 14\text{kDa}$ ) and the species at higher sedimentation coefficient corresponding to monomeric Dcp1/Dcp2(1-266) ( $\text{MW}_{\text{monomer}} \sim 44\text{kDa}$ ). **c**, AUC of 40  $\mu\text{M}$  Dcp1/Dcp2(1-266) gives rise to peak at  $\sim 9\text{S}$ , which most closely fits with a dimeric species ( $\text{MW}_{\text{dimer}} \sim 88\text{kDa}$ ).

Because phase separation at higher concentrations of Dcp1/Dcp2<sub>ext</sub> may confound AUC analysis, we studied Dcp1/Dcp2<sub>HLM-1</sub>. At concentrations below the critical concentration, Dcp1/Dcp2<sub>HLM-1</sub> is also monomeric (**Fig. 4.4b**). Increasing Dcp1/Dcp2<sub>HLM-1</sub> concentration to near the critical point for Dcp1/Dcp2<sub>ext</sub> phase separation still resulted in a predominantly monomeric

state, a small fraction of dimeric species is observed (**Fig. 4.4c**). This species may become more populated as the concentration is increased to recapitulate that observed in droplets. Targeted mutations predicted to destabilize dimerization of Dcp1/Dcp2<sub>HLM-1</sub> can be tested and then made in Dcp1/Dcp2<sub>ext</sub> to look for defects in phase separation. The results of these experiments have broad implications for understanding how phase separation can be utilized by enzymes to establish new mechanisms of regulation.

### **mRNA decapping maintains fluidity in condensates and causes structural rearrangements**

Biomolecular condensates are characterized by the exchange of molecules between the dense droplet environment and surrounding dilute solution<sup>19</sup>. The rate of exchange between these phases is often used to describe how liquid-like a condensate is with more rapid exchange corresponding to a more liquid-like environment. Condensates studied both *in vitro* and *in vivo* exhibit a wide range of exchange behavior and it can change over time for a given droplet<sup>20</sup>. An oft-observed phenomenon of condensates is that the exchange of molecules between the dense and dilute phase slows as they age, resulting in a more viscous droplet<sup>21</sup>. The functional consequences of condensate aging are context-dependent but are meaningful to understand the arrestation of cellular processes and progression of pathogenic aggregation.

P-bodies exhibit properties consist with increased viscosity *in vivo* and decapping condensates undergo aging *in vitro*<sup>22-24</sup>. Mutations that inhibit decapping cause an increase in P-body size and abundance *in vivo*, and is predicted to arise from increased RNA abundance in the cell<sup>22,25</sup>. A study examining the direct effects of decapping on the rheological properties is lacking. Therefore, we sought to use catalytically active Dcp1/Dcp2/Edc3 condensates to study how aging effects their ability to decap mRNA. We performed two independent experiments using the fluorescent mRNA probe: Mg<sup>2+</sup> was added 1) 0.5 hours after Dcp1/Dcp2/Edc3 droplet formation and 2) after 20h incubation of the condensates to initiate catalysis and fluorescence

was monitored by microscopy. Decapping rates observed in droplets were indistinguishable between condensates initiated at 0.5 or 20 hours after formation ( $0.19 \pm 0.02 \text{ min}^{-1}$  and  $0.23 \pm 0.02 \text{ min}^{-1}$ , respectively) as indicated by loss of Fluorescein- $m^7\text{GDP}$  intensity in droplets (**Fig. 4.5a**). Localization of the RNA body was also unchanged in both instances as shown by Cy5 fluorescence (**Fig. 4.5b**). We conclude aging does not affect the ability of Dcp1/Dcp2/Edc3 condensates to perform catalysis.

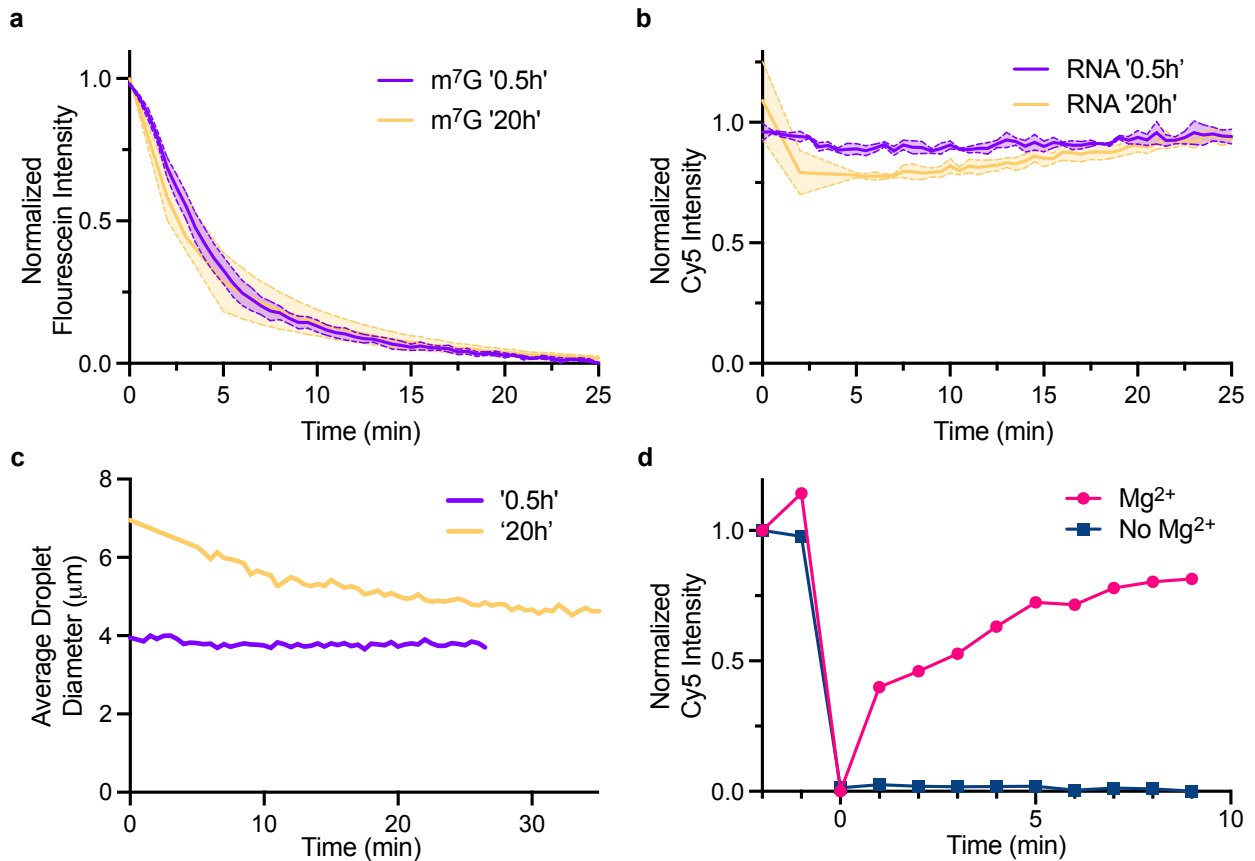


**Figure 4.5: Decapping in aged Dcp1/Dcp2/Edc3 condensates restores size and RNA exchange to resemble liquid-like condensates more closely.** **a**, Fluorescein- $m^7\text{GDP}$  intensity in condensates formed with  $5 \mu\text{M}$  Dcp1/Dcp2<sub>ext</sub> and  $80 \mu\text{M}$  Edc3 following initiation of catalysis with  $\text{Mg}^{2+}$  after 0.5h (purple) or 20h (gold) incubation of condensates with  $100 \text{ nM}$  dual-labeled mRNA probe. **b**, As in **a**, but monitoring RNA-Cy5 fluorescence. **c**, Average size of droplets incubated with  $100 \text{ nM}$  mRNA probe for 0.5h (purple) or 20h (gold) following initiation of decapping with  $\text{Mg}^{2+}$ . **d**, Fluorescence recovery after photobleaching (FRAP) of dual-labeled mRNA localized to Dcp1/Dcp2/Edc3 droplets and incubated for 20h in the absence (dark blue) and presence (pink) of  $\text{Mg}^{2+}$ .

Following initiation of decapping, we noticed droplet size decrease during image acquisition. Plotting the average droplet diameter as a function of time shows droplets incubated for 20h have an initial average diameter of seven micrometers, 1.75x larger than droplets

imaged after 0.5h (**Fig. 4.5c**). During catalysis, the average size decreased to 4.8  $\mu\text{m}$ , plateauing near the size observed for droplets imaged 30 minutes after formation, which did not exhibit any change in average size. The rate of the size decrease ( $0.07 \pm 0.01 \text{ min}^{-1}$ ) observed for aged droplets is slower than the measured rate of decapping, suggesting rearrangements in the droplet environment occur after catalysis and are rate-limiting. While it is unknown what the nature of these rearrangements are, we predict it could be the result of an alteration to the interactions promoting phase separation and a change in partitioning that reflects restored exchange of molecules in condensates. This latter prediction is supported by the observation that the RNA becomes more mobile in condensates following initiation of decapping (**Fig. 4.5d**). More work is needed to better understand this phenomenon, but it is tempting to speculate catalysis is important for maintaining and restoring the liquid-like behavior of decapping condensates. Consequently, P-body morphological and rheological properties could reflect their enzymatic state and dictate their functional roles in mRNA storage and decay.

**Table 4.1: Effect of Dcp2 aromatic mutations on decapping rates and specificity for methylated cap**

Construct	$k_{\text{max}} (\text{min}^{-1})$ $\text{m}^7\text{GpppRNA}$	$k_{\text{max}} (\text{min}^{-1})$ GpppRNA	Specificity ( $k_{\text{m}^7\text{GpppRNA}}/k_{\text{GpppRNA}}$ )
Dcp1/Dcp2	1.2	0.3	4
Dcp1/Dcp2(W43A)	0.03	0.02	1.2
Dcp1/Dcp2(Y92A)	1.6	0.4	3.8
Dcp1/Dcp2(W117A)	0.3	0.2	1.5
Dcp1/Dcp2(Y220A)	1.7	0.3	5.8

**Table 4.2: Qualitative evaluation of mutations in Dcp2 on ms- $\mu\text{s}$  dynamics**

Dcp2 construct	ms- $\mu\text{s}$ dynamics
WT	+++
E39A	++
W43A	-
D47A	-
Y92A	+
W117A	+++
Y220G	-

## REFERENCES

1. Deshmukh, M. V. *et al.* mRNA Decapping Is Promoted by an RNA-Binding Channel in Dcp2. *Mol. Cell* **29**, 324–336 (2008).
2. Floor, S. N., Jones, B. N., Hernandez, G. A. & Gross, J. D. A split active site couples cap recognition by Dcp2 to activation. *Nat. Struct. Mol. Biol.* **17**, 1096–1101 (2010).
3. Mugridge, J. S., Ziemniak, M., Jemielity, J. & Gross, J. D. Structural basis of mRNA-cap recognition by Dcp1–Dcp2. *Nat. Struct. Mol. Biol.* **23**, 987–994 (2016).
4. Ziemniak, M. *et al.* Two-headed tetraphosphate cap analogs are inhibitors of the Dcp1/2 RNA decapping complex. *RNA* **22**, 518–529 (2016).
5. Mugridge, J. S., Tibble, R. W., Ziemniak, M., Jemielity, J. & Gross, J. D. Structure of the activated Edc1-Dcp1-Dcp2-Edc3 mRNA decapping complex with substrate analog poised for catalysis. *Nat. Commun.* **9**, 1–10 (2018).
6. Paquette, D. R., Tibble, R. W., Daifuku, T. S. & Gross, J. D. Control of mRNA decapping by autoinhibition. *Nucleic Acids Res.* **46**, 6318–6329 (2018).
7. Tibble, R. W., Depaix, A., Kowalska, J., Jemielity, J. & Gross, J. D. Biomolecular condensates amplify mRNA decapping by biasing enzyme conformation. *Nat. Chem. Biol.* **17**, 615–623 (2021).
8. Aglietti, R. A., Floor, S. N., McClendon, C. L., Jacobson, M. P. & Gross, J. D. Active Site Conformational Dynamics Are Coupled to Catalysis in the mRNA Decapping Enzyme Dcp2. *Structure* **21**, 1571–1580 (2013).
9. Wurm, J. P., Holdermann, I., Overbeck, J. H., Mayer, P. H. O. & Sprangers, R. Changes in conformational equilibria regulate the activity of the Dcp2 decapping enzyme. *Proc. Natl. Acad. Sci.* **114**, 6034–6039 (2017).
10. Charenton, C. *et al.* Structure of the active form of Dcp1–Dcp2 decapping enzyme bound to m<sup>7</sup> GDP and its Edc3 activator. *Nat. Struct. Mol. Biol.* **23**, 982–986 (2016).

11. She, M. *et al.* Structural Basis of Dcp2 Recognition and Activation by Dcp1. *Mol. Cell* **29**, 337–349 (2008).
12. She, M. *et al.* Crystal structure and functional analysis of Dcp2p from *Schizosaccharomyces pombe*. *Nat. Struct. Mol. Biol.* **13**, 63–70 (2006).
13. Floor, S. N., Borja, M. S. & Gross, J. D. Interdomain dynamics and coactivation of the mRNA decapping enzyme Dcp2 are mediated by a gatekeeper tryptophan. *Proc. Natl. Acad. Sci.* **109**, 2872–2877 (2012).
14. Chang, C.-T., Bercovich, N., Loh, B., Jonas, S. & Izaurralde, E. The activation of the decapping enzyme DCP2 by DCP1 occurs on the EDC4 scaffold and involves a conserved loop in DCP1. *Nucleic Acids Res.* **42**, 5217–5233 (2014).
15. Brady, J. P. *et al.* Structural and hydrodynamic properties of an intrinsically disordered region of a germ cell-specific protein on phase separation. *Proc. Natl. Acad. Sci.* **114**, E8194–E8203 (2017).
16. Kim, T. H. *et al.* Phospho-dependent phase separation of FMRP and CAPRIN1 recapitulates regulation of translation and deadenylation. *Science* **365**, 825–829 (2019).
17. Boczek, E. E. *et al.* *HspB8 prevents aberrant phase transitions of FUS by chaperoning its folded RNA binding domain.* 2021.04.13.439588  
<https://www.biorxiv.org/content/10.1101/2021.04.13.439588v1> (2021)  
doi:10.1101/2021.04.13.439588.
18. Wong, L. E., Kim, T. H., Muhandiram, D. R., Forman-Kay, J. D. & Kay, L. E. NMR Experiments for Studies of Dilute and Condensed Protein Phases: Application to the Phase-Separating Protein CAPRIN1. *J. Am. Chem. Soc.* **142**, 2471–2489 (2020).
19. Banani, S. F., Lee, H. O., Hyman, A. A. & Rosen, M. K. Biomolecular condensates: organizers of cellular biochemistry. *Nat. Rev. Mol. Cell Biol.* **18**, 285–298 (2017).
20. Boeynaems, S. *et al.* Protein Phase Separation: A New Phase in Cell Biology. *Trends Cell Biol.* **28**, 420–435 (2018).

21. Jawerth, L. *et al.* Protein condensates as aging Maxwell fluids. *Science* **370**, 1317–1323 (2020).
22. Xing, W., Muhlrad, D., Parker, R. & Rosen, M. K. A quantitative inventory of yeast P body proteins reveals principles of composition and specificity. *eLife* **9**, e56525 (2020).
23. Fromm, S. A. *et al.* In Vitro Reconstitution of a Cellular Phase-Transition Process that Involves the mRNA Decapping Machinery. *Angew. Chem. Int. Ed.* **53**, 7354–7359 (2014).
24. Schütz, S., Nöldeke, E. R. & Sprangers, R. A synergistic network of interactions promotes the formation of in vitro processing bodies and protects mRNA against decapping. *Nucleic Acids Res.* **45**, 6911–6922 (2017).
25. Decker, C. J. & Parker, R. P-Bodies and Stress Granules: Possible Roles in the Control of Translation and mRNA Degradation. *Cold Spring Harb. Perspect. Biol.* **4**, a012286 (2012).



## CHAPTER 5

### CONCLUDING REMARKS

Our work into the mechanisms regulating eukaryotic mRNA decapping has illuminated a link between mesoscopic organization, atomic structure, and enzymatic activity. We predict our results have implications for the localization of mRNA degradation to dynamic, highly regulated sites in cells. Phase separation sequesters the 5'-3' mRNA decapping machinery, providing a robust mechanism to limit their cellular distribution. These sites can inhibit or activate decapping relative to the surrounding cytoplasm depending on the interactions promoting phase separation (**Fig. 5.1**). As a result, aberrant degradation events would be limited since the available pool of decapping factors are no longer widely distributed. The liquid-like behavior of condensates also allows for rapid reorganization of molecules, potentially altering the fate of localized mRNAs and providing an additional mechanism for ensuring degradation is only permitted when specific conditions are met. Conversely, when drastic changes to the mRNA pool are needed, the expression of Edc1-type activators co-opts the conformational regulation of decapping to promote decay independent of phase separation.

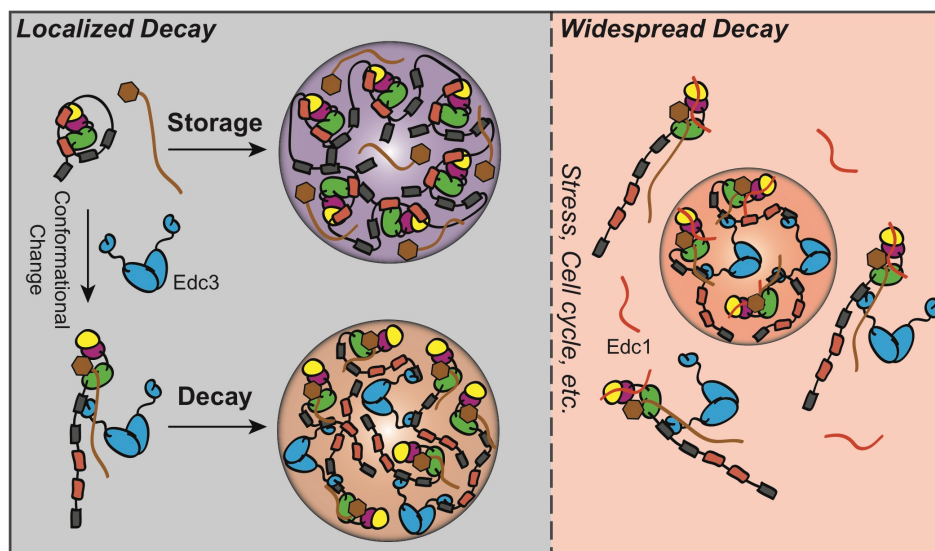


**Figure 5.1: Model of how phase separation regulates mRNA decapping.** Molecular conformation and interactions dictate the functional state of Dcp1/Dcp2 in condensates to cause localized sites of mRNA storage (intermolecular Dcp1/Dcp2 IM—IM interactions) and decay (Dcp1/Dcp2 HLM—Edc3 interactions).

Edc1-type activators strongly activates decapping to override the localized regulation and cause widespread decay.

While this dissertation provides a framework for understanding how intrinsically disordered regions and phase separation can lead to emergent regulatory mechanisms of enzymatic reactions, it does not capture the full complexity of cellular mRNA degradation. An exciting prospect for future research is the ability to reconstitute the complete 5'-3' mRNA decay pathway *in vitro*, which is the result of tireless efforts by many researchers. Simultaneously studying these concerted processes will likely reveal additional modes of molecular crosstalk that may elucidate how the various complexes are assembled on mRNA to coordinate its destruction. With this information we can make incisive hypotheses about the interplay between stability and degradation. The challenges of working with this complexity are formidable, but the prospects of gleaning new insights into RNA biology are rich.

## Publishing Agreement

It is the policy of the University to encourage open access and broad distribution of all theses, dissertations, and manuscripts. The Graduate Division will facilitate the distribution of UCSF theses, dissertations, and manuscripts to the UCSF Library for open access and distribution. UCSF will make such theses, dissertations, and manuscripts accessible to the public and will take reasonable steps to preserve these works in perpetuity.

I hereby grant the non-exclusive, perpetual right to The Regents of the University of California to reproduce, publicly display, distribute, preserve, and publish copies of my thesis, dissertation, or manuscript in any form or media, now existing or later derived, including access online for teaching, research, and public service purposes.

DocuSigned by:  
  
7ED41B150DC0407... Author Signature

9/13/2021  
Date